University of Nottingham
UK | CHINA | MALAYSIA

Deposition behaviour of carbon fibres processed by automated dry fibre placement (ADFP)

by

Shimin Lu, MSc

Thesis submitted to the University of Nottingham for the degree of Doctor of Philosophy

February 2024

Abstract

Automated Dry Fibre Placement (ADFP) is a derivative of Automated Fibre Placement (AFP) where bindered dry carbon fibre tapes instead of prepregs are deposited. ADFP uses similar deposition hardware as AFP but it has low cost potential and fewer resin build-up issues compared to AFP. However, material behaviour of the bindered dry carbon fibre tape is poorly understood which limits the rate and quality of ADFP process. This thesis seeks to understand the material behaviour of the bindered dry carbon fibre tape under ADFP consolidation in order to improve the quality of ADFP manufactured preforms.

The influence of three key process parameters in ADFP: compaction force, process temperature and deposition velocity on the quality of ADFP manufactured preforms is investigated. Compaction behaviour of dry carbon fibre tapes and compaction rollers is characterised. A material model of dry carbon fibre tapes in the through-thickness direction is developed. A finite element (FE) model of roller compaction on carbon fibres is established and experimental validated to research the compaction pressure distribution on complex tool geometries. Thermal properties, including pressure dependent thermal conductivity and temperature dependent specific heat, of carbon fibre tapes are characterised. Joule heating of carbon fibre tapes with configurations representative of an ADFP deposition head are investigated experimentally. Analytical models for joule heating are also built and experimentally validated to predict the joule heating temperature and efficiency. A dynamic FE heat transfer model is built to simulate the temperature history of deposited carbon fibre tapes.

Experimental studies show that bindered carbon fibre tapes have stiffer and more stable response in through thickness direction compared to normal carbon fibre tows. The interlayer bonding of carbon fibre tapes samples manufactured by the ADFP consolidation is dramatically weaker that of the samples manufactured by long term isothermal consolidation (oven heating) and it is also significantly weaker than AFP manufactured prepreg samples. Therefore, process parameters for ADFP need to be chosen more carefully and controlled precisely. Joule heating can be used in ADFP when the contact resistance between carbon fibre tapes and electrodes, and the distance between heating region and nip point are reduced.

From the FE model of roller compaction on carbon fibres, it is found that the force applied by the deposition head when using different roller materials should be

adjusted to obtain equivalent compaction pressure on the preform. Target force windows for roller compaction on tools with different curvatures have been obtained from model results. Softer rollers exhibit larger target force window and increased suitability for tools with larger curvature. From the dynamic FE heat transfer model results, it is found when deposition velocity is high, deposited tapes accumulate heat and have a relatively high temperature (around 130 °C when deposition velocity is 600 mm/s) during the deposition of the next layer. It is also shown that adjusting heat inputs for different layers based on the substrate temperature could reduce the high reheating temperature and differences of temperature histories between different layers of tapes.

Control methods for compaction force and heating temperature in ADFP process are developed with the help of the understanding of ADFP tapes behaviour and the finding from the process models. A model-based feed-forward force control method is developed in order to handle the large deformation of carbon fibre tapes and deposition roller, and to accurately control deposition on complex tools. A PID controller with a pulse-width modulation power control method is developed for joule heating temperature control between two electrodes. The two methods are implemented and tested in an ADFP rig. A high level of control accuracy of compaction force and joule heating temperature can be achieved.

Acknowledgements

I would like to express my sincere gratitude to my supervisors Dr Thomas Turner and Dr Anthony Evans for their continuous advice, support and encouragement during my PhD study.

Thanks go to Paul Johns, Liam Sprake, Dr Adam Joesbury, Jason Greaves, Dr Zhe Liu, Graham Malkinson and Richard Homer for their technical support. Thanks also go to Biruk Nega for his help with running and testing the ADFP rig.

The external support from Peihao Song at the University of Oxford and Professor Francois Robitaille, Chengqian Liao at the University of Ottawa is highly appreciated.

The financial support from the Engineering and Physical Sciences Research Council [grant number EP/P006701/1], as part of the EPSRC Future Composites Manufacturing Research Hub, [grant number EP/V061798/1], as part of the Made Smarter Innovation – Materials Made Smarter Research Centre is also acknowledged.

Lastly, my thanks go to my parents, girlfriend and friends for their encouragement and support.

Research outputs

Journal paper:

Lu S, Evans A, Turner T. Analysis of roller compaction pressure distribution in automated dry fibre placement. **Composite Structures**. 2023;316.

Conference:

(1) **Lu S**, Evans A, Turner T. A model-based feed-forward force control strategy for Automated Dry Fibre Placement (ADFP) on complex tools. International Conference on Manufacturing Advanced Composites 2022 **(ICMAC 2022)**: Sheffield, UK.

(2) **Lu S**, Evans A, Turner T. Application of Joule Heating in Automated Dry Fibre Placement (ADFP). International Conference on Composite Materials **(ICCM 23)**: Belfast, UK.

Contents

List of figures

List of tables

1 Introduction

Carbon fibre reinforced polymer composite materials have been widely used in many industries such as aerospace, automotive, wind energy and sports, because of their high specific strength, high specific stiffness and ability to have their properties tailored to suit specific applications. Automated composites manufacturing processes have been developed to meet the high demand of composites parts and to reduce costly touch labour. With the help of automation, composites parts can be manufactured at high rates, with high repeatability, high quality and low waste. Automated fibre placement (AFP) is a commonly used automated composites manufacturing technique in the aerospace industry. It has been used to manufacture large structural components, such as fuselage, wing skin and spars of several commercial and military aircraft programmes.

1.1 Automated fibre placement (AFP)

Narrow unidirectional carbon fibre prepreg tapes with a typical width of 3.125 mm, 6.35 mm or 12.7 mm are used in the AFP process. Several (typically 8, 16 or 32) prepreg tapes are heated and compressed onto a tool or substrate (i.e. previously deposited layers) continuously by a deposition head mounted on a gantry system or a robotic arm. Figure 1-1 shows a sketch of a typical AFP deposition head. The consolidation roller is used to provide compaction pressure in order to conform prepreg tapes to the required shape. The heating source is used to provide enough heat in order to improve the tack of thermoset prepregs or to facilitate the bonding of thermoplastic prepregs to substrates. The prepreg tapes are cut on-the-fly in the deposition head and near net shape prepreg preforms can be manufactured. There is no limitation on the fibre orientation in AFP process and curved fibre paths can also be deposited with machine steering or tow shearing. These enable novel composites design like ‘double-double’ [1] and variable stiffness laminates [2] where non-conventional fibre orientations or curved fibre paths are used. AFP has been proven to reduce manufacturing cost and material wastage over hand lay-up. AFP also eliminates the labour-intensive hand layup methodology and significantly increases production rates. Literatures [3, 4] summarize recent research and future directions in AFP area.

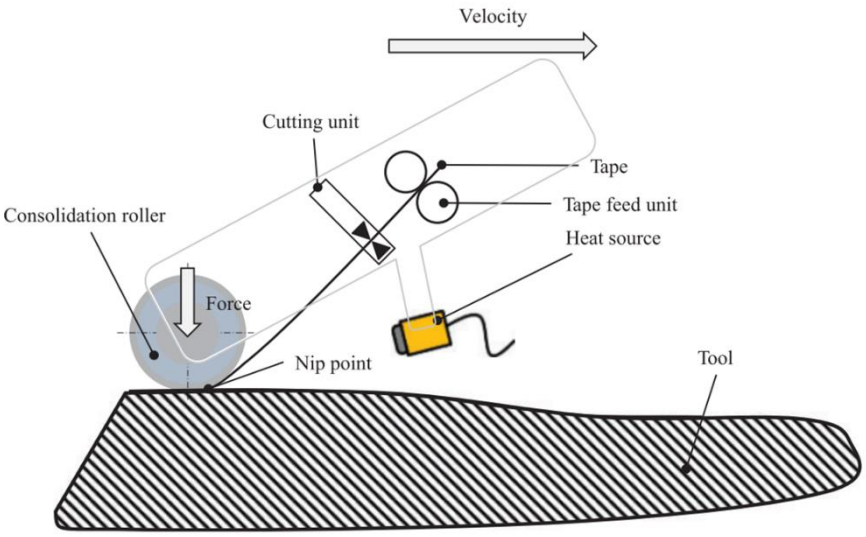

Figure 1-1 Sketch of a deposition head of AFP machine [5]

1.2 Automated dry fibre placement (ADFP)

Automated dry fibre placement (ADFP) process uses similar deposition hardware as AFP but substitutes a bindered dry carbon fibre tape for the prepreg materials. After the deposition stage is completed, ADFP-manufactured preforms are then transferred to a liquid resin injection process such as resin infusion or resin transfer moulding (RTM). This provides the benefit of allowing deposition on low cost tooling where the costly cure tool is used solely for the curing step.

ADFP has advantages over AFP and dry fibre material manual layup processes. The big potential benefit of ADFP over AFP is reduced costs because dry carbon fibre tapes have simpler storage requirements and can be combined with a low cost out-of-autoclave process for resin curing. ADFP tape lacks a matrix resin which eliminates resin build-up issues. Downtime events and repair times due to resin build-up in deposition hardware are significantly reduced when using dry fibre tapes [6]. Compared with the hand layup technique, laminates manufactured by ADFP with vacuum resin infusion process show a 9 % increase of fibre volume fraction and decreases of porosity and thickness variation than laminates manufactured by manual layup with vacuum resin infusion [7, 8].

There are also some significant challenges for ADFP: The low cost potential is not yet fully realised because commercial ADFP tapes are expensive and highly engineered to suit deposition hardware originally designed for prepreg use. Typical commercial ADFP tapes have permeability enhancement materials to accelerate the resin infusion process and binder materials to provide adhesion to the substrate [9]. The

highly engineered tapes have different properties compared to prepreg tapes and normal dry fibre reinforcement therefore experience gained in AFP and dry fibre forming processes may not be directly applied to ADFP. The material behaviour of ADFP tape is also poorly understood which could limit the rate and quality of ADFP process. The binder in dry carbon fibre tapes needs a relatively high activation temperature and laser heating is typically required for high rate deposition of dry carbon fibre tapes [6]. Using laser heating creates health and safety issues [10] and also increases costs.

Two trends in automation of composites manufacturing have been observed: The first trend is towards the smart factory - process automation combined with widespread data exchange and autonomous decision making is now widely established across all areas of manufacturing technology and has become known as 'Industry 4.0'. Critical to this transition is the development of cyber-physical systems which can monitor processes based on detailed and accurate virtual copies of real systems. This trend means more emphasis on sensors for data collection and exchange, and more emphasis on exploiting the advances in computing power for real-time simulation and autonomous decision making. The second trend is the fast development of process models. Process models tend to become more complex and to contain multi-physics and multi-scale simulation in order to provide accurate prediction for complex composites manufacturing process. Machine learning and artificial intelligence methods are also applied to the process models when high non-linearity, poorly understood or non-determined mechanisms are involved in the composite manufacturing process. A recent literature [11] presents a review of current status of machine learning and its application to polymer composites process simulation.

For relatively simple manufacturing process with well understood raw materials, like the CNC milling process, the two trends are relatively easy to pursue because the process, machine and material behaviour for CNC milling are all well understood and highly predictable. For automated composites manufacturing process like AFP and ADFP, there are several challenges: The composite design and manufacturing process are more complex to monitor. AFP and ADFP composites layup have a hierarchical structure: laminate, layer, course and tape. It is hard to monitor the whole hierarchical structure during deposition especially for information at tape level such as tape position, width, thickness and quality [10]. The material behaviour under manufacturing process is poorly understood. Therefore process models have not

been fully developed to include the complex physics in AFP and ADFP in order to provide prediction with a sufficiently high level of accuracy.

1.3 Research objectives

This work is a part of a core project 'Technologies framework for Automated Dry Fibre Placement' within the EPSRC Future Composites Manufacturing Research Hub. The aim of this work is to investigate the material behaviour of carbon fibre tapes under ADFP consolidation and develop process models for ADFP based on the deposition behaviour. The models are used to facilitate real-time control of the ADFP process which could help the ADFP process follow the 'Industry 4.0' trend with consequent improvements in rate and quality. The following research question is proposed.

Research question:
How can we enhance the quality of preforms manufactured by ADFP via improved understanding of both the deposition behaviour of dry carbon fibre tapes and the interactions between them and the deposition machine?

The following objectives are derived to answer this research question:

I. Review the state of art research in AFP, ADFP and related dry fibre processing techniques to determine the knowledge gaps.

II. Understand the influence of process parameters on the quality of preforms manufactured by ADFP consolidation.

III. Understand the material behaviour of carbon fibre tapes under ADFP process conditions and develop models to simulate the material behaviour.

IV. Apply the understanding of material behaviour and developed models in the process parameter control of ADFP.

1.4 Thesis outline

This thesis is organised as shown in Figure 1-2 and each chapter outlines are as below:

- In Chapter 2, the state of art research of quality factors and influence of process parameters on parts quality in AFP, ADFP and related dry fibre processing techniques is reviewed.
- Chapter 3 presents the investigation on the influence of deposition process parameters on the bonding quality of dry fibre preforms manufactured by ADFP consolidation.

- In Chapter 4, the compaction behaviour of carbon fibre tapes and roller compaction pressure on dry fibrous bed are characterised experimentally and numerical models are developed.
- In Chapter 5, the thermal properties of carbon fibre tapes are characterised. A novel joule heating of dry carbon fibre tapes approach is investigated. The temperature history of deposited dry carbon tapes are analysed by a finite element heat transfer model.
- Chapter 6 presents real-time compaction force and heating temperature control methods based on the understanding of compaction and thermal behaviour of dry carbon fibre tapes, and developed models in Chapter 4 and Chapter 5. Demonstrations for the control methods are also presented.
- Chapter 7 shows conclusions from this thesis and discussion of potential future work for research in ADFP.

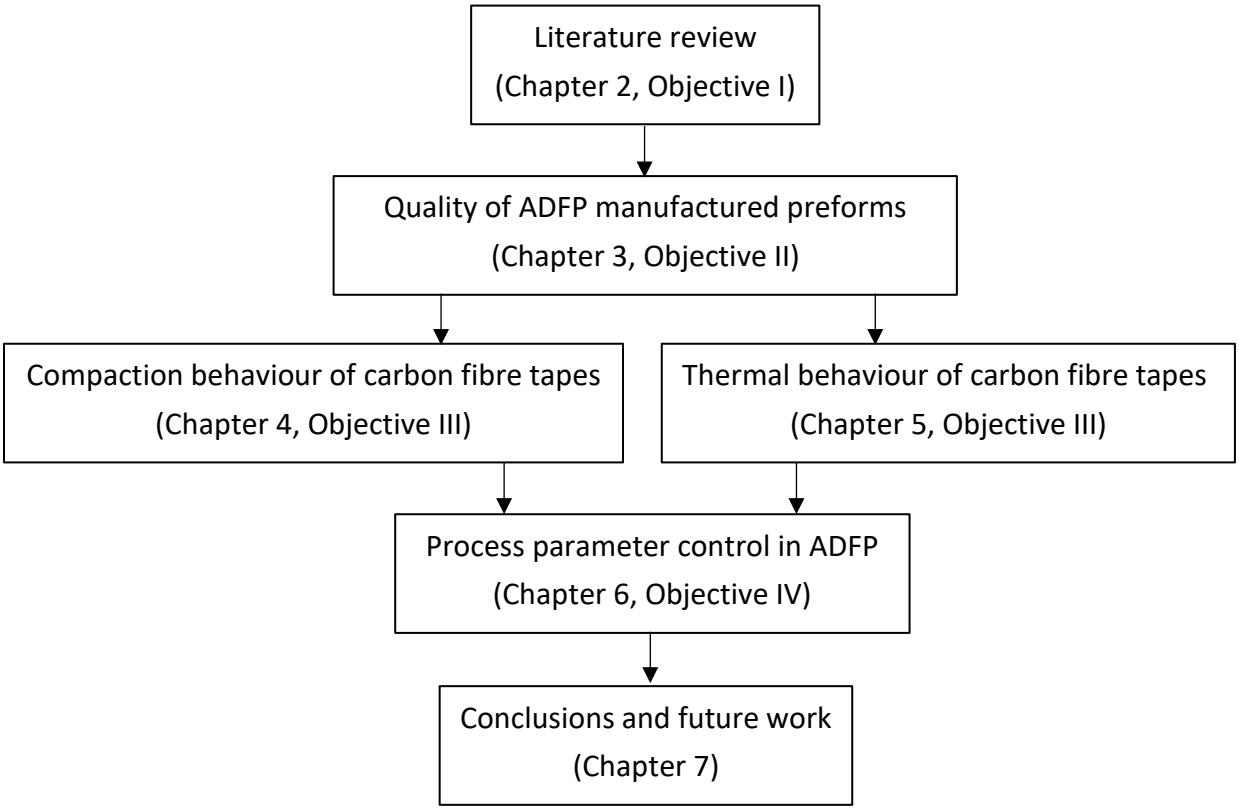

Figure 1-2 Thesis organisation

2 Literature review

In AFP and ADFP processes, the compaction force, the heating temperature and the deposition velocity are the three key process parameters. The compaction force enables the conformance of the tapes on the tool surface and increases the contact area between a compaction roller and substrates. Heating in the process could soften the resin in prepreg tapes or activate the binder in dry fibre tapes to ensure enough tack or bonding is achieved. The deposition speed influences the heating time, pressing time and the production rate. Research on the influence of process parameters on the quality of AFP and ADFP manufactured parts and are reviewed. Research on material behaviour and process conditions related to compaction and heating is then reviewed. Process control related research is also reviewed. Research on AFP and ADFP is reviewed in two separate sections.

2.1 AFP

2.1.1 Quality measure and process parameters optimisation

Tack is considered to be an important property of thermoset prepregs for AFP [10]. It keeps the prepreg on the tool and resists the tendency of tapes pull off. A continuous application-and-peel testing apparatus was developed to investigate the impact of the process parameters on the tack between the prepregs and the tool surface [12-14]. It was found that the tack is sensitive to the temperature and the feed rate. The time-temperature superposition method could be used to predict required temperature in a different feed rate to achieve same tack based on the known results. The apparatus was also used to conduct the tack testing on aerospace grade thermoset prepregs and it was found that the maximum tack between the tool and the prepregs is achieved at low feed rates when temperature is low while when the temperature is increased the maximum tack is achieved at increased feed rates [12-14]. The apparatus was modified to investigate the interlaminar tack and the influence of the compaction force and the roller material [15, 16]. It was reported that the maximum interlaminar tack is significantly larger than prepregs-tool tack and the interlaminar tack increases when compaction force increases and reaches a plateau with further increase of the compaction force. It was also found that a compliant roller could generate larger tack than a stiffer roller at the same level of the compaction force because the compliant roller could increase the contact area and the duration time of compaction. Probe tests are also used to measure the tack of thermoset prepregs [17, 18]. The load-displacement curves from probe tests can fit the traction-separation curve in the cohesive contact in ABAQUS simulation therefore the tack can be simulated as a cohesive contact. The cohesive contact

modelled tack combined with the shear and bending properties of prepregs can be used to simulate the steering induced defects such as blisters and wrinkles [18, 19]. The influence of process parameters on the critical steering radius is also investigated [19]. A floating roller peel test was also conducted to determine the adhesion properties of the prepreg-tool interface. The influence of the compaction force, the heating temperature and the layup speed was investigated. A two-level full factorial design of experiments analysis was conducted to investigate the effect of the individual parameter and the interaction between the parameters [20]. It was found that the temperature has the greatest effect on the peel force and the two-level full factorial design of experiments analysis results could be used to predict the peel force under different process parameters.

Similar to tack, the bonding quality of thermoplastic prepreg is important for AFP. The wedge peel test and the T-peel test were used to characterise the interlaminar bonding of thermoplastic prepregs processed by the AFP and investigate the influence of the process parameters [21-23]. An intimate contact with polymer healing theory was developed to simulate the interlaminar bonding of thermoplastic prepregs processed by the AFP [24, 25]. The simulation results showed similar trend with the peel force results from the wedge peel test. A consolidation model and a thermal model were combined with the intimate contact and polymer healing theory in order to investigate the influence of the process parameters. The intimate contact with polymer healing theory was modified and combined with a multi-pass pressure model and a heat transfer model to obtain the homogeneity of interlaminar bonding strength by using different process parameters when depositing different layers [26, 27]. The wedge peel test results showed that the method could achieve the same level of the bonding strength of every interlaminar region. A concept of effective intimate contact, which is based on the resin content at the surface, is introduced in literature [28]. It is shown that in addition to the squeeze flow mechanism, which is the base for the previous intimate contact models, through-thickness percolation flow of the resin needs to be considered to explain the effective intimate contact development. The influence of heating temperature, compaction force, tool temperature, deposition velocity on the degree of effective intimate contact is also investigated.

Research is also conducted on the process parameter optimisation for AFP. In literatures [29, 30], the prepregs preforms processed by the AFP were evaluated by marking them scores based on their quality. The response surface method and the machine learning method were used to analyse the process parameters sensitivity

and optimise the process parameters to achieve the highest score. A multiscale method was built to optimise the process parameters for the AFP process [31-33]. This multiscale method includes a marco-scale FEA model, an energy transfer model and a molecular dynamics model. High adsorption energy, high diffusion coefficient, stable viscosity and low entropy, which indicate good layup quality, were achieved by optimising the process parameters using the multi-scale method.

AFP enables the manufacturing of the variable stiffness laminates by introducing curved fibre path using the tow steering or shearing. Researchers developed different fibre path optimisation strategies such as using the lamination parameters [34] and the polar parameters [35] to improve some specific performance of the variable stiffness laminates. Introducing curved fibre path by the tow steering or shearing leads to the tow deformation and defects during the deposition process. The steered tow deformation mechanism [36], the steer-induced defects [18, 37] and the influence of the tow deformation and defects on the fibre path planning [38, 39] were investigated. Some researchers [2, 40, 41] applied the manufacturing defects and constraints in the fibre path optimisation strategies to provide practical designs. The layup strategies for different surfaces used in the AFP process including 3D complex surfaces, planer surfaces with a hole in the centre, conical surfaces and cylindrical surfaces were also developed [42]. However, most of the optimisation strategies and the layup strategies remain in the theoretical and the simulation stage and have not been used to manufacture variable stiffness composite laminates. One reason for this might be that no automated method has been developed to convert the optimised fibre path to the control codes for machine deposition. The fibre path needs to be converted to the tow path. The fibre placement head delivers several tows in the same path at the same time and these tows form a course. Thus, the tow path also needs to be converted to the course path, which is the tool path of the deposition head. This conversion process is less developed in the literature.

During the AFP process, several types of defects could be induced including gaps, overlaps, bridging, wrinkle, twisted tow, missed tow, tow drop, folded tow and foreign objects [43-45]. Research on the formation and the prediction of the defects were conducted [46-48]. The influence of the defects on the mechanical properties of the AFP produced laminates were investigated [49-52]. When manufacturing large parts using the AFP, the defect inspection and rework process could take up around 40 % of the total production time [44]. In-process defects detection methods, such as laser vision system [53, 54] and thermal monitoring system [55, 56] have been developed to tackle this issue. The fibre Bragg grating sensors [57] and the eddy

current methods [58] also show potentials to facilitate the in-process defects detection.

2.1.2 Compaction

In the AFP process, prepreg materials are compressed on the tool or the substrate layers by a compaction roller in the deposition head. The compaction force applied to the roller influences the quality of the preforms and final parts. Therefore the compaction force needs to be precisely controlled. The tack between prepreg materials and the tool partially determines the quality of the parts and is strongly influenced by the compaction force [15, 16, 20, 59]. The intimate contact and bonding between adjacent layers are influenced by the compaction force [26, 27, 60]. Mechanical properties, such as the interlaminar shear strength, facture toughness and bending modulus, of AFP-manufactured laminates are influenced by the compaction force [25, 61-64]. Physical characteristics such as cured ply thickness and the formation of defects, such as wrinkles and voids [24, 65, 66] are also influenced.

The roller transfers the compaction force applied by the machine to the compaction pressure on the plies. A high level of uniformity of compaction pressure is required in the AFP process to achieve optimal quality. Several researchers have analysed rollers and sought to optimise the roller geometry to achieve a uniform compaction pressure. For compaction on flat tools, the uniformity of pressure generated by solid rollers with wide range of modulus, diameters and lengths is higher than 80% [67] but perforated rollers have been shown to reduce the uniformity of the pressure distribution compared with solid rollers and this reduction could lead to defect generation [65, 68]. For compaction on non-flat tools, the pressure uniformity of rollers could be reduced from 89% to 16% [67]. This non-uniform pressure distribution restricts the application of AFP on parts with high curvature. The roller geometry therefore needs to be optimised to tackle this issue. For simple non-flat tools such as tools with single curvature or ramps, FE models have been built to investigate the influence of roller material and geometry on the pressure uniformity [46, 67, 69]. It is concluded that soft, compliant rollers generate a larger contact area and a more uniform pressure distribution than stiff rollers. It is also found that carbon fibre reinforced PA6 composites manufactured by an elastomer encased roller exhibit better flexural strength, lap-shear strength, and percentage of crystallinity than those of composites manufactured by a stiff steel roller [70]. In addition, rollers with larger diameter and shorter length can generate more uniform pressure distribution. Roller geometry selection criteria have been established based on the deformability of rollers on surfaces with single curvature [71]. For complex irregular

tools, a theoretical model has been built and validated to investigate the pressure distribution applied by the compaction roller [72]. This model has been used to analyse a segmented roller and it is found that for irregular tools, a segmented roller could generate a more uniform pressure than a solid roller [73]. Besides optimising the geometry or material of rollers, the pressure uniformity can also be improved by dynamically controlling the yaw and roll angle of the head based on the tool geometry [66]. These works focus on situations where the roller is compacted on either the tool surface or with one layer of prepreg between them. No research has been found investigating the pressure distribution on other common situations in the AFP process, such as thick prepreg substrates and substrates with gaps and overlaps.

2.1.3 Heating

During AFP, heating the tapes could soften or melt the resin to obtain enough tack or bonding of the tool-tape and the interlaminar interface. Several heating methods have been used. In the AFP process, the heat source is typically hot gas torch [26], infrared radiation [74], laser [75], flashlamp [3, 76]. The properties of the resin are sensitive to the heating temperature. Thus, it is important to obtain the nip point temperature and the temperature history of the tapes. Research on the influence of the heat input power, the heating device configuration on the heat transfer and the nip point temperature in the AFP deposition process has been conducted [74, 75, 77]. Several thermal models have been developed to investigate the nip point temperature [5, 78, 79]. Temperature history of deposited materials is also important because it can be used in intimate contact model, autohesion model, crystallinity model and residual stress model and to predict interlaminar bonding between layers, crystallisation of prepreg tapes, and residual stresses development [80]. A Lagrangian formulation with changing boundary conditions method [81], a birth-death element strategy [82] and a model expansion method [83] were developed to simulate the entire temperature history of the tapes during the AFP process. Heat transfer model for AFP deposition on complex tool geometry such as C-beam was also established [84]. The information of path points as well as the heating time are incorporated to the heat transfer model to predict the temperature distribution in C-beam structure.

In the thermal model for AFP, the characterisation of the thermal conductivity of the tapes and the interlaminar thermal contact resistance are important for the accuracy of the models. For prepreg materials, the thermal conductivity of the tapes remains consistent under the compaction but the interlaminar thermal contact resistance is influenced significantly by compaction pressure. The interlaminar thermal contact resistance reduces the effective through-thickness conductivity by the factor of two

and the thermal contact resistance is reduced when then compaction pressure increases [85, 86]. Add thermal contact resistance to simulation could improve the prediction accuracy of temperature history [87]. The effect of the compaction pressure on the interlaminar thermal contact resistance has not been applied to the thermal models mentioned above.

2.1.4 Process parameters control

In the AFP process, the defect inspection and rework process could take up around 40 % of the total production time [44]. This might be attributed to the offline control where no adjustment can be performed when defects or machine errors are detected. If real-time control is applied, the quality of parts and the production rate will be improved. To facilitate the real-time control, sensor data is collected and the defects are required to be detected online. The real-time model is running based on the online data to evaluate the influence of the events, such as defects. Decisions are made based on the results from the real-time model. The manufacturing database is used to save the sensor data and the events in the deposition process [88, 89]. In this section, real-time control in AFP related research are reviewed including online data collection, real-time model and the manufacturing database.

The online data collection includes the process parameter monitoring and the online defect detection. The process parameter monitoring could be achieved by using different sensors. For the online defect detection, the laser vision system [53, 54] and thermal monitoring system [55, 56] could be used. The laser profile scanner, the rings of LED lights with sensor array and the image capture camera could be integrated to the AFP deposition system to achieve online fibre orientation measurement and the defects detection [89]. Thermal images taken by the IR camera in the deposition system combined with the image process algorithm such as the convolution neural network could facilitate the online defect recognition [88, 90].

An artificial neural network based real-time model is developed in literature [91] and it could generate the relationship between the compaction pressure, the applied force and the contact width. This model runs online to obtain the real-time compaction pressure based on the sensor data of the applied force and then adjust the force input in real-time to achieve the constant compaction pressure along the deposition path. Similar concept has been developed for the real-time adjustment for the tool centre point to reduce the unwanted forces and torques [92]. Online deposition path correction methods based on the vision or vision-force scheme have been developed to improve the deposition accuracy and to reduce the gaps and

overlaps [93-95]. A surrogate model has been built to generate the knock-down factor (decrease of the safety margin) of different properties caused by the manufacturing defects. It could achieve online evaluation of the effects of the defects [89, 96]. A inline tape width control method is developed to compensate the width variation of prepreg tapes in order to reduce gaps [97]. The width of tape can be controlled by changing compaction force during deposition. In literature [98], a real-time defect detection and correction methods is developed. Defects such as wrinkles are detected using laser scanner in real-time and the wrinkles are corrected by automatically increasing the local compaction level and heating when depositing next layer on the wrinkles position.

The manufacturing database could store the sensor data and the defect detection and recognition results to produce a digital twin for the manufactured preforms [89]. The information stored in the manufacturing database could be analysed by the machine learning method to investigate the influence of the process parameters on the quality of the parts and to optimise the process parameters [88, 90]. The manufacturing database could also store the path planning information and the process information [90]. The HDF5 file and the XML file has been used to produce the manufacturing database. In literature [99], a smart interface is built in MAIO platform to unify and automate data capture from multiple sources in AFP process. Data from each source is contextualised in order to translate each measured data point into to localised Cartesian position on the preform. A demonstration was conducted on a complex tool and data of layup speed, compaction force, nip point surface temperature and preform thickness can collected and visualised. In literature [100], a data mapping technique has been developed and it enables the evaluation of spatial data from many different sources within the AFP process. A global array of data can be generated that includes all aspects of AFP manufacturing such as design data, manufacturing data, inspection data and prediction data. The technique is used to map data of a doubly curved part manufactured by AFP. It is shown that the technique has the ability to map multimodality data into a uniform format.

2.2 ADFP and related dry fibre process techniques

Automated dry fibre placement (ADFP) is a relatively new technique to manufacture large aerospace components [101]. The ADFP process uses similar deposition hardware as AFP but substitutes a bindered dry fibre reinforcement for the prepreg materials. Five types of commercial bindered dry fibre tapes, which could be used in the ADFP were compared using the analytical hierarchy process and the comparison

criteria were based on the quality of the raw materials, preforms and laminates produced from the raw materials. It was found that the TX1100 (Solvay) dry fibre tapes has the highest score among the five materials based on the comparison method [9]. ADFP has many advantages over manual layup process. Laminates manufactured by ADFP with vacuum resin infusion process show a 9% increase of fibre volume fraction and decreases of porosity and thickness variation than laminates manufactured by manual layup with vacuum resin infusion [7, 8]. A 12 to 16% increase of flexural strength and a 6% increase of interlaminar shear stress compared with hand layup are also observed [7]. Compared with AFP, the manufacturing costs of ADFP are theoretically reduced because of the use of low-cost raw materials, liquid resins and out-of-autoclave process. Bindered dry fibre reinforcement used in ADFP has no matrix resin, which could result in a decrease in downtime events and repair times for the deposition machine and an increase of laydown rates comparing with AFP [6]. The ADFP process could be combined with the through-thickness reinforcement, such as stitching and tufting [102, 103]. ADFP process can be followed by thermoplastic resin infusion to produce thermoplastic composites [104].

2.2.1 Quality measure and process parameters optimisation

Similar to AFP, the tack or bonding quality of ADFP carbon fibre tapes are important. A shear tests tack measurement method where the pulling direction is along the fibre direction is developed for bindered dry fibre rovings [105]. It is found that the tack of bindered dry fibre rovings remains on a high level once the temperature is higher than the activation temperature and the binder is fully melted. The tack can be increased slightly by applying more compaction pressure. In literature [106], the wrinkle formation of the dry carbon fibre tapes induced by the carbon fibre tapes steering was investigated and it is found that the tack, which is determined by the process parameters, has a great influence on the critical steering radius.

Research on the bonding quality of preforms manufactured by ADFP has not been found but research on the binder bonding in other dry fibre preforming techniques is reviewed here. The binder bonding of the dry fibre preforms could be influenced by the binder chemical properties, the binder content and particle size, the compaction pressure, the heating temperature and the process time. The thermoset binder and the thermoplastic binder have different bonding properties [107, 108]. The fibre-binder chemical interaction could also influence the bonding strength [109]. The size of the binder particles has influence on the bonding strength and the larger binder particle size generates higher bonding strength [110]. The bonding strength

increases initially with the increase of the binder content but reaches a plateau when the interlayer region is fully covered by the binder [108, 111, 112]. The heating temperature has great influence on the bonding strength. Low temperature does not activate the thermoset binder or melt the thermoplastic binder while the too high temperature will result in the binder flowing into the tow, which cannot contribute to the interlayer bonding [107, 112]. Unnecessary long process time leads to poor bonding strength because the binder might flow into the tow [112]. The compaction pressure influences the bonding strength since it might change the binder coverage area but no research has been conducted on this aspect for dry fibre materials. In the ADFP process with high deposition velocity, the compaction time and the heating time are much shorter than them in the research above and the binder behaviour might show some differences. In the ADFP process, the physical nature of the binder is spreading a viscoelastic polymer melt over the porous carbon fibre under the compaction pressure [107], which is complex and different from the intimate contact situation in the AFP process. No model for the binder flow and bonding has been found, but intimate contact model with the polymer healing theory [24-27], the capillary pressure model and the fibre wetting characterisation [107, 110] might be helpful for building a binder flow and bonding model.

The preforms produced by the ADFP process have low permeability compared with normal textile preforms. Several research was conducted on the characterisation of the permeability of preforms produced by the ADFP [113-115] and the infusion process for the ADFP preforms [8]. Gaps and overlaps are the common defects in the ADFP process and their influence on the permeability was investigated [115-117]. Introducing gaps into the preforms could lead to higher permeability and it is shown that intentionally introducing gaps with 0.4 mm size between fibre tapes in the ADFP layup can increase the out-of-plane permeability 17 times and reduce the compressive strength and modulus by 6 % and 7.2 % [118]. However, the engineering gaps could have large geometry variation which leads to large variation of the permeability [115, 117]. The influence of the through-thickness reinforcement (stitching and tufting) on the preform permeability and the laminate properties was investigated [102, 103].

The influence of compaction pressure, heating temperature and deposition speed on the fibre volume fraction of the preforms produced by ADFP have been investigated [90]. The process parameters optimisation for the fibre volume fraction was conducted on five types of the commercial bindered dry fibre tapes. No research was

conducted on the ADFP process parameters optimisation for other quality factors such as the binder bonding, the permeability and the defects formation.

2.2.2 Compaction

Like AFP, in ADFP the compaction force could also influence the bonding of dry fibre tape to the tool and adjacent dry fibre layers. Compaction pressure is even more important in ADFP than AFP because the compaction pressure directly influences the fibre volume fraction of the preforms which determines the mechanical properties of the final laminates. Uniformity of compaction pressure is required in the ADFP to manufacture preforms with consistent fibre volume fraction. The compaction on dry fibres is a complicated process and the elasticity, plasticity, relaxation, viscoelasticity and cyclic effects appear in the process [119]. Research on the compaction is also important for the liquid composites moulding technique and the main focus is the relationship between the compaction pressure and the fibre volume fraction. This relationship is commonly described by a power law equation [119]. However in ADFP, it has been shown that high compaction pressure can lead to lower fibre volume fraction of the preforms [120, 121]. It is surmised that this reduction is caused by the high compaction-induced through-thickness shear stress which leads to the breakdown of the binder bond and the subsequent deconsolidation of the preforms. This assumption needs further research on the stress field of the dry fibre-roller interaction.

Using dry fibre reinforcement in automated placement process also brings challenges. Dry fibre reinforcement exhibits a large geometry change under process conditions. Thickness reduction of dry carbon fibre tows has been found to be higher than 20% under sufficient compaction [119, 120] while that of thermoset prepregs under AFP process conditions has been found to be less than 10% [122]. In practice, however, commercial materials for ADFP are highly engineered to give consistent in-process performance in the through-thickness direction. But the large thickness change still exists and it can bring difficulties for ADFP force control. Commercial deposition hardware tends to include some built-in compliance in the form of a pneumatic cylinder in order to maintain a roughly constant compaction force. This compliance introduces uncertainty in that the height of the deposition head is not known, there may also be issues in responding to rapid changes in thickness or tool geometry.

Several material models for the dry fibre compaction were developed to describe the compaction behaviour and generate the relationship between the compaction pressure and the fibre volume fraction. For the elasticity, the isotropic linear elastic

model [123], the linear transverse isotropic model [124], the elastic orthotropic model with the non-linear response in the transverse direction [125], the hyperelastic model [126] and the porous elastic model [127] have been developed. Models for the plasticity [128] and the viscoelasticity [129] have been built. For the cyclic compaction behaviour, no model has been built but some experimental research has been conducted [130-132]. It is shown that the compaction response of dry carbon fibre reinforcement shows differences between different compaction cycles and the plastic strain is cumulative with successive compaction cycles. In the ADFP process, cyclic compaction behaviour needs to be determined and a material model considering the cyclic effects should be built. This is because every layer in the preform has a different compaction history and, therefore, a different response to the compaction and different thickness.

No research on experimental or simulation study of roller compaction pressure distribution on dry fibres has been found. Related research in AFP as reviewed in section 2.1.2 might be adopted for ADFP but the compaction behaviour of dry carbon fibre tapes needs to be considered.

2.2.3 Heating

In the ADFP process, the binder activation temperature is relatively high and the laser heating is commonly used [6, 10, 75]. The joule/resistive heating [133, 134] and hot gas torch heating [118] are also used. For laser heating, the influence of the heat input power, the heating device set up on the heat transfer and the nip point temperature in the deposition process has been conducted [75].

Carbon fibres are electrically conductive and there is little resin present in the ADFP tapes, therefore joule heating could potentially be a suitable heating method for ADFP consolidation. Joule heating enables fast, efficient and local heating [133]. It has many applications in the composites industry, such as curing of composite laminates [135], de-icing [136], and towpreg manufacturing [137]. Joule heating in these areas utilises different configurations especially the contact between carbon fibre and electrodes compared with ADFP conditions. In ADFP process, cylinder or roller electrodes are suitable for joule heating to ensure smooth feeding for carbon fibre tapes. The contacts between cylinder electrodes and carbon fibre tapes are not perfect and the electrical contact resistance therefore exists. The electrical contact resistance consumes energy and causes heating in contact area therefore it needs to be reduced. Research in [138] characterised the contact resistance between carbon fibre tows and cylinder electrodes and it is found that the existence of contact

resistance leads to the heating in the contact region and increasing fibre tension results in a decrease of contact resistance. However, the contact resistance between carbon fibre tapes used in ADFP and the cylinder electrodes has not been investigated.

For the thermal properties of dry fibre reinforcement, only the effective thermal conductivity of the dry fibre fabrics was investigated. Both the in-plane and through-thickness effective thermal conductivity increase with the increasing fibre volume fraction, which is achieved by increasing the compaction pressure [139-142]. No research has been conducted on the thermal conductivity of the single layer of dry fibres and the interlaminar thermal contact resistance of dry fibre preforms. The heat transfer model for the ADFP process should consider the effect of the compaction pressure.

For AFP process, many heat transfer models have been built to investigate the nip point heating temperature and temperature history of deposited materials to achieve thermal management of AFP process as reviewed in section 2.1.3. However, no related research has been found for ADFP.

2.2.4 Process parameters control

Research on the process parameters control in ADFP is limited. For temperature control, an open-loop laser heat power control method based on a semi-empirical model is developed and used in ADFP deposition in literature [75]. Real-time control strategies developed for AFP process as reviewed in section 2.1.4 have potentials to be used in ADFP but the material behaviour of dry carbon fibre tapes needs to be characterised and incorporated to the strategies.

2.3 Summary of findings

AFP and ADFP use similar deposition hardware but their process conditions have differences. Table 2-1 presents the heating, pressure conditions, post processing steps and main advantages of AFP using thermoset prepreg, thermoplastic prepreg and ADFP using bindered dry fibre tapes. It is noted that the pressure range for thermoplastic AFP and ADFP is less conclusive than heating temperature requirement because in most related research compaction force instead of compaction pressure is used. Compared to AFP, ADFP is a new manufacturing technique and ADFP related research is limited. ADFP brings new challenges and

research opportunities. From literature review, it is found that research in following subjects is helpful for improving the quality of ADFP manufactured preforms:

I. Influence of process parameters on the bonding quality of ADFP manufactured preforms and process parameter optimisation methods/models for ADFP.
II. Bonding formation mechanisms and models for the binder in dry carbon fibre tapes under ADFP process conditions.
III. Cyclic compaction behaviour and models of dry carbon fibre tapes.
IV. Roller compaction pressure distribution on dry carbon fibrous bed.
V. Characterisation of fibre volume fraction dependent thermal conductivity of dry carbon fibre tapes.
VI. Characterisation of fibre volume fraction dependent thermal contact resistance of tape/tool contact and tape/tape contact.
VII. Application of joule heating in ADFP configurations.
VIII. Heat transfer analysis of the heating of dry carbon fibre tapes for nip point temperature investigation.
IX. Heat transfer analysis for deposited dry carbon fibre tapes for their temperature history.

Table 2-1 Process conditions of AFP and ADFP

	Thermoset AFP	Thermoplastic AFP	ADFP
Heating requirement	Low heat: typically less than 70 °C [62, 65, 122]	High heat: around 400 °C for PEEK [28, 143]	Medium heat: around 200 °C for TX1100 tapes [8, 121]
Pressure range	Low pressure: typically less than 0.3 MPa [62, 122, 144]	0.3 to 0.9 MPa [28]	~ 0.25 to 0.87 MPa [7, 121]
Post processing	Autoclave curing for best quality	Autoclave consolidation for best quality	Resin infusion and curing
Main advantage	Well understood Low heat and pressure	Sustainability In-situ consolidation potential	Low cost

3 Influence of process parameters on the quality of carbon fibre preforms manufactured by ADFP

3.1 Introduction

The influence of process parameters on the quality of ADFP manufactured preforms and final laminates are poorly understood. Limited research has been conducted on the influence of process parameters on the key quality measures of fibre volume fraction and permeability as reviewed in section 2.2.1. The tool-ply and interlayer bonding or tack behaviour has been found to be a key quality factor for AFP manufactured thermoplastic or thermoset composite laminates as reviewed in section 2.1.1. However, research on tool-ply / interlayer bonding behaviour for ADFP manufactured preforms has not been found in the literature. The interlayer bonding behaviour of dry fibre preforms (e.g. those manufactured for subsequent processing via RTM) under long term (in minutes or hours) isothermal consolidation conditions (constant temperature through the whole preform) has been investigated as reviewed in section 2.2.1. However, high speed dry fibre consolidation shows significant differences to isothermal consolidation. The process time period is very short (the process time is 0.4 s when the contact length is 40 mm and the deposition velocity is 0.1 m/s) and the deposited tapes make contact with cooler substrates. The heat transfer between deposited tapes and cooler substrates also influences the bonding quality. In this chapter, two sets of dry fibre tape samples are manufactured by both long term isothermal consolidation and also via mock ADFP consolidation. The interlayer bonding quality of the manufactured samples is characterised by T-peel tests. The interlayer bonding quality of samples manufactured by the two conditions is compared. The influence of three important process variables: temperature, compaction force and deposition velocity on the interlayer bonding quality of ADFP manufactured preforms is also investigated.

3.2 Sample manufacturing and peel resistance characterisation

3.2.1 Materials

24K TX1100 (Solvay) unidirectional bindered carbon fibre tapes with a width of 6.35 mm, a nominal thickness of 0.275 mm and an areal weight of 212 g/m^2 were used to manufacture samples. The tapes have binder particles on one surface (termed binder surface in later sections) and veils on the other surface (termed veil surface in later sections) [9] as shown in Figure 3-1. During deposition of the tapes, the binder surface faces down and makes contacts with either tool surfaces or veil surfaces of substrate tapes.

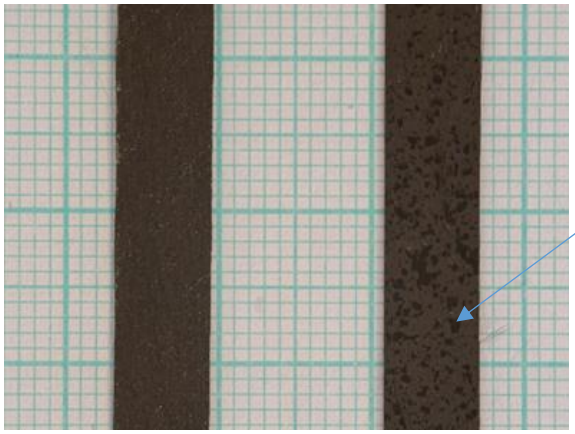

Figure 3-1 TX1100 carbon fibre tapes showing veil (left) and binder (right) surfaces (1 mm minor grid spacing)

3.2.2 Sample preparation

Two sets of samples were manufactured. The samples manufactured using an oven under long term isothermal consolidation are termed 'static samples' and the samples manufactured using an ADFP rig are termed 'dynamic samples'.

3.2.2.1 Static samples preparation

The TX1100 tapes were cut into a length of 200 mm. Two tapes were laid up together with the veil surface of one facing the binder surface of the second. A piece of release film with a length of 50 mm was inserted in one end of the interlayer region of each sample to produce a pre-crack. Six samples were laid up and compacted by a vacuum pressure 0.1 MPa using a silicone rubber vacuum bag whilst heating in an oven to a consolidation temperature to activate the binder. A thermocouple was connected to the tool surface to measure the process temperature. When the thermocouple measured temperature reached the consolidation temperature, this temperature was maintained for 10 minutes before cooling. Vacuum pressure was applied until they were cooled down to room temperature. Figure 3-2 shows the setup for static sample preparation during the cooling period.

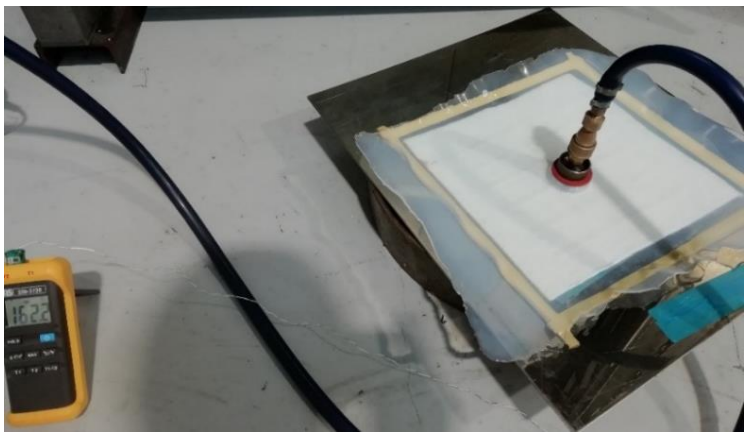

Figure 3-2 Vacuum consolidation setup for static samples: six samples can be observed through the breather layer

3.2.2.2 Dynamic sample preparation

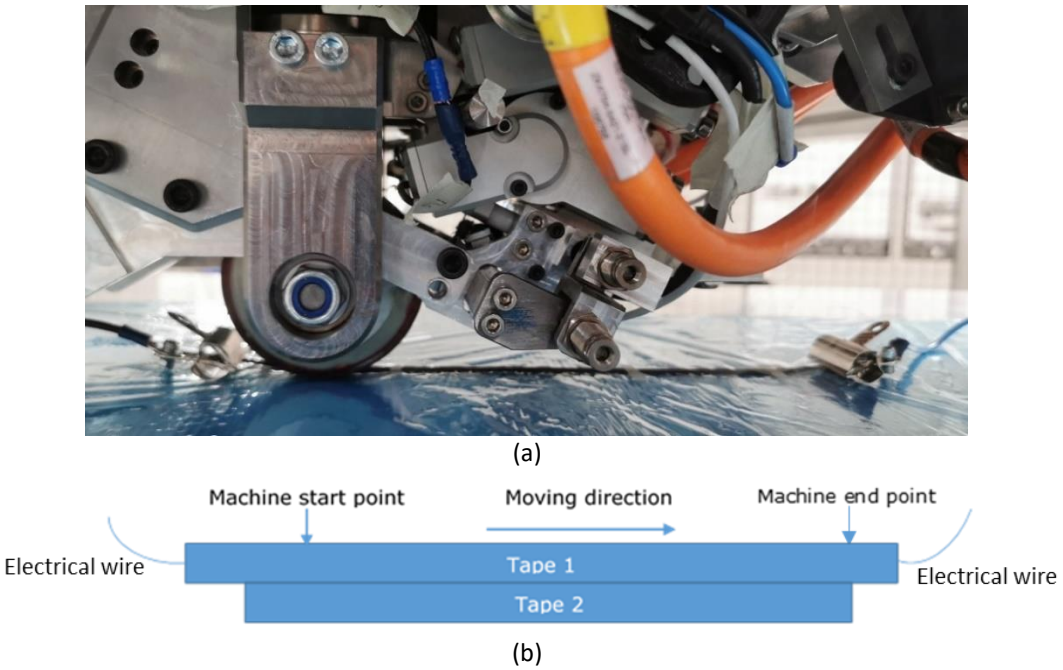

Figure 3-3 Mock ADFP consolidation setup for dynamic samples (a) experimental setup (b) sketch for tapes position and machine moving path (Two electrical wires are connected to a power supply.)

For dynamic samples manufacturing, a mock ADFP consolidation setup was used because the lab-scale ADFP rig was not fully developed. Figure 3-3 shows the experimental setup and the sketch for the mock ADFP consolidation conditions. A piece of TX1100 tape with a length of 200 mm is fixed on the tool surface with two pieces of adhesive tape on the two ends and the binder surface faces the tool surface. The other piece of TX1100 tape with a length of 240 mm is placed on the top of the substrate tape with binder surface facing down and is fixed with four pieces of adhesive tape. A joule heating method is used to heat the top tape (tape 1 in Figure 3-3 (b)) and details of the joule heating mechanism is given in section 5.3. The two ends of the top tape are connected to an electric circuit using clips and wires. A power supply (Velleman LABPS3010SM) is used to provide constant voltage to the circuit to heat the top tape. The lab-scale ADFP rig is used to apply a compaction force with a prescribed deposition velocity. The machine movement length (bonding length) is 25 mm shorter than the interlayer contact length. The initial uncompacted 25 mm length is considered as a pre-crack. During the sample manufacturing process, the top tape is firstly heated for 15 s to reach a nearly steady state heating temperature and the deposition head then starts movement with certain compaction force and deposition velocity. The joule heating stops when the deposition head arrives at the end point. This consolidation conditions partially replicates the real ADFP conditions. The main difference is in the cooling period: In real ADFP consolidation, tapes are heated before the nip point and cooled with compaction during deposition while in

this mock setup, top tapes are heated continuously before and after compaction. The cooling of tapes then occurs without compaction.

3.2.3 Experimental design

The choices of three process parameters: process temperature, compaction force and deposition velocity are described in this section.

3.2.3.1 Process temperature

For static samples manufactured using an oven, the isothermal condition is achieved, therefore the thermocouple measured temperature (tool temperature) can accurately represent the temperature in the interlayer bonding region. Four process temperatures: 180, 200, 220, 240 °C are chosen because the activation temperature of the tapes is around 160 °C [120]. These temperatures are termed 'interlayer temperature'.

For dynamic samples manufactured using the ADFP rig, the joule heating method is used and the power supply voltages are varied to achieve different heating temperatures. The heating temperatures generated by different voltage supplies are characterised experimentally using the same setup as shown in Figure 3-4 (a). The top tape is heated around 15 s and the heating temperatures of the top tape are then measured using a FLIR C5 thermal camera. Figure 3-4 (b) shows an example of heating temperature measurement. Average temperature in the centreline of the top tape is calculated and recorded as heating temperature. Five measurements are conducted for each voltage. Figure 3-5 shows the relationship between the power supply and heating temperature for the mock ADFP setup. Five voltages 11, 12, 13, 14 and 15 V are chosen, and these voltages result in 136, 155, 193, 233 and 254 °C heating temperature. These temperature can only represent the surface temperature of top tape and are termed 'heating temperature'. This heating temperature is slightly higher than the average temperature of the whole surface area of the tape because the edges (across the width) of the tape exhibit lower heating temperature than the centre area as shown in Figure 3-4 (b).

(a)

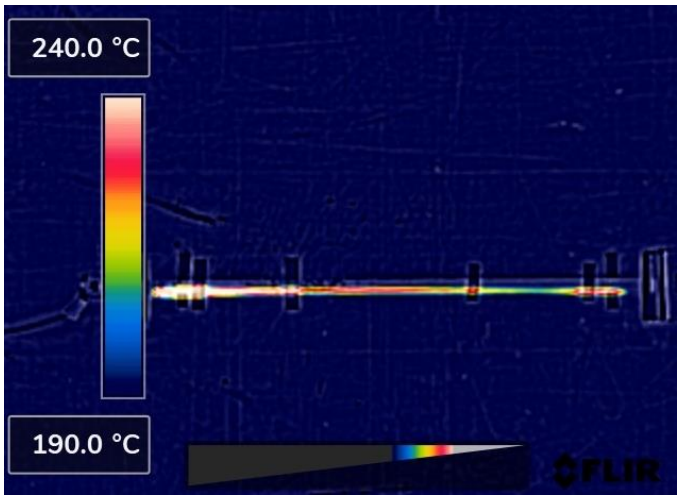

(b)

Figure 3-4 Joule heating temperature characterisation for mock ADFP setup (a) joule heating setup (same as Figure 3-1 (b)) (b) thermal camera measurement of heated tapes

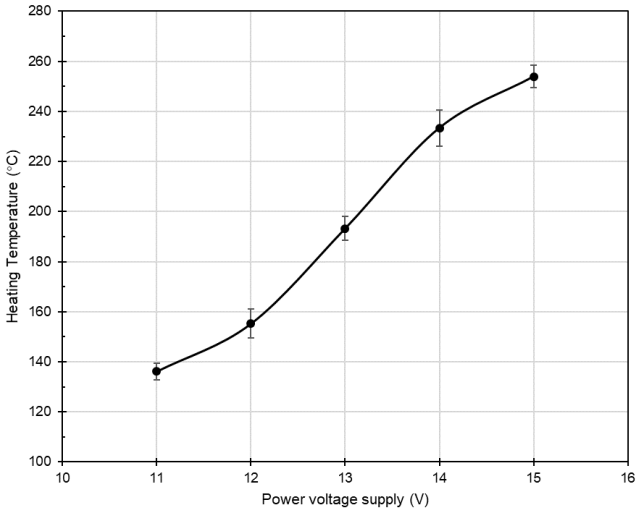

Figure 3-5 Joule heating temperature generated by different voltage supplies for the mock ADFP setup

3.2.3.2 Compaction force

For static samples manufactured using an oven, a full vacuum pressure (around 0.1 MPa) as used in many dry fibre process techniques is applied via a vacuum pump and a lab manufactured silicone rubber vacuum bag which could withstand the high process temperatures.

For dynamic samples manufactured using the ADFP rig, the compaction force is applied by the deposition head with a proportional integral derivative (PID) controller, details of which are given in section 6.2. The force data is collected by a force torque

sensor (ATI Industrial Automation Axia80). Four compaction forces 10 N, 20 N, 30 N and 40 N are chosen. These four forces result in four nominal pressures (average pressure over contact area): 0.51 MPa, 0.77 MPa, 0.94 MPa and 1.05 MPa based on simulation results shown in Figure 4-15 in section 4.3.2.5. These compaction pressure values cover the range of commonly used compaction pressure in composites manufacturing process and they are within the range of pressure used in ADFP research in literature [121].

3.2.3.3 Deposition velocity

For deposition velocity, relatively low velocities are used because the lab scale ADFP rig is not fully developed and high-speed deposition performance is not stable. Four speeds 2, 5, 10, 20 mm/s are then chosen. The velocity data is collected from motion data in the ADFP rig. The acceleration and deceleration stages on the two ends of tapes are short (full deposition velocity is reached within 0.11 s for deposition velocity of 20 mm/s) and then ignored.

In total 17 combinations of process parameters were used to manufacture dynamic samples. Six repeat samples were manufactured for each combination. Table 3-1 shows the process parameters for all combinations.

Table 3-1 Process parameters combinations for dynamic samples manufacturing

Sample reference	Voltage (V)/ temperature (°C)	Compaction force (N)	Deposition velocity (mm/s)
1	11 / 136	20	10
2	12 / 155	20	10
3	13 / 193	20	10
4	14 / 233	20	10
5	15 / 254	20	10
6	14 / 233	10	10
7	14 / 233	30	10
8	14 / 233	40	10
9	12 / 155	20	5
10	13 / 193	20	5
11	14 / 233	20	5
12	15 / 254	20	5
13	14 / 233	10	5
14	14 / 233	30	5
15	14 / 233	40	5
16	14 / 233	20	2
17	14 / 233	20	20

3.2.1 Peel testing methods

Peel tests are commonly used to characterise the bonding behaviour. Among different peel test methods, the T-peel type was chosen to compare the bonding quality of manufactured samples as it uses simple equipment and it is a quick method for comparison purposes. T-peel tests were conducted on an Instron universal testing machine with a 1 KN load cell and the load rate was 75 mm/min. Figure 3-6 shows the T-peel test apparatus. Six samples were tested for each combination of process parameters. The total peel distance was around 300 mm and the average peel forces and maximum peel forces were calculated from peel distance 50 mm to 250 mm, as shown in the shaded area in Figure 3-7.

Figure 3-6 Experimental setup for T-peel tests

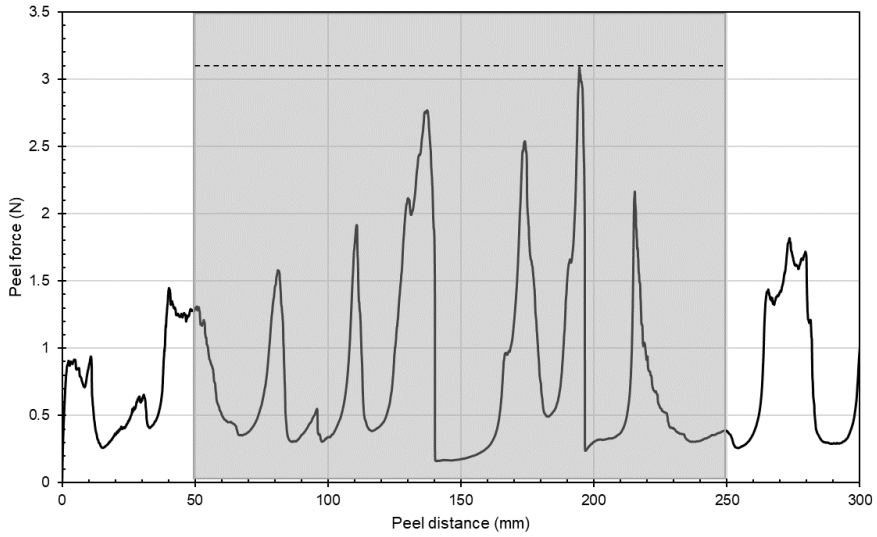

Figure 3-7 Peel force curve from T peel test (average peel force is calculated from shaded area; maximum peel force is from dash line)

3.3 Experimental results of bonding quality

The peel resistance of static and dynamic samples are firstly compared in this section. The influence of compaction force, temperature and deposition speed on the peel resistance is then investigated.

3.3.1 Comparison between static and dynamics samples

Figure 3-8 shows the peel resistance characterisation results for static and dynamic samples. For dynamic samples, the highest peel resistance results in all 17 combinations are shown in the 233 °C data points in Figure 3-8 (b). It is observed that the peel resistance results show large variation especially for dynamic samples. The average peel forces are around 0.5 % of the full rated output of the load cell and the reading error could be 5 % at this low point according to the manufacturer. The reading error could contribute to the large variation of results. The maximum peel forces are much higher than the average peel forces and load cell error is much less (within 0.25%). Therefore, maximum peel forces are more valuable results. For both static and dynamic samples, the process temperature has a great influence on peel resistance and this is discussed in section 3.3.3. Static samples have significantly larger average peel forces and maximum peel forces than dynamic samples at all process temperatures. The maximum peel forces of dynamic samples are even smaller than the average peel forces of static samples. Figure 3-9 shows peel force curves along the peel distance of typical individual static sample and dynamic sample. It is observed that the peel resistance along the length of samples is not uniform which could be caused by nonuniformity distribution of the binder and veil of tapes. For both static and dynamic samples, peel force curves consist of peaks and low plateaus. Peaks indicate the initiation of interlayer bonding crack and low plateaus indicate the crack propagation. The shapes of peel force curves are in agreement with the T-peel curves of in literature carbon fibre reinforced polypropylene samples manufactured by AFP [22]. Static sample have more peaks with higher peel force value. Dynamic samples have fewer peaks and their values are much lower than static samples. These agree with the results shown in Figure 3-8. The distribution of peaks are uniform along the peel distance for static samples while the most peel force peaks of dynamic samples are located towards one end along the peel distance. Different sections of dynamic samples have different heating time before and after roller compaction, and the heating temperature is not uniform along the sample length as shown in Figure 3-4 (b). These could lead to the non-uniform peel force peaks distribution.

Compared with carbon fibre reinforced polypropylene samples manufactured by AFP in literature [22], the maximum peel force per unit width of the dynamic samples is about tenth of that of AFP samples. This significant low peel resistance is due to the lack of matrix resin in the interlayer region. The low peel resistance means lower robustness and requires more precise process parameter control than AFP.

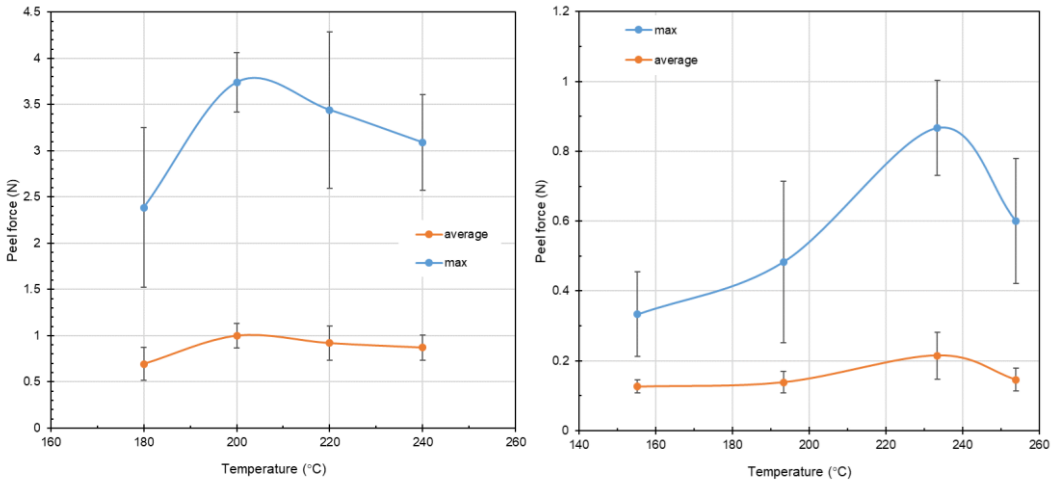

(a) (b)

Figure 3-8 Average and maximum peel forces of (a) static samples (b) dynamic samples under different process temperatures (different y axis scales for (a) and (b))

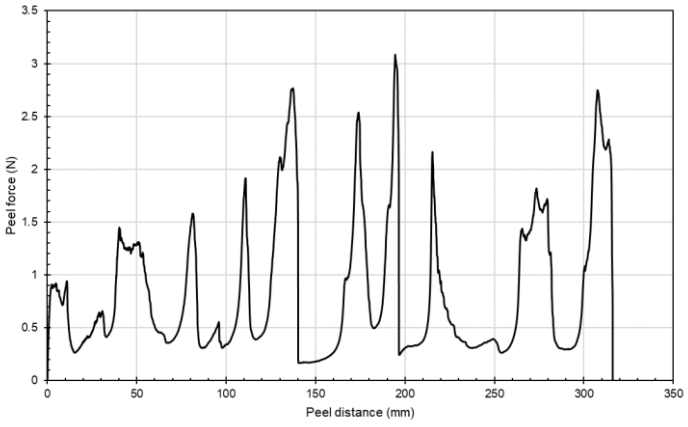

(a)

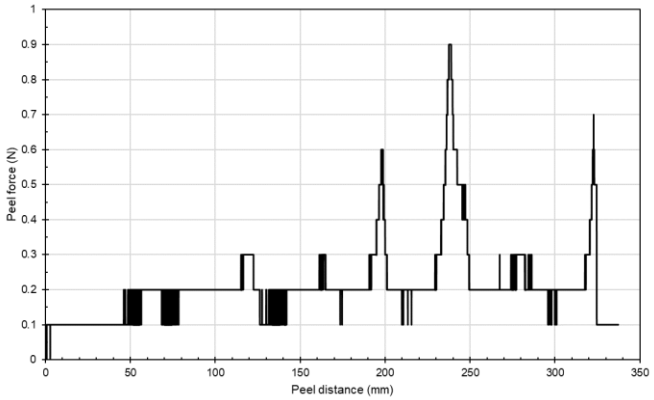

(b)

Figure 3-9 Peel force curve from (a) static sample (b) dynamic sample(different y axis scales for (a) and (b))

To investigate the failure mechanisms behind the large differences of peel resistance between static samples and dynamic samples, macro-pictures are taken using a mirrorless camera with a macro-lens for unprocessed tapes, peeled surfaces of static and dynamic samples. Figure 3-10, Figure 3-11 and Figure 3-12 show the macro-pictures for unprocessed tapes, peeled static samples and peeled dynamic samples.

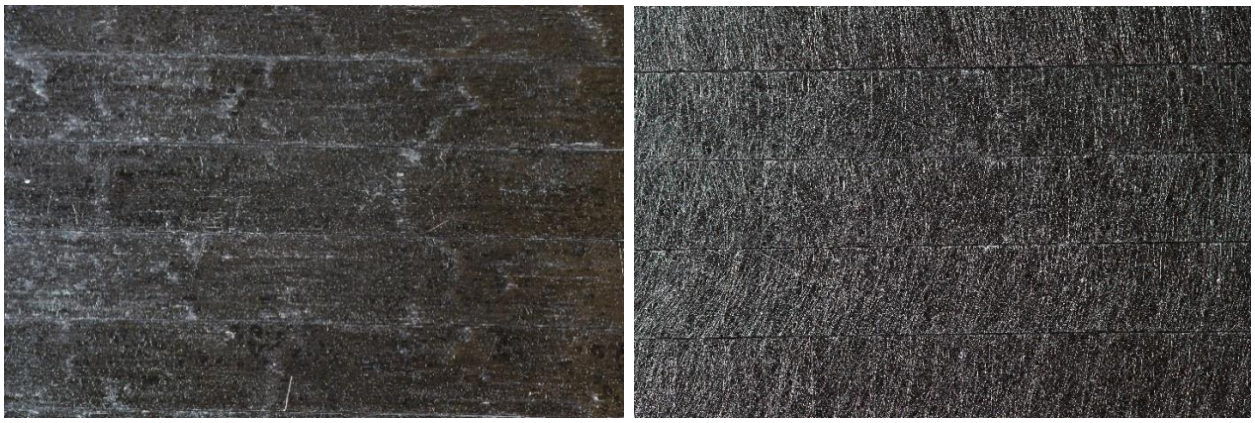

(a) (b)

Figure 3-10 Macro-photographs of unprocessed TX1100 tape (a) binder surfaces (b) veil surfaces

Figure 3-11 Macro-photograph of binder surfaces of processed and peeled static samples at the boundary region between precrack area (right) and peeling area (left) (Veils left on the binder surfaces are shown on the left-hand side. Peeling direction is from right to left.)

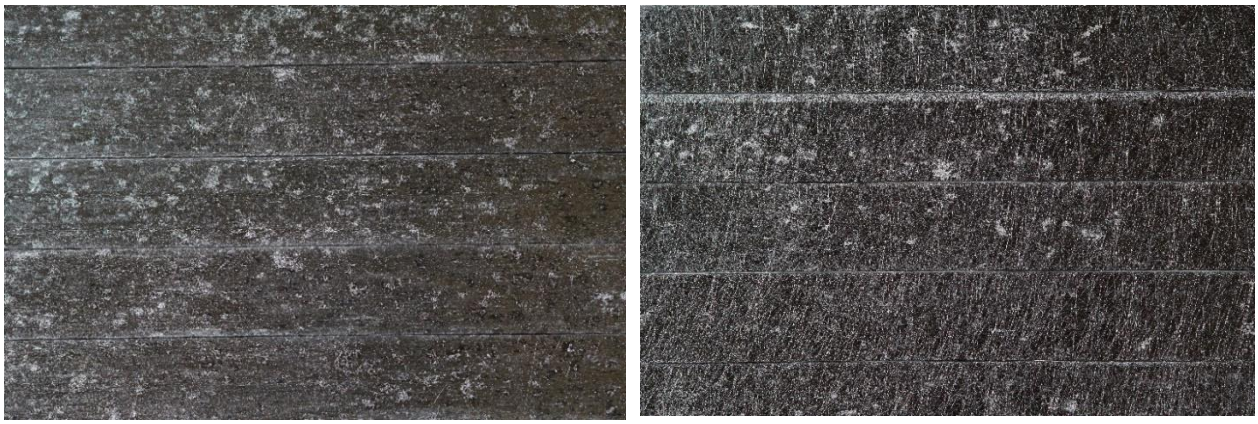

(a) (b)

Figure 3-12 Macro-photographs of processed and peeled dynamic samples (a) binder surfaces (b) veil surfaces

For static samples, Figure 3-11 shows pre-crack regions (on the right) and initial peel regions (on the left) of binder surfaces. Clear boundaries between pre-crack regions and peel regions can be observed. It is also found that veils from opposite tapes remain on the binder surfaces after peel testing. Strong bonding was formed between the powder binder and the veil, and the peeling action leads to cohesive failure of the veil in the interlayer region. Figure 3-13 (b) shows the sketch of peeled samples with cohesive failure and the location of the clear boundaries between pre-crack regions and peel regions.

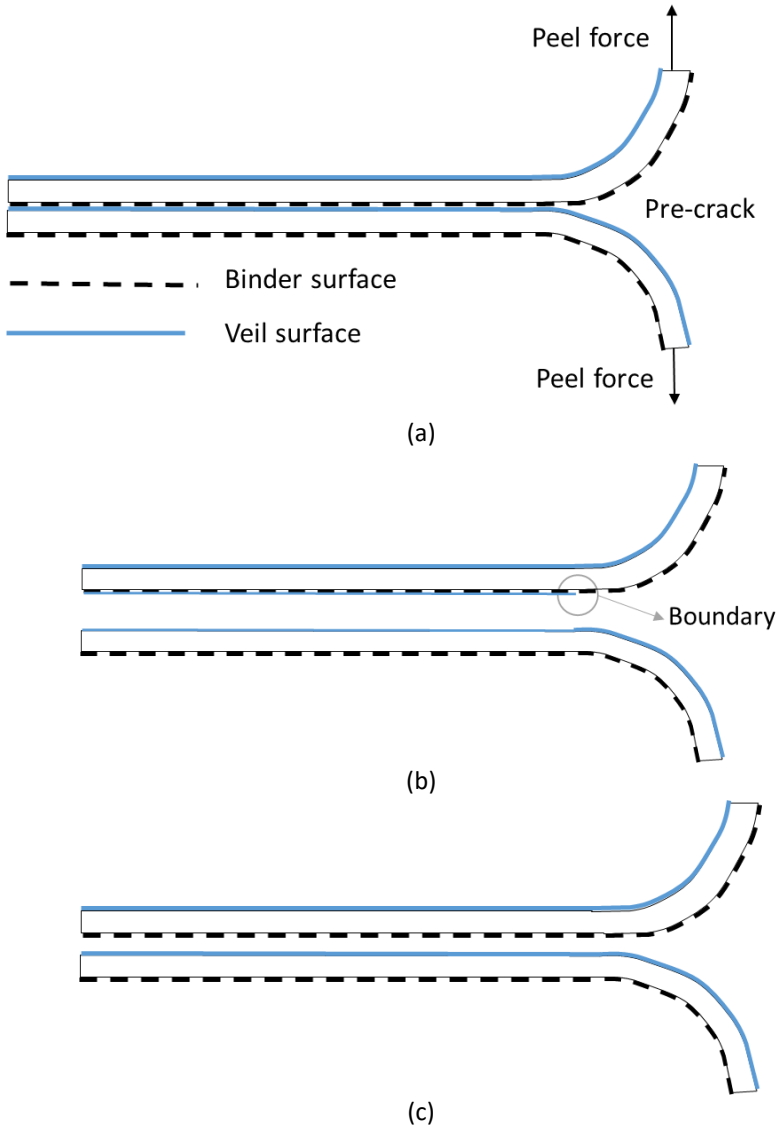

Figure 3-13 Sketch of (a) Bonded tapes under T-peel test (b) peeled tapes with cohesive failure where veils left on binder surfaces (Boundary region is shown in Figure 3-11) (c) peeled tapes with adhesive failure

For peeled dynamic samples as shown in Figure 3-12, only small amount of veils or binder (small white dots) are found left on the opposite tapes compared with unprocessed samples as shown in Figure 3-10. It is concluded that adhesive failures

are dominant for dynamic samples which results in much weaker bonding. Figure 3-13 (c) shows the sketch of peeled samples with adhesive failure.

There are various possible explanations for the observed lower bonding quality of dynamic samples compared to the static samples. In the mock ADFP consolidation, the process is non-isothermal which could lead to lower bonding strength. Joule heating is used and its heating temperatures across the width of the tapes are not uniform. The heating temperature of the edge of the tapes is lower than that of the centre of the tapes as shown in Figure 3-4 (b). The heated tapes make contact with a cooler roller and substrate. The compaction time of tapes might not be long enough for forming good bonding. The tapes are still heated after roller compaction which may degrade the bonding, but this only occurs in the mock ADFP consolidation.

3.3.2 Influence of compaction force on peel resistance

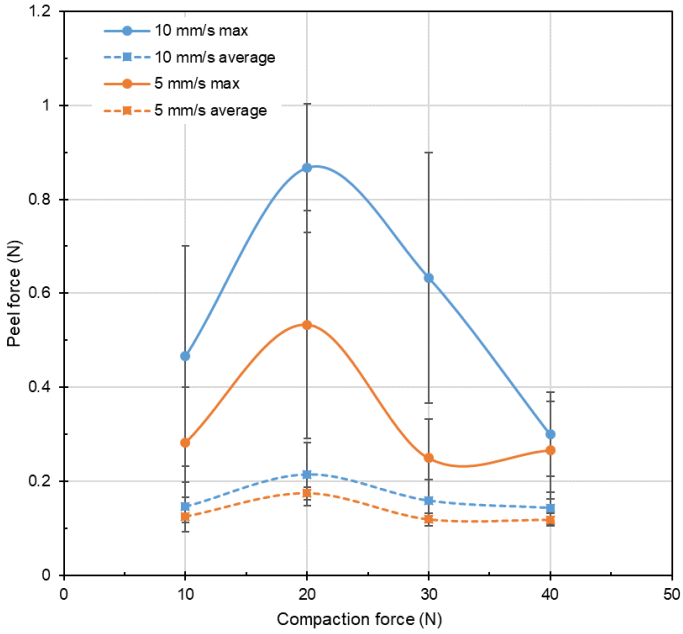

Figure 3-14 Peel tests results of dynamic samples for different compaction forces under 233 °C heating temperature and 5, 10 mm/s deposition velocity

Figure 3-14 shows the influence of compaction force on the peel resistance of dynamic samples. For 10 mm/s deposition velocity, increasing compaction force from 10 N to 20 N leads to an 86% increase of maximum peel force and a 47% increase of average peel force. High compaction force (40 N) results in lower peel resistance than small compaction force (10 N). At 5 mm/s deposition velocity, the findings are same as 10 mm/s deposition velocity but the peel force values are lower. The detrimental influence of high compaction pressure agrees with the findings in the literature [120, 121], where it is shown that high compaction pressure can lead to lower fibre volume fraction of the preforms and it is assumed that this reduction is caused by the high

compaction-induced through-thickness shear stress and through-thickness tensile stress. These stresses result in the breakdown of the binder bond and the subsequent deconsolidation of the preforms [120, 121]. Other published research [62, 143] shows that high compaction pressure also has negative influence on the interlayer peel strength and interlaminar facture toughness of samples manufactured by AFP.

3.3.3 Influence of process temperature on peel resistance

For static samples, the temperature in Figure 3-15 (b) is considered to be 'interlayer temperature' because it is a long term isothermal process. Figure 3-15 (b) shows that peak peel resistance is observed at 200 °C and further increase of interlayer temperature causes slightly decrease of peel resistance. High interlayer temperature (220 °C and 240 °C) could generate better bonding than low interlayer temperature (180 °C).

For dynamic samples, the temperature in Figure 3-15 (a) is the 'heating temperature' which could only represent the surface temperature of the upper tape. During the manufacturing of samples, it was found that under voltage input 11 V (133 °C heating temperature), fragile bonding was formed after manufacturing but the bonding was broken during handling process. To obtain acceptable bonding quality, the heating temperature needs to be increased to a critical temperature, in this mock ADFP conditions, around 150 °C. It was also found that weak bonding could be formed at high temperature (233 °C and 254 °C) without roller compaction.

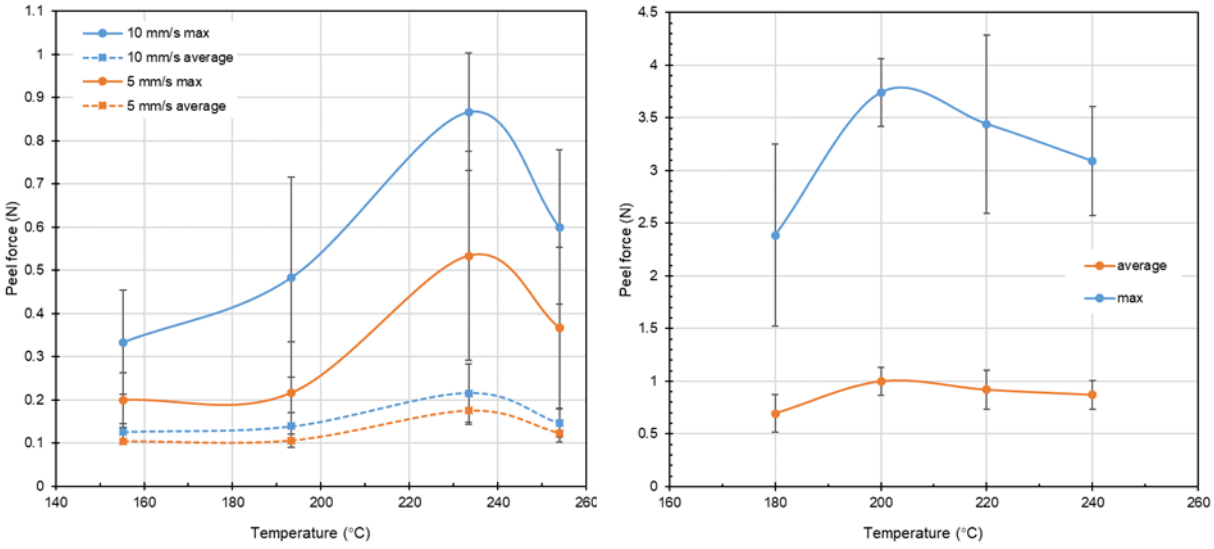

(a) (b)

Figure 3-15 Peel tests results under different process temperatures for (a) dynamic samples with 5, 10 mm/s deposition velocity (b) static samples (different y axis scales for (a) and (b))

Figure 3-15 (a) shows the influence of heating temperature on the peel resistance of dynamic samples. The curve of dynamic samples shows similarity with the curve of static samples. Both curves display peaks in the response and further increase of process temperature decreases peel resistance. High heating temperature (254 °C) leads to higher peel resistance than low heating temperature (155 °C and 193 °C). Higher heating temperature of dynamics samples (233 °C compared with 200 °C interlayer temperature for static samples) is needed to obtain peak peel resistance. Two potential causes for this temperature difference are determined. The heated tapes made contact with cooler underneath tapes under roller compaction therefore the temperature in contact region is lower than the heating temperature. In addition, the heating temperature is characterised in the centre line of tape and the average heating temperature of the whole tape is slightly lower than the characterised heating temperature.

At two deposition velocities 5 mm/s and 10 mm/s, the heating temperature has same influence on the peel resistance but the peel forces values are lower at 5 mm/s.

3.3.4 Influence of deposition speed on peel resistance

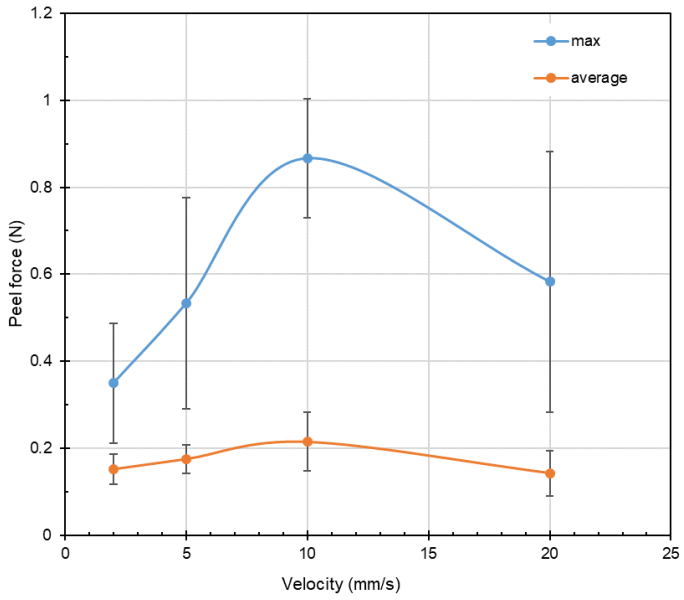

Figure 3-16 Peel tests results of dynamic samples for different deposition velocities under 233 °C heating temperature and 20 N compaction force

Figure 3-16 shows the influence of deposition velocity on the peel resistance of dynamic samples. The peel resistance increases with the increase of deposition velocity from 2 mm/s to 10 mm/s. The peel resistance decreases with further increase of deposition velocity to 20 mm/s. At lower deposition velocity, the tapes have more compaction time which is helpful for forming good bonding but the tapes

also have more heating time after compaction. This long heating time without compaction and the resulting loss of consolidation while the binder is still softened may cause relaxation and lead to poorer bonding quality.

In this mock ADFP consolidation, the deposition velocity influences compaction time, heating time before compaction and heating time after compaction of dry carbon fibre tapes. It is more complex than real ADFP consolidation where deposition velocity only influences the compaction time of dry fibre tapes. The observations found in this mock ADFP consolidation may therefore not agree with the real ADFP consolidation. At two deposition velocities 5 mm/s and 10 mm/s, no coupling effects between deposition velocity and compaction force, between deposition velocity and heating temperature are founded as shown in Figure 3-14 and Figure 3-15 (a). Changing deposition velocity has minimal influence on the shape of curves in the two figures. However, only two velocities are investigated with difference compaction forces and heating temperatures and the differences between the two velocities is small. Therefore, to determine the coupling effects of three process parameters, a full factorial experimental design is recommended to be conducted in the future.

3.4 Conclusions

In this chapter, two sets of dry fibre tape samples are manufactured by oven heating with vacuum pressure and also via joule heating with the ADFP deposition head compaction. The interlayer peel resistance of the manufactured samples are characterised by T-peel tests. The peel tests results are analysed and the following conclusions are obtained:

The interlayer bonding of samples manufactured by the mock ADFP consolidation (dynamic samples) is dramatically weaker that of the samples manufactured by long term isothermal consolidation (static samples). The failure mechanism of static samples is the cohesive failure of veils in the interlayer region while for dynamic samples, the adhesive failure of bonding is dominant. The non-uniform heating, cooler substrate and shorter compaction time of the dynamic samples could lead to weaker interlayer bonding. The interlayer bonding of dynamic samples is also significantly weaker than AFP manufactured prepreg samples. Therefore, process parameters for ADFP need to be choose more carefully.

The process temperature has a great influence on the interlayer bonding quality. The carbon fibre tapes need to be heated to a critical temperature to activate the binder

in order to provide sufficient interlayer bonding. For both static samples and dynamic samples, when increasing process temperature above the critical temperature, the peel resistance is increased significantly (around 71% for dynamic samples) before decreasing slightly with further increases of process temperature. Compared with static samples, dynamic samples require higher process temperature to obtain peak peel resistance because of the cooler substrate.

The compaction force/pressure also has a great influence on the interlayer bonding quality. Sufficient compaction level is required to obtain good interlayer bonding. However, excessive compaction forces could decrease the interlayer peel resistance up to 57%. The negative influence of excessive compaction forces agree with the research on the fibre volume fraction of ADFP manufactured preforms [120, 121], interlayer bonding of thermoplastic composites manufactured by AFP [143] and tensile properties of thermoset composites manufactured by robotic lay-up of towpregs [144].

The effect of deposition velocity is less conclusive; maximum interlayer peel resistance is obtained at 10 mm/s but lower deposition velocities could not generate better interlayer bonding in the mock ADFP conditions. The observed influence of deposition velocity here may not fully represent real ADFP conditions. Further research is recommended to be conducted using a fully developed ADFP deposition head to investigate the influence of deposition velocity in the future.

Research as reviewed in section 2.1.1 shows that the tool/tape tack or bonding is significantly lower than the interlayer tack or bonding in AFP. It is assumed that this lower bonding quality between tool surface and dry carbon fibre tapes can also be found in ADFP and it could bring more difficulties when depositing the first layer of dry fibre tape. Precise control of process parameters for depositing first layer on tool surfaces is therefore more crucial. However, the dry carbon fibre tapes/tool surfaces bonding quality needs further investigation in the future.

The binder bond formation mechanism are complex. Binder melting, flow or curing and binder solidification could occur during the formation of the bond and these processes are influenced by temperature, pressure, process time and their coupling effects [107, 110]. To fully capture the science behand it, the temperature dependent viscosity of binder, the wettability of binder on dry fibres, the cure kinematics of binder and etc. need to be characterised and a multi-physics binder flow model needs to be established. These are out of scope of this thesis. The experimental results in

this chapter show the importance of proper choice and precise control of process parameters. Fragile bonding or even no bonding will be formed if process parameters are out of control. To implement precise control of process parameters, understanding the compaction and heat transfer behaviour of dry fibre tapes under ADFP consolidation are required and these are investigated in the following two chapters.

4 Compaction behaviour of carbon fibres processed by ADFP

4.1 Introduction

In the ADFP process, dry fibre tapes are compressed on the tool or the substrate layers by a compaction roller mounted on a robotic arm or gantry system. The compaction force applied to the roller influences the quality of manufactured preforms, such as fibre volume fraction [121] and peel resistance as evidenced by the results in section 3.3.1. The roller transfers the compaction force applied by the machine to the compaction pressure on the plies. The compaction pressure is the real factor determining the preform quality. A high level of uniformity of compaction pressure is required in the ADFP process to achieve optimal quality. The compaction pressure distribution depends on compaction roller geometry and materials, compaction behaviour of dry carbon fibres, and tool geometry. In state-of-art ADFP deposition hardware, only compaction force instead of compaction pressure can be monitored and controlled. The required compaction force targets for the hardware controller need to be determined based on the compaction pressure requirement. The force targets are not straightforward because the contact areas are difference for different roller and the compaction pressure is not uniform especially for complex tools. In this chapter, a roller compaction on dry carbon fibres model is developed to bridge the gap between the compaction force and compaction pressure distribution.

The compaction mechanism of the dry fibres is complicated and includes elasticity, plasticity, relaxation, viscoelasticity and cyclic effects [119]. In the ADFP process, the compaction time is short (the compaction time is 0.4 s when the contact length is 30 mm and the deposition velocity is 0.1 m/s) therefore the relaxation and viscoelasticity of dry fibres are not investigated. In this chapter, the elastic and cyclic compaction behaviour of dry carbon fibre materials are characterised experimentally. A power-law based material model is used to describe the through-thickness elastic properties of dry carbon fibre materials. The roller materials are also characterised experimentally. A finite element (FE) model is then developed to analyse the roller-applied pressure on the fibrous reinforcement bed. The model has been validated by using a pressure sensitive film. The influence of roller material, tool curvature and substrate thickness on the pressure distribution are investigated. To obtain the compaction force targets for the hardware controller, a target pressure requirement is chosen. The compaction pressure distribution simulation results under different compaction force are analysed and force target bounds for tools with different curvature are determined.

4.2 Compaction behaviour of dry carbon fibres

In this section, the compaction behaviour of dry carbon fibre reinforcement materials is characterised and a compaction material model is then explained.

4.2.1 Compaction experiments

4.2.1.1 Materials and experimental setup

24K TX1100 (Solvay) bindered carbon fibre tapes and normal 24K carbon fibre tows with a measured width of 6.92 mm, an areal weight of 237 g/m^2 were also used. The tapes and tows were cut into lengths of 60 mm. One piece of tape or tow was tested under compaction at a time. Testing was conducted on an Instron 5969 universal machine with a 50 KN load cell and two parallel circular platens as shown in Figure 4-1. Two Linear Variable Differential Transformers (LVDT) (MICRO-EPSILON D6/02500ARA-L10) were used to measure the instantaneous thickness of the tape and the average value of the two sensors was used to calculate the fibre volume fraction of the tape using equation (4.1). The initial fibre volume fraction of the tape was calculated using measured thickness of the tape when the load was 5 N before starting to increase. The peak compaction force was 500 N and the loading rate was 0.3 mm/min. The load 5 N for initial fibre volume fraction calculation is very small compared to the load cell capacity 50 KN and the force reading could have 5 % error. The force error could lead to initial fibre volume fraction error up to 0.4 % (calculated from measured thickness value at force range of 5 N ±5%). A single compaction test and a 15-cycle cyclic compaction test were conducted. The compaction loading curves were recorded. From the compaction loading curves, the compaction pressure and tape material properties at loading stage can be obtained. While the viscoelastic and relaxation behaviour of the tape cannot be investigated.

$$V_f = \frac{A_F}{\rho_f t} \tag{4.1}$$

Where A_F is the areal weight of the carbon fibre tapes. ρ_f is the fibre density. t is the thickness of the tape.

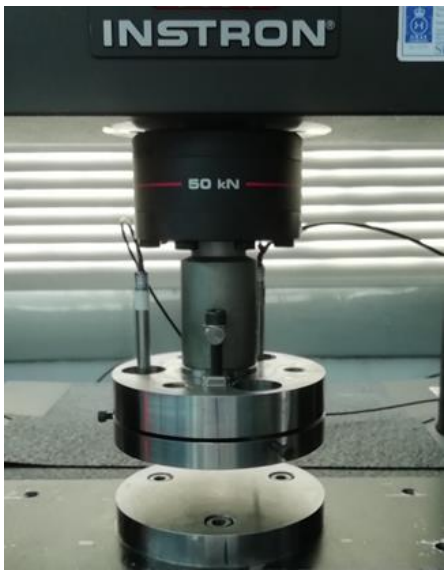

Figure 4-1 Dry fibre tapes and tows compaction testing experimental apparatus

4.2.1.2 Compaction experimental results

Figure 4-2 (a) shows the compaction curves of the normal 24 K carbon fibre tow and the TX1100 tape. The two curves exhibit same power-law shape, which describes the compaction behaviour for most dry carbon fibre reinforcement materials [119]. However, to achieve same fibre volume fraction, less compaction pressure is needed for the TX1100 tapes. Figure 4-2 (b) shows the thickness change under different compaction pressure. The TX1100 tape shows less thickness change and stiffer compaction response than the normal 24 K carbon fibre tow. Compared to the compaction results of commercial prepreg materials in literature [122], the TX1100 tapes show a 136 % greater reduction of thickness under same compaction pressure in the room temperature. This large deformation can bring difficulties for ADFP force control. In the cyclic compaction testing, TX1100 tapes show a more stable response than 24 K tows, as shown in Figure 4-3. Their thickness shows a minimal change after five compaction cycles, while for 24 K carbon fibre tows, after ten compaction cycles, obvious cycle-to-cycle thickness change is still evident. Figure 4-4 shows the cyclic compaction curves of two materials. The TX1100 tapes show relatively consistent compaction response after a few compaction cycles. For 24 K tow, the compaction response shows noticeable increased stiffness under each compaction cycle. The stable compaction response of the TX1100 tapes under cyclic compaction testing may require fewer debulk cycles after deposition. The two materials have different format, which leads to the different compaction response. The TX1100 tapes are highly engineered and they have veils on one side and powder binder particles on the other side. They were also consolidated during their manufacturing process. These contribute to a more stable response. The 24 K carbon fibre tows only have a small amount of sizing without pre-consolidation.

In the ADFP process, when using different dry carbon fibre materials, the compaction pressure setting and control should be adjusted because dry fibre materials with different format shows large differences in compaction response. The dry carbon reinforcement bed is compacted multiple times and the cyclic effects should be considered when choosing compaction pressure requirement for different layers. This cyclic effect is less concerned for highly engineered commercial tapes because they have more stable response.

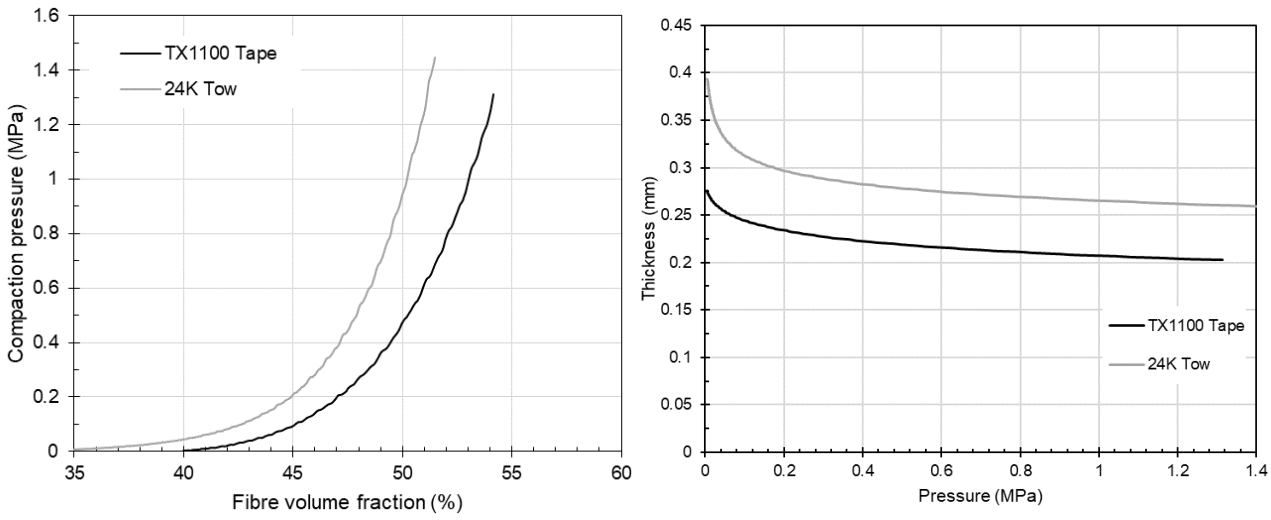

(a) (b)

Figure 4-2 Compaction results of two carbon fibre materials (a) fibre volume fraction (b) thickness

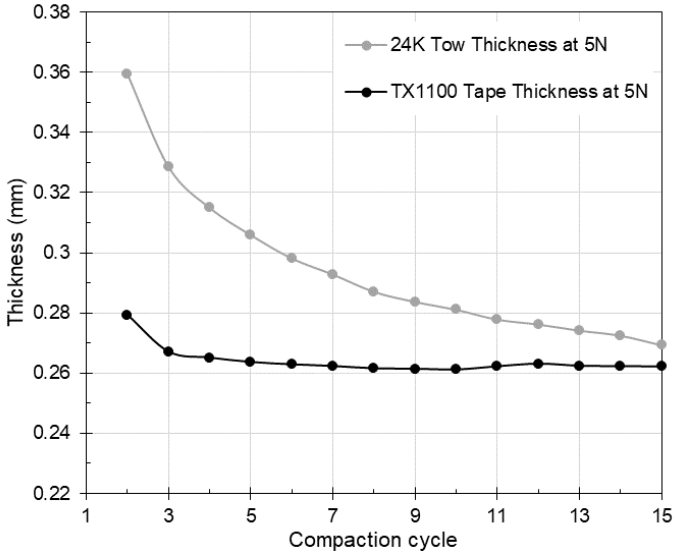

Figure 4-3 Thickness of two carbon fibre materials at the beginning of each compaction cycle

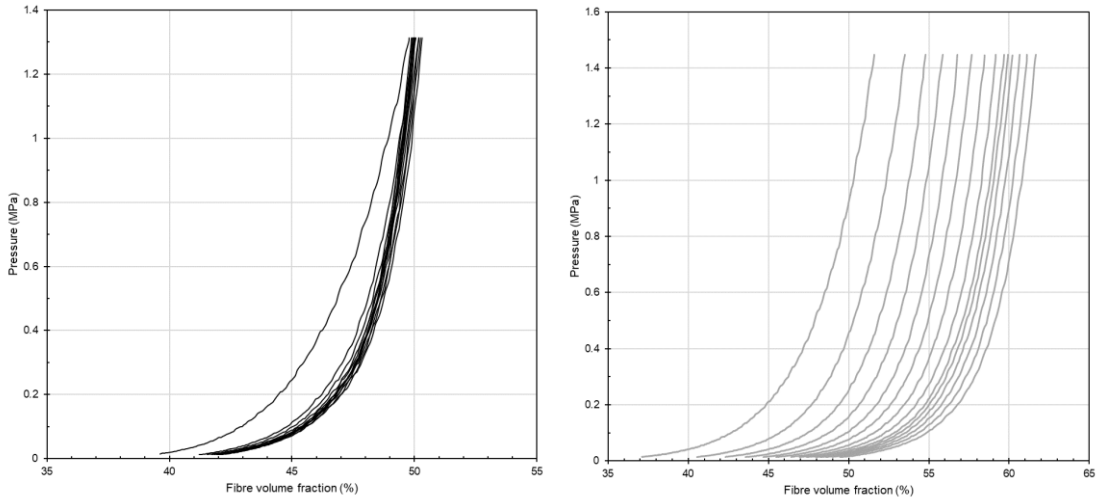

(a) (b)

Figure 4-4 Cyclic compaction curves for two materials (a) TX1100 tape (b) 24K tow

4.2.2 Compaction material model

4.2.2.1 Power law empirical model

Power law equation is a commonly used empirical model to describe the elastic compaction behaviour of dry fibre materials [119]. Figure 4-5 shows the experimental compaction curve of the TX1100 carbon fibre tapes and the power law fitted curve. The power law is also applicable for TX1100 tapes and it shows good agreement with the experimental curve when the compaction pressure is higher than 0.1 MPa. A power-law equation $P = 4975\ {V_f}^{13.42}$ is the best fit for the experimental curve. This was obtained by using a nonlinear least squares method provided by the Matlab curve fitting toolbox. This results in an R squared value of 0.998.

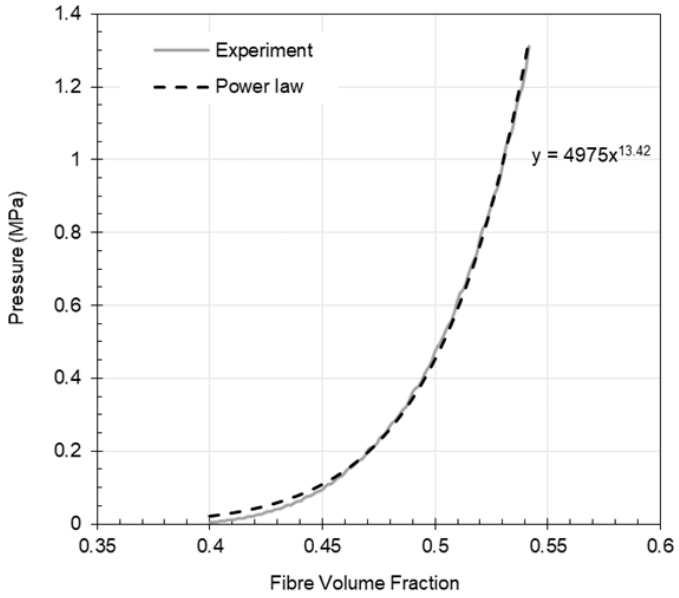

Figure 4-5 Compaction curve of TX1100 tapes from experimental results with power law fitted curve

4.2.2.2 Power law based material model for compaction behaviour

The power law model shows the relationship between compaction pressure and fibre volume fraction of carbon fibre tapes. The method developed by Sherburn [145] is modified to obtain the elastic stress-strain relationship of dry fibre tapes in the through-thickness direction using the power law fitted equation. In the through-thickness direction, the stretch ratio λ can be expressed as:

$$\lambda = \frac{t}{t_0} \tag{4.2}$$

Where t is the thickness of deformed carbon fibre tapes and t_0 is the initial thickness of undeformed carbon fibre tapes. The logarithmic strain ε is then expressed as:

$$\varepsilon = ln\ (\frac{t}{t_0}) \tag{4.3}$$

$$exp(\varepsilon) = \frac{t}{t_0} \tag{4.4}$$

Substituting equation (4.1) to equation (4.4), the fibre volume fraction V_f during compaction is calculated by:

$$V_f = \frac{V_{f_0}}{exp\ (\varepsilon)} \tag{4.5}$$

Where V_{f_0} is the initial fibre volume fraction of the dry fibre tapes before compaction. The relationship between the compaction pressure P and the fibre volume fraction V_f is fitted using a power law with two parameters a and b according to the following equation:

$$P = a\, V_f{}^b \tag{4.6}$$

The through-thickness stress σ has the same value as the compaction pressure P but with a minus sign:

$$\sigma = -P \tag{4.7}$$

Substituting equation (4.5) and (4.6) to (4.7), the stress-strain relationship in the through-thickness direction is obtained:

$$\sigma = -a \left(\frac{V_{f_0}}{exp(\varepsilon)}\right)^b \tag{4.8}$$

4.3 Roller compaction on dry fibres

In section 4.2, the compaction behaviour of dry fibre materials is investigated. In ADFP process, the dry fibre reinforcement bed is compacted by a compaction roller. In this section, compaction rollers are characterised and roller compaction on dry fibre reinforcement bed is investigated experimentally. A roller compaction on dry fibre model is then established and the roller compaction pressure distribution is investigated using model results.

4.3.1 Roller compaction on dry fibres experiments

4.3.1.1 Roller materials, manufacturing and characterisation

The roller is made from four parts: a rubber cover, a sleeve, a shaft and two bearings as shown in Figure 4-6. Three materials: silicone rubber (Polycraft FS30) with a shore A hardness of 28, silicone rubber (Easycomposites AS40) with a shore A hardness of 40, and polyurethane rubber with a shore hardness of 95 (DuroFlex 95) were used to manufacture the roller cover. The hardness level is comparable with the hardness level of rollers used in commercial AFP machines [28, 121]. Steel was used to manufacture the sleeve and the shaft. For the two silicone rubber covers, the silicone rubber and the cure catalyst were mixed thoroughly with the weight ratio of 10:1 and the mixture was then degassed with a vacuum chamber. The degassed mixture was filled into the roller mould containing the sleeve. They were transferred to an oven

with a temperature of 50 °C. The silicone rubber was then cured in the oven in an hour. The rubber cover with the co-moulded sleeve was then demoulded. For the polyurethane rubber cover, the polyurethane part A and part B were mixed thoroughly with the weight ratio of 1:1 and the manufacture proceeded as above. The diameter of the rollers is 70 mm and their width is 28 mm. The diameter of the sleeve is 35 mm. The dimension of three rollers is same as the dimension of the roller used in a lab-scale ADFP rig [146] to lay down four tows each course. The diameter of the rollers is same with the diameter of rollers in commercial AFP machines [28, 121].

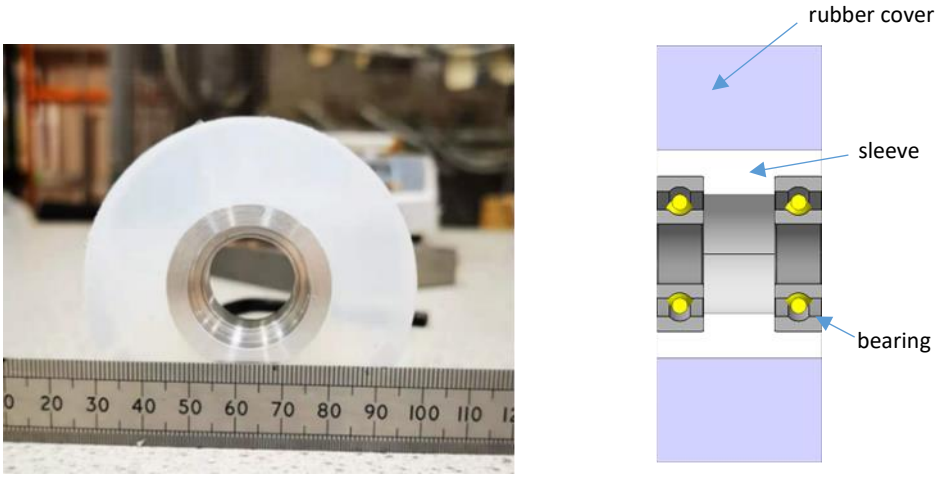

Figure 4-6 Compaction roller (a) Manufactured roller (b) Cross-section view of roller in CAD

4.3.1.2 Testing description

The properties of rollers were characterised by conducting compression testing of rollers. The rollers were installed on an Instron 5966 universal machine with a fixture as shown in Figure 4-7. The rollers were compacted on a flat rigid surface with the compaction force of 700 N and a load rate of 2 mm/min. The roller was rotated 90° after one test and four repeats were conducted in total to check the influence of the material uniformity of the roller. The load-displacement curves of the rollers were obtained.

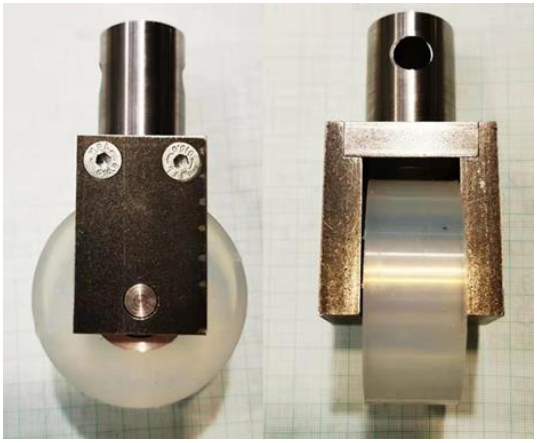

Figure 4-7 Compaction roller with fixture for roller compaction testing

The roller compaction on fibre test were conducted after the roller characterisation test. Static roller compaction testing on a fibre bed was conducted in this research. In the real ADFP process, the roller is rotating dynamically but at the velocities of interest the roller rotation has a negligible influence on the value of compaction pressure [67]. For analysis of compaction pressure, static testing can therefore generate valuable results. Five TX1100 tows with a length of 100 mm were placed on a steel flat tool with no gaps between them. The binder surfaces were adjacent to the tool surface. The width of the roller is slightly larger than the width of one course which contains four tows. When depositing the current course, the extra width of the roller compacts the previous course. Thus, five tows in total are compacted during the deposition. Pressure sensitive films were placed on top of the five tows. The roller was compacted on the centre of the tapes covered with the pressure sensitive films by an Instron 5966 universal machine. The experimental setup is shown in Figure 4-8. Three load levels were tested on the three rollers as shown in Table 4-1. The load rate was set to achieve the load level in around 5 s and the load was then held in 2 minutes according to the pressure sensitive film manual. The pressure distribution was then measured by the pressure sensitive films.

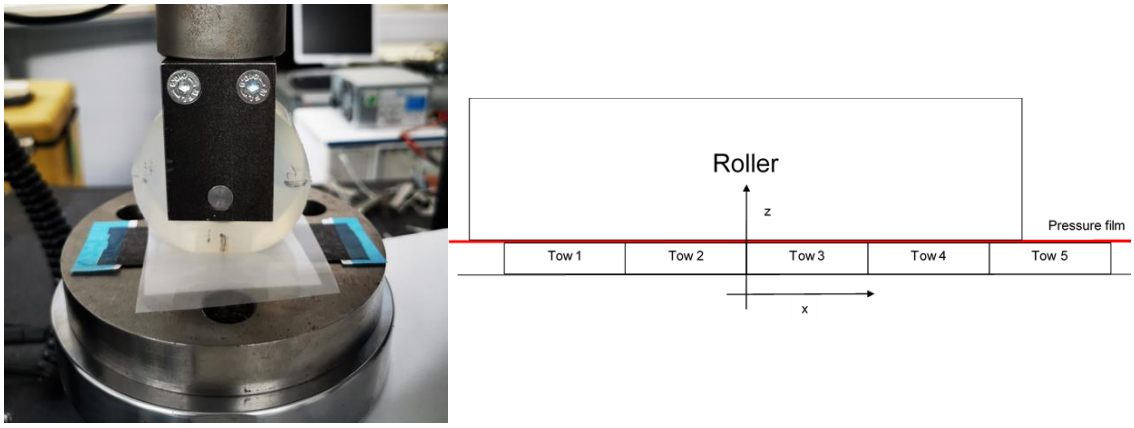

(a) (b)

Figure 4-8 Experimental setup for compaction on fibres test (a) machine setup (b) illustration of the relative location of the roller and fibre tows (x direction is along the width of tapes. z direction is along the thickness of tapes.)

Table 4-1 Forces used to determine compaction behaviour

Roller Hardness (HA)	Load level 1 (N)	Load level 2 (N)	Load level 3 (N)
28	100	250	400
40	70	200	380
95	20	30	50

4.3.1.3 Pressure measurement method

Fujifilm LLLW pressure sensitive films with measurement range from 0.2 MPa to 0.6 MPa were used to measure the compaction pressure. The films show different colour density of red colour after being compressed. The procedure developed by He *et al*. and Jiang *et al*. [72, 73] was used to obtain the pressure values from the pressure film. The manufacturer manual which has all sample red colours rectangular pattern and their colour density ρ is scanned by a flatbed scanner. The average grayscale a of each sample colour rectangular pattern is calculated by Matlab. The relationship between the sample colour density ρ and their average grayscale a is then fitted as $\rho = f(a)$. The relationship between the sample colour density ρ and the pressure value P is provided as a curve by the manufacturer and can be fitted as $P = g(\rho)$. The relationship between the average grayscale a and the pressure value is then obtained as $P = g\big(f(a)\big) = F(a)$. The pressure sensitive films were scanned alongside a paper scale in a flatbed scanner. The grayscale of each pixel in the scanned picture is calculated by Matlab and then the pressure distribution is calculated by using the relationship $P = F(a)$. Figure 4-9 shows the compacted pressure sensitive films and the pressure results. It is shown that the pressure values are scattered instead of continuous due to the inhomogeneous red dots in the pressure sensitive films. To reduce this inhomogeneity, the average greyscale value of 0.5 mm by 0.5 mm area instead of the greyscale of each pixel is used to calculate the pressure value for the whole area, since the relationship $P = F(a)$ is obtained using average grayscale values of sample colours. The use of 0.5 mm by 0.5 mm reduces the inhomogeneity without losing many resolutions. Values below 0.2 MPa are deleted and the values above 0.6 MPa are set to 0.6 MPa due to the measurement range of the film. Figure 4-10 shows the comparison of pressure values along the centreline of the tow in y direction (the dash line in Figure 4-9) obtained by raw data and averaged data. The experimental pressure values in following sections are obtained using the averaging method described above.

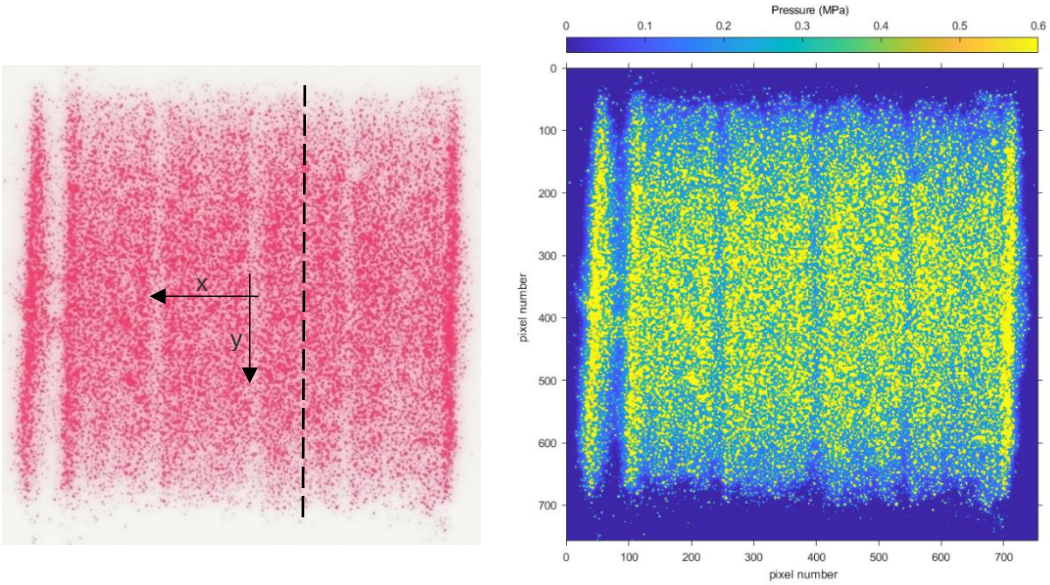

(a) (b)

Figure 4-9 Pressure film and pressure results (a) scanning picture of pressure sensitive film (x direction is along the width of tapes and y direction is along the length of tapes) (b) calculated pressure values from Matlab

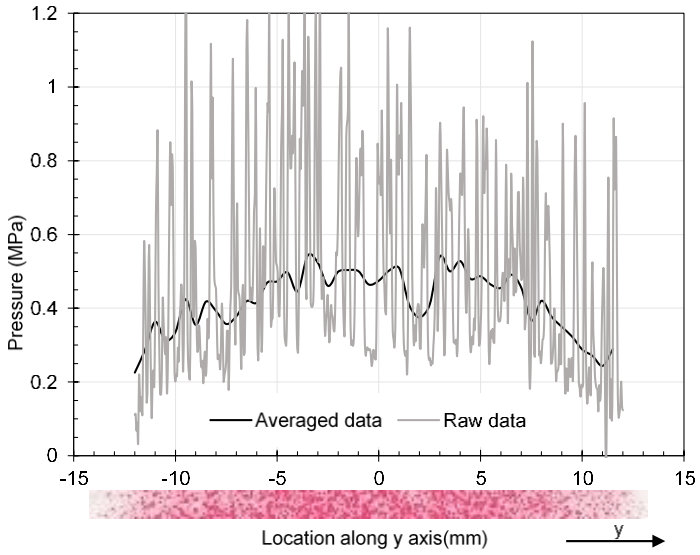

Figure 4-10 Averaged pressure results along tow centreline in y direction (the dash line along the length direction of tapes in Figure 4-9 (a)) calculated using average grey scale of 0.5 mm by 0.5 mm area)

4.3.1.4 Experimental Results

Figure 4-11 shows the load-displacement curves of the rollers from the experiments and the FE model (shown in section 4.3.2) with fitted linear elastic material properties. It is found that the hardest 95 HA roller had a very low displacement in the compaction direction compared to the softer rollers under the same compaction force. This low displacement makes precise force control difficult, particularly when the positional accuracy of deposition head is limited. Table 4-2 shows the compaction pressure distribution of the three rollers with the three load levels from Table 4-1.

Peak pressure (a pressure spike) is observed at the area around the roller edges. Pressure drops are found between adjacent tows although the tows were butted together without visible gaps. It is found that for the same load level, the hardest 95 HA roller generates the smallest contact area with a highly non-uniform pressure, which is not desirable for the requirements of the manufacturing process. Thus, 95 HA roller is not analysed in later sections.

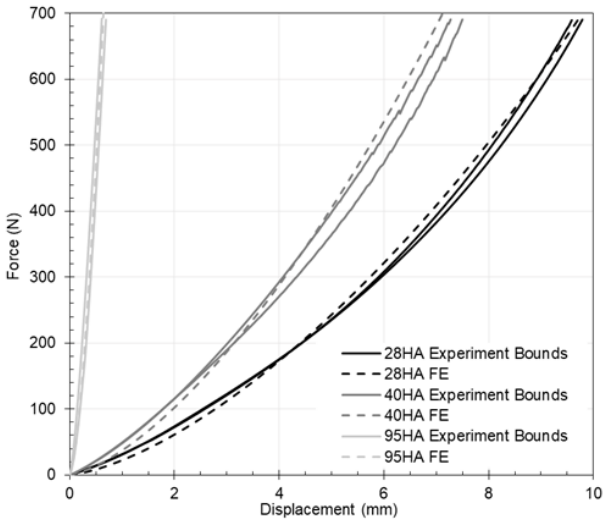

Figure 4-11 Load displacement curves of three rollers from experimental and FE results (experimental curves show upper and lower bounds based on four repeats)

Table 4-2 Compaction pressure distribution results from pressure sensitive films under three different load level for three rollers

Roller Hardness	Load Level 1	Load Level 2	Load Level 3
28	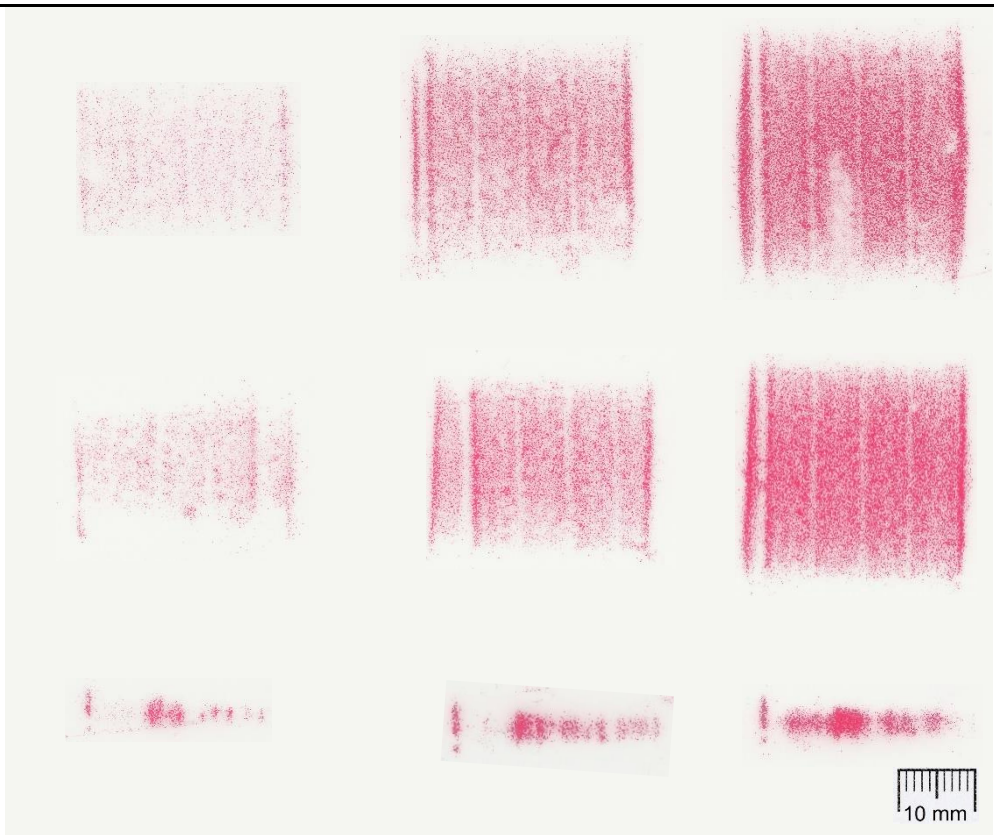		
40			
95			

4.3.2 FE model of roller compaction on dry carbon fibres

4.3.2.1 FE model description

A finite element model of roller compaction on dry carbon fibres is established using ABAQUS/CAE. The model consists of four parts: a sleeve, a tool, a rubber cover and dry carbon fibre tapes. Because of the symmetry of the structure and the load, half of the structure and the load are used during the FE analysis as shown in Figure 4-12, and symmetric boundary conditions are used. The sleeve with a diameter of 35 mm is modelled as a rigid body and the compaction force is applied to its reference point. The tool is constrained as a fixed rigid body. The dimension of the half tool is 45 mm × 40 mm. The interactions between the rubber cover and the sleeve, between the dry fibre tapes and the tool are modelled as tie constraints. The contact between the rubber cover and the dry fibre tapes and the contact between the rubber cover and the tool are modelled as hard contact conditions. The degrees of freedom of displacement of the rubber cover except in the through-thickness direction are constrained to zero and the 8-node linear brick C3D8 element is chosen for the rubber cover. For the dry fibre tapes, five tows are modelled as one part with the dimensions 40 mm × 31.75 mm × 0.275 mm and again the C3D8 element is chosen. The relative location of the roller and fibre tows is the same as the experimental setup shown in Figure 4-8 (b). After a mesh size dependency analysis, the mesh size for the top and bottom half rubber cover is chosen to be 2 mm and 0.75 mm respectively. The mesh size for the dry fibre tapes is chosen to be 0.18 mm. A modified transversely isotropic elastic material model with a nonlinear response in the through-thickness direction based upon the method developed by Lin and Sherburn [125, 145] is used for the dry fibre tapes, the details are given in the section 4.3.2.3.

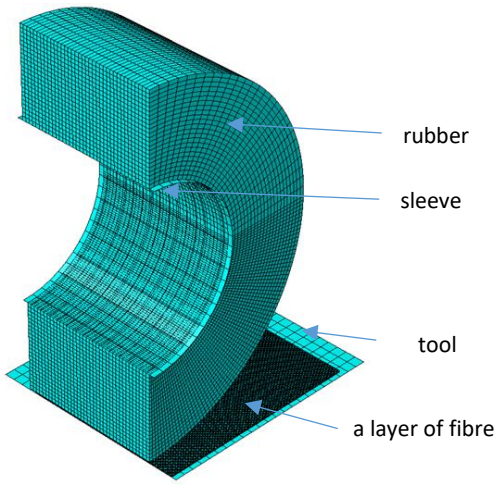

Figure 4-12 FE model setup for roller compaction on a layer of dry carbon fibre

4.3.2.2 Material model and properties for roller

For the silicone rubber, a linear elastic isotropic material model is chosen. The material property parameters are obtained by fitting the load-displacement curve from the roller characterisation testing as shown in Figure 4-11. It is shown that the linear elastic model used for the rubber cover can provide good agreement with the experimental data. The material properties used for the three rollers are shown in Table 4-3.

Table 4-3 Input values for material model of three rollers

Roller Hardness (HA)	Modulus (MPa)	Poisson's Ratio
28	0.165	0.475
40	0.275	0.475
95	12.5	0.475

4.3.2.3 Material model and properties for carbon fibres

The compaction mechanism of the dry fibres is complicated and includes elasticity, plasticity, relaxation, viscoelasticity and cyclic effects [119]. This model focuses on the quasi-static compaction pressure distribution when the dry fibre tapes are compacted by the roller and only the elasticity is currently considered in this model. In the longitudinal fibre direction, the modulus is modelled as a linear function of the fibre volume fraction V_f of the dry fibre tapes [125]. In the compaction testing conducted by the authors and in literature [132], the length of the dry fibre tow shows no change after the compaction. Thus, the values of the Poisson's ratio ν_{12}, ν_{13}, ν_{31} and ν_{21} are assumed to be zero. The stress in the longitudinal direction is then described by the following equation:

$$\sigma_1 = E_0 V_f \varepsilon_1 \tag{4.9}$$

Where E_0 is the modulus of the carbon fibre. V_f is the fibre volume fraction of the dry fibre tapes.

In the through-thickness direction, the response is nonlinear. Equation (4.8) is used to calculate the through-thickness stress σ_3.

$$\sigma_3 = -a \left(\frac{V_{f_0}}{exp(\varepsilon_3)}\right)^b \tag{4.10}$$

In compaction testing, the Poisson's ratio ν_{23} shows a nonlinear relationship with the through-thickness strain ε_3 and its value is typically lower than 0.1 [132, 147]. For simplicity, its value is assumed to be zero in this model. The through-thickness stress σ_3 is then the function of only ε_3 as shown in equation (4.10). The transverse isotropic model is used, and the in-plane transverse direction shows the same

response as the through-thickness direction. The stress σ_2 is defined according to the following equation:

$$\sigma_2 = -a\left(\frac{V_{f_0}}{exp(\varepsilon_2)}\right)^b \quad (4.11)$$

For the shear stresses, the shear moduli G_{12}, G_{13}, G_{23} are described by linear elastic material models. The material property inputs are shown in the Table 4-4. E_0 is obtained from the fibre manufacturer datasheet. G_{12} and G_{13} are obtained from literature [125]. Data for G_{23} is limited but it has minimal influence on the compaction response. Thus G_{23} assumed to be a small value of 2 MPa. V_{f_0}, a, b are generated from the experiments described in section 4.2.1.2. This dry fibre material model is implemented using the subroutine UMAT in Abaqus.

Table 4-4 Input values for material model of TX1100 dry carbon fibre tape

Input	Symbol	Value
Power law parameter	a	4975
Power law parameter	b	13.42
Initial Fibre volume fraction	V_{f_0}	0.3997
Modulus of fibre	E_0	290 GPa
Poisson's Ratio	ν_{12}, ν_{13}, ν_{23}	0
In-plane shear modulus	G_{12}, G_{13}	5 MPa
Transverse shear Modulus	G_{23}	2 MPa

4.3.2.4 Experimental validation of FE model

Figure 4-13 shows the compaction pressure distribution along the tow centre line in y direction from the pressure sensitive film measurement compared to the FE model results. Pressure from load level 1 is smaller than the measurement range of pressure film, therefore pressure distribution from load level 2 and load 3 are compared with the FE results. It is shown that the experimental curves have significant fluctuations due to the inherent variability of the pressure sensitive film, and the FE result curves have good agreement with experimental curves although the pressure values show low level differences. The ±10% measurement error of the pressure sensitive film, the pressure calibration method and the averaging method all contribute to the pressure fluctuations and differences observed.

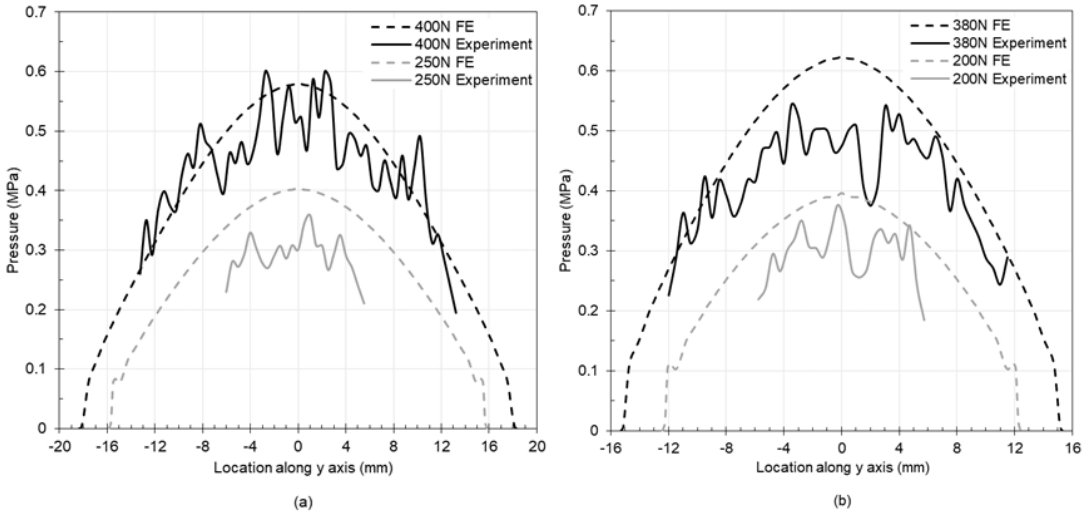

Figure 4-13 Compaction pressure distribution along tow centreline in y axis from experimental and FE results (a) 28 HA Roller (b) 40 HA Roller (y direction is along the length of tapes.)

4.3.2.5 Parameter analysis

A flat tool and tools with radius of curvature of 20 mm, 30 mm, 50 mm, 100 mm, 200 mm and 500 mm are chosen to investigate the influence of tool geometry on the pressure distribution uniformity which is calculated by equation (4.12). The tool and dry fibres have a single curvature and the direction of the curvature is shown in Figure 4-14. The relative location of roller and dry fibre tows is shown in Figure 4-8 (b). The boundary between tow 2 and tow 3 is positioned at the highest point of the tool. Three sets of material properties for the rubber cover materials are used to investigate the influence of the roller material. These are chosen to fit the load-displacement curves obtained from the experiments described above. Investigation of thick dry fibre substrates is also conducted. The thickness of dry fibre substrates are chosen as 0.275 mm (1 layer), 2 mm, 5 mm and 10 mm. The model is slightly simplified for the thick dry fibre substrate cases to speed up the simulation. The width of the dry fibre substrate in the x direction is set as the same width as the width of the roller. Coarser mesh sizes are chosen for thick substrates. Mesh sizes of 0.4 mm, 0.5 mm and 0.7 mm are used for dry fibre substrates with the thickness of 2 mm, 5 mm and 10 mm respectively.

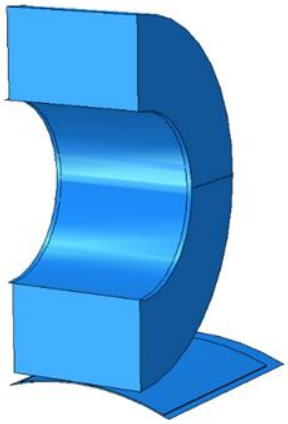

Figure 4-14 FE Model setup of roller compaction on dry carbon fibre with single curvature tools

Compaction pressure uniformity calculation

$$u = 1 - \sqrt{\frac{1}{n}\sum_{i=1}^{n}\left(\frac{p_i - \overline{p}}{\overline{p}}\right)^2} \quad (4.12)$$

Where n is the number of nodes. p_i is the contact pressure value at the node i . $\overline{p}$ is the average contact pressure value of all nodes.

Influence of roller material on roller deformation and contact area

Table 4-5 Simulation results of the roller deformation and the contact area of three rollers under a compaction force of 400 N

Roller	Roller Deformation	Contact Area
28 HA	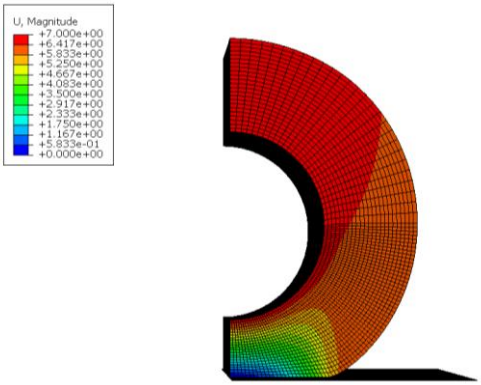	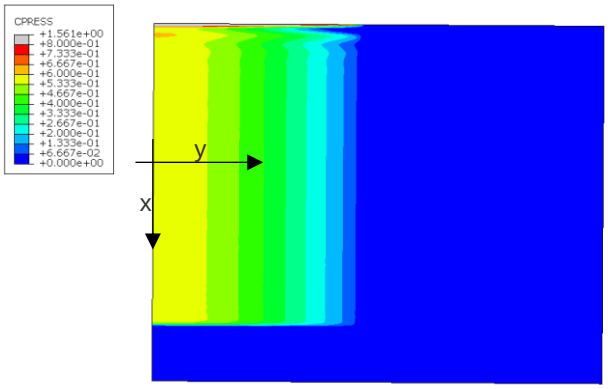 26.7 mm × 18.5 mm
40 HA	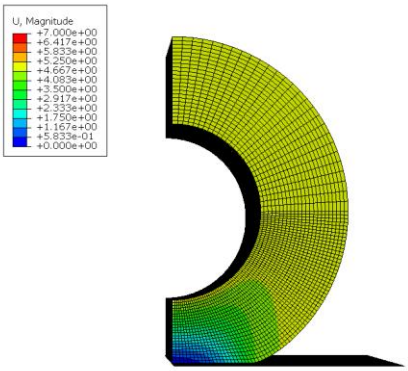	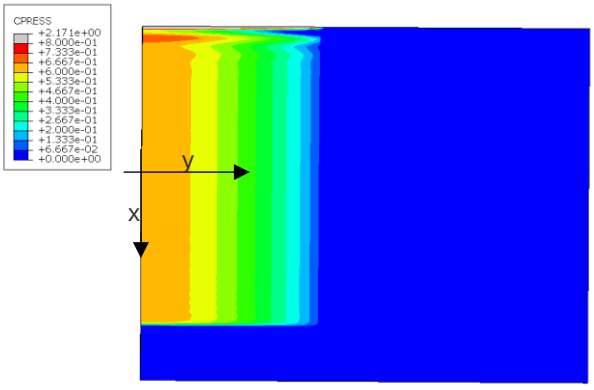 26.7 mm × 16.1 mm
95 HA	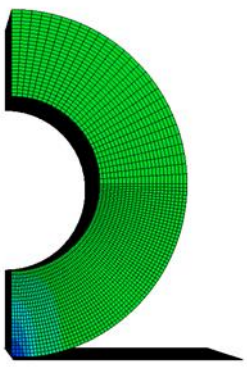	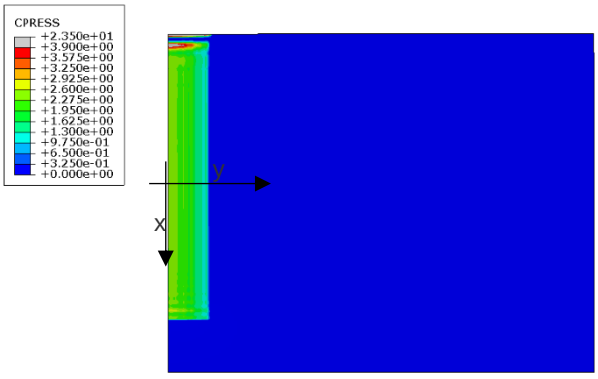 26.7 mm × 4.1 mm

Table 4-5 shows the roller deformation and the contact area of 28 HA, 40 HA and 95 HA rollers under a compaction force of 400 N. It is found that under same compaction force, the 95 HA roller exhibits lowest deformation and smallest contact area compared with the 28 HA and 40 HA rollers hence the compaction pressure from 95 HA roller is the highest among three rollers. Figure 4-15 shows the average compaction pressure (nominal compaction pressure) calculated by the compaction divided by the contact area for three rollers. The nominal pressure generated by 95 HA roller is around three times higher than that generated by the other two rollers.

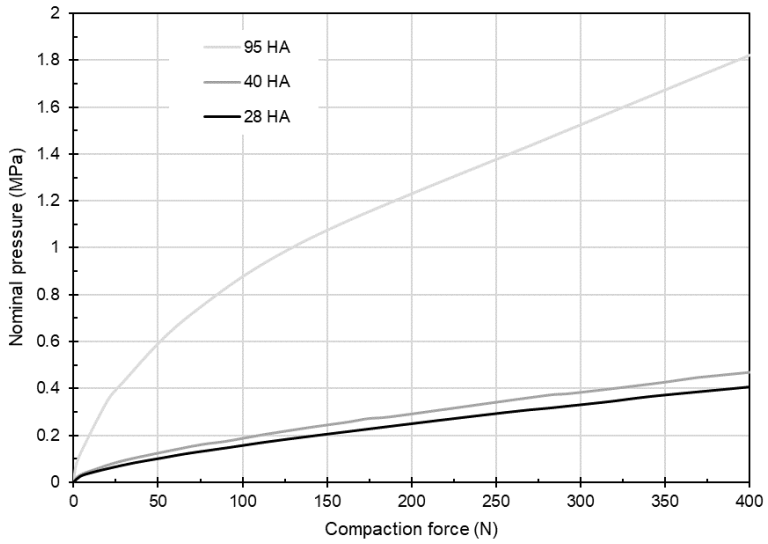

Figure 4-15 Nominal compaction pressure for three rollers under compaction force up to 400 N (Nominal pressure is calculated by force divided by contact area.)

Influence of tool curvature on compaction pressure

Figure 4-16 shows the compaction pressure distribution along the x-direction under a compaction force of 600 N generated by the two softer rollers on both a flat tool and the curved tools. A pressure spike is observed at the edge of the contact area which was also found in the compacted pressure sensitive film. It is shown that for flat tools, the compaction pressure is uniform except in the pressure spike area for both rollers and that the pressure generated by the 40 HA roller is higher than that generated by the 28 HA one. Whilst for the convex tools, the compaction pressure has a convex shape and the shape becomes more pronounced when decreasing the radius of curvature. 40 HA roller has a less uniform compaction distribution than the 28 HA roller under the same radius of curvature. Figure 4-17 shows the influence of radius of curvature on the pressure uniformity under a compaction force of 600 N. Pressure uniformity is calculated from the nodes on the tow 3 and tow 4 shown in Figure 4-8 (b) to avoid the influence of the local pressure spike. It is shown that the 28 HA roller has higher pressure uniformity than the 40 HA roller under the same radius of curvature, which is in agreement with the observations in Figure 4-16. For

both rollers, the pressure uniformity decreases slightly with an increase of curvature when radius of curvature is higher than 100 mm before decreasing dramatically for radii smaller than 100 mm.

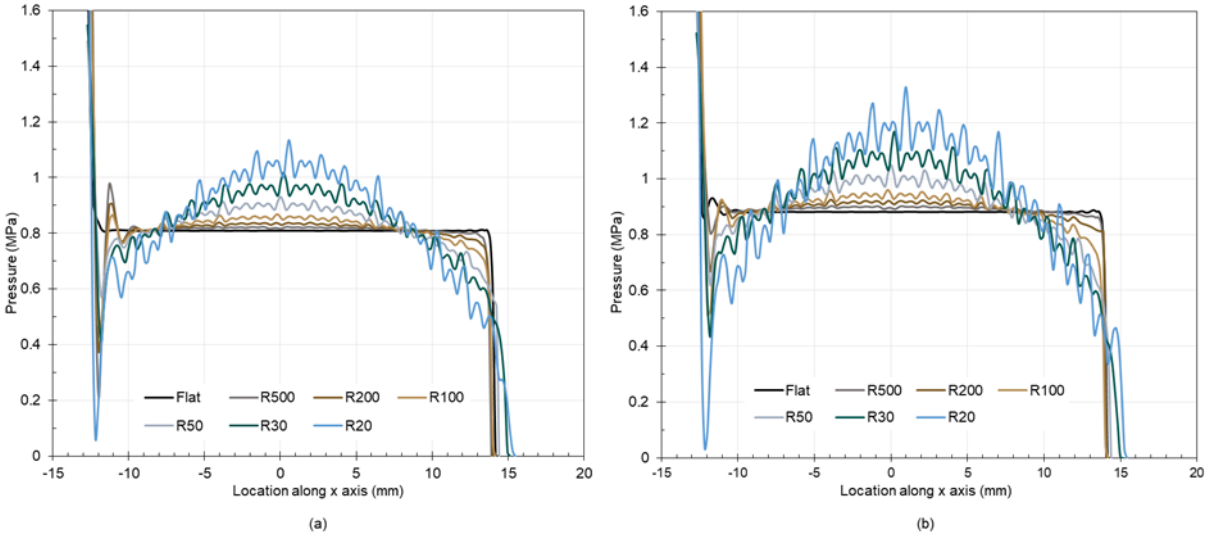

Figure 4-16 Simulated compaction pressure distribution of (a) 28 HA roller and (b) 40 HA roller on curved surfaces under a compaction force of 600 N (0 in x axis is positioned at the boundary between tow 2 and tow 3 shown in Figure 4-8 (b). X direction is along the width of tapes.)

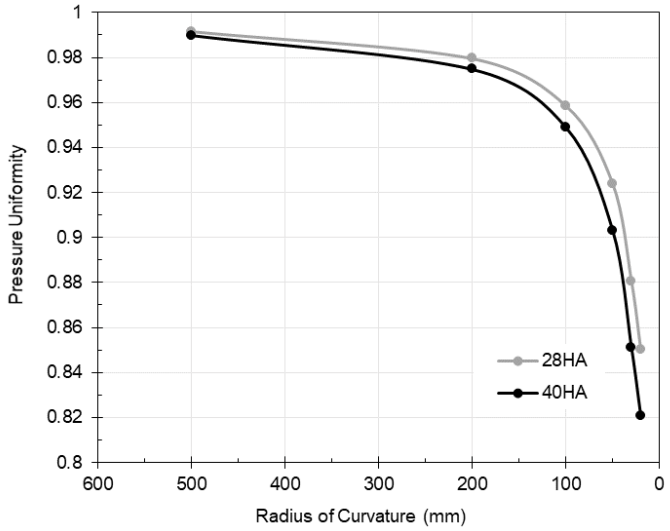

Figure 4-17 Pressure uniformity (calculated using equation (4.12) for tow 3 and tow 4 shown in Figure 4-8 (b))) of two rollers on curved surfaces under a compaction force of 600 N

Target force windows of rollers on curved tools

In other research on roller compaction on curved tools, the pressure uniformity given by different compaction rollers was compared for the same applied force. However, the pressure generated by different hardness rollers vary under the same applied force (due to the difference in effective contact area). In this work the pressure uniformity is found to depend on the force input according to the curves shown in Figure 4-18. For both rollers, pressure uniformity increases monotonically with the

applied compaction force. At a low level of compaction force, the rate of increase is almost constant but this then decreases more gradually above 200N. In this research, instead of comparing the pressure uniformity of two rollers under the same force input, force 'windows' of the two rollers are determined for curved tools to satisfy the compaction pressure requirement (between 0.5 MPa and 0.9 MPa in this case), to ensure good consolidation of the bindered tape without excessive force.

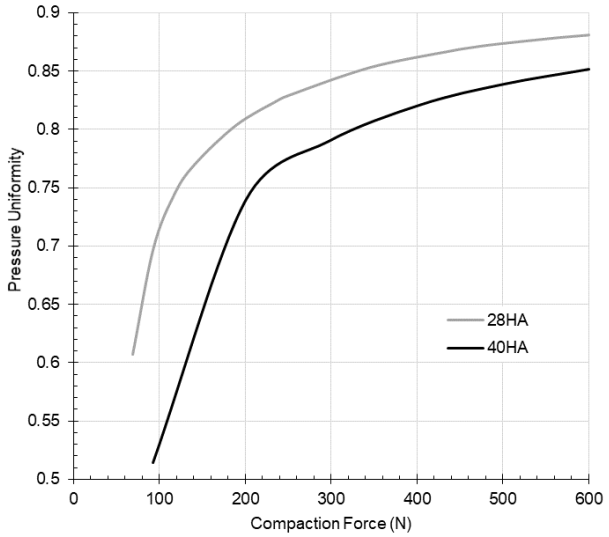

Figure 4-18 Influence of compaction force on pressure uniformity (calculated using equation (4.12) for tow 3 and tow 4 shown in Figure 4-8 (b))) for roller compaction on the tool with radius of curvature of 30 mm

Figure 4-19 shows the influence of applied force on the maximum and minimum contact pressure between the roller and the dry fibre substrate for the 28 HA roller on a tool with a radius of 30 mm. The maximum and minimum pressures are calculated from nodes in tow 3 and tow 4 as shown in Figure 4-8 (b) to avoid the influence of the pressure spike. It is found that maximum and minimum pressure shows a linear relationship with compaction force when the force is higher than 200 N. The other compaction results on different tool curvatures and roller materials show similar trends. The target force window is obtained from the intersection points of maximum and minimum pressure curves with the target pressure requirement bounds. Target force window results for other combinations are shown in Table 4-6. The maximum force applied in the FE simulation is 600 N but in reality, the actual upper bound of force which satisfies the compaction pressure requirement is above 600 N for 28 HA roller compaction on tools with radius of curvature greater than 100 mm. It is found that neither roller meets the pressure requirement for tools with radius of curvature of 20 mm, but the 28 HA roller can satisfy the requirement for a radius of curvature of 30 mm while the 40 HA roller cannot. For tools with other curvatures, 28 HA roller has a larger force window than the 40 HA roller. These force windows provide guidance for the force control of the ADFP process and it is

recommended that forces toward the upper end of the acceptable range should be chosen for force input since the pressure uniformity has been shown to increase with increasing compaction force. These force windows are used as the target force inputs for a force control strategy shown in section 6.2.

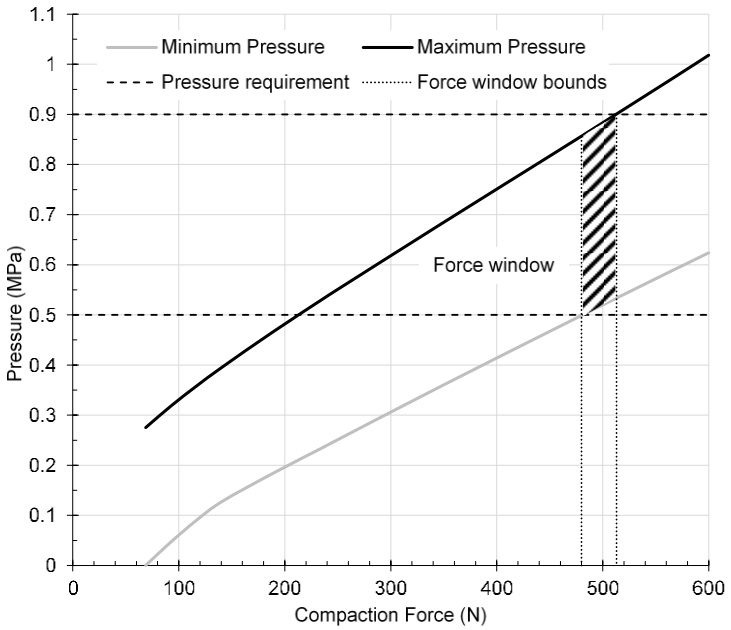

Figure 4-19 Influence of compaction force on maximum and minimum observed contact pressure between 28HA roller and the tool with radius of curvature of 30 mm

Table 4-6 Force windows of two rollers for tools with different curvatures

Radius of Curvature (mm)	28 HA Roller	40 HA Roller
20	-	-
30	480-513 N	-
50	435-563 N	447-492 N
100	398-600* N	350-538 N
200	347-600* N	320-557 N
500	338-600* N	304-597 N

*Actual upper bound is larger than 600 N.

Influence of substrate thickness

The simulation results show that the thickness of dry fibre substrate has minimal influence on compaction pressure since uniform material properties are used in this model for the dry fibre substrate. However, different layers of dry fibres have different compaction properties due to their different compaction history [131, 132]. The cyclic properties of carbon fibre are beyond the scope of this research and the model will be improved to consider the non-uniform properties of thick dry fibre

substrates in the future. Thick dry fibre substrates exhibit large deformation which is greater than twice the deformation of thermoset prepregs in the AFP process [122]. This larger deformation leads to larger displacement of the roller during the deposition process as shown in Figure 4-20. This larger displacement potentially complicates force control. If a position/displacement-based control strategy is used and the large displacement of the 10 mm dry fibre substrate is not considered, a force error around 43% can be produced. Thus, a force-based control strategy instead of position/displacement-based control strategy should be used for ADFP. Commercial deposition hardware deals with this issue by including some kind of built-in compliance (often in the form of a pneumatic cylinder) in order to maintain a roughly constant compaction force. The method developed here to use a target force window, when combined with real-time force feedback and knowledge of local tool geometry has the potential improve the quality of preforms by having tighter control over height and force. This idea is implemented by a force control strategy shown in section 6.2.

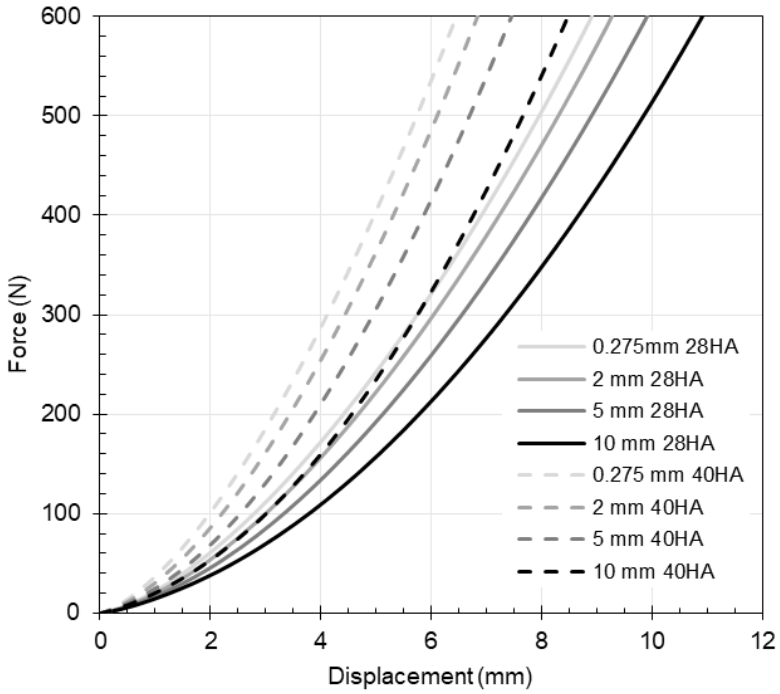

Figure 4-20 Load displacement curves for two compaction rollers on dry fibre substrates with different thickness (Displacement consists of the deformation of rollers and dry fibre substrates.)

4.4 Conclusions

In this chapter, compaction behaviour of dry carbon fibres and compaction rollers is investigated. A material model of dry carbon fibres in the through-thickness direction is developed. A FE model of roller compaction on carbon fibres is established to research the compaction pressure distribution. The following conclusions are obtained:

Commercial ADFP tapes have the same shape of compaction curve as normal dry fibre tows but they exhibit a stiffer response. The widely used power law equation can fit the compaction curve of commercial ADFP tapes with good agreement. For cyclic compaction properties, commercial ADFP tapes have a much more stable response than normal dry fibre tows and the tapes show minimal thickness change after 5 cycles of compaction.

The force applied by the deposition head when using different roller materials should be adjusted to obtain equivalent compaction pressure on the preform in order to optimise the binder performance in the finished preform. Harder rollers generate smaller contact areas and greater pressure non-uniformity. Precise force control is more challenging for harder rollers due to their low compliance under compaction. Therefore, harder rollers are not recommended for ADFP hardware.

For deposition on curved tools, compaction pressure uniformity decreases with increasing tool curvature for a given force. However, for a given curvature, pressure uniformity is directly proportional to applied force. Target force windows for roller compaction on tools with different curvatures have been obtained. Softer rollers exhibit larger force control window and increased suitability for tools with larger curvature. Given the high influence of tool curvature on required force, *a priori* knowledge of the tool curvature could significantly improve preform quality.

Thick dry fibre substrates exhibit large deformation under compaction during the ADFP process which brings complexity to the force control strategy. If an improper control strategy is used and the large deformation of thick dry fibre substrates is disregarded, a force error up to 43% can be generated.

These results provide guidance for the choices of roller and force control strategy for ADFP process. In common with existing research on AFP, it is recommended that compliant rollers should be used in ADFP process because they are more applicable

for precise force control and deposition on curved tools. Thermal resistant surface layer or coating is also recommended to protect compaction roller from high temperature dry carbon fibre tapes. Target force windows for roller compaction on curved tools provide force control input for ADFP. A force-based control strategy, instead of a position-based control strategy, is recommended for ADFP process especially for deposition on thick dry fibre substrates. Details of force control strategies are described in section 6.2.

5 Joule heating and heat transfer analysis of ADFP process

5.1 Introduction

Process temperature has great influence on the quality of both AFP and ADFP manufactured parts as evidenced by quality chapter 3.3.3 and literature review section 2.1.1 and 2.2.1. For AFP process, research on configurations of heating devices, nip point heat transfer analysis and temperature history of deposited materials are being conducted to improve the thermal management of AFP process and the quality of manufactured parts as shown in literature section 2.1.3. However for ADFP, the related research are limited. This chapter's work contributes to the research.

The thermal properties of commercial dry carbon fibre tapes are less understood. The tapes used in ADFP process are highly engineered with complex structures (veils, binders) which could lead to large differences in thermal properties compared with dry fibre tows and prepregs. In this chapter, thermal properties of commercial ADFP tapes, including temperature dependent specific heat capacity, binder thermal behaviour and fibre volume fraction dependent thermal conductivity, are firstly characterised.

In state of art of ADFP, laser heating is commonly used but the laser heating creates health and safety issues [10]. Since there is little resin present in the ADFP tapes, joule heating could potentially be a suitable heating method for ADFP consolidation. Joule heating has many applications in the composites industry, such as curing of composite laminates [135], de-icing [136], and towpreg manufacturing [137]. Joule heating in these areas utilises different configurations compared with ADFP conditions. In this chapter, the joule heating of dry fibre tapes with configurations representative of an ADFP deposition head are investigated experimentally. Analytical models have been built and experimentally validated to predict the joule heating temperature and efficiency. The models are used to predict the heating temperature with different power inputs and deposition velocities.

After heated by joule heating, the carbon fibre tapes make contacts with cooler substrates at the nip point. The temperature history after contact influences the properties therefore it is important to obtain the temperature history carbon fibre tapes after deposition. A finite element model is built in this chapter to analyse the heat transfer of dry carbon fibre tapes through the whole deposition process. It is

also used to investigate the effect of the process parameters on the temperature history of deposited dry fibre tapes.

5.2 Thermal characterisation of dry carbon fibre tapes

No published data of thermal properties of the TX1100 tapes has been found. Therefore, in this section, the fibre volume fraction dependent thermal conductivities of dry carbon fibre tapes are measured in the through-thickness and in-plane directions. The temperature dependent specific heat capacity and binder thermal behaviour of dry carbon fibre tapes are characterised by using modulated differential scanning calorimeter (MDSC). The characterised properties are also used as the input of models developed in later sections of this chapter.

5.2.1 Thermal conductivity measurement

5.2.1.1 Experimental setup

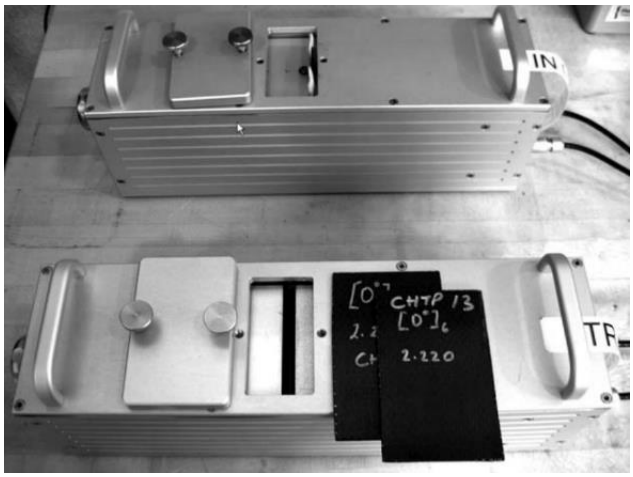

Figure 5-1 Hukseflux devices: THASYS (front) for through-thickness measurement and THISYS for in-plane measurement (back) [148]

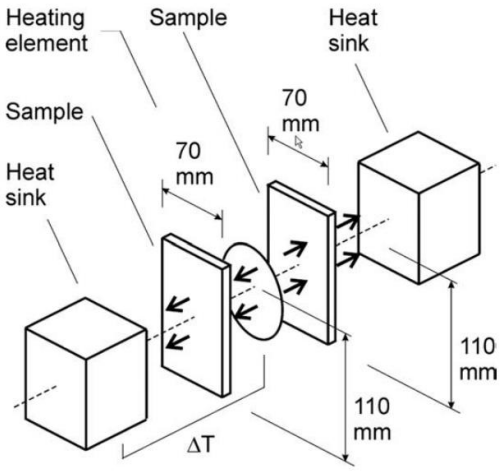

Figure 5-2 Configuration of THASYS device for through-thickness thermal conductivity measurement [148] (Through-thickness heat flow and temperature difference between heat sink and heating element are measured and used to calculated through-thickness thermal conductivity.)

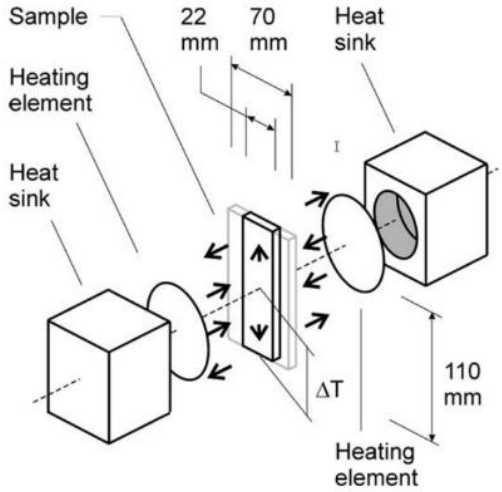

Figure 5-3 Configuration of THISYS device for in-plane thermal conductivity measurement [148] (In-plane heat flow and temperature difference between the centre of the sample and the edge of the sample are measured and used to calculated in-plane thermal conductivity.)

The thermal conductivity measurement used the methods described in [142, 148]. The through-thickness and in-plane thermal conductivity were measured using Hukseflux THASYS^{TM} and THISYS^{TM} devices as shown in Figure 5-1, Figure 5-2 and Figure 5-3. The devices require one or two flat samples with dimensions around 70 mm by 110 mm. TX1100 tapes were used to manufacture samples for thermal conductivity measurement. Tapes were cut into length of 110 mm. Nine tapes were butted together unidirectionally without visible gaps to form a layer with dimension of 69.85 mm by 110 mm. Eight layers in total were laid up together to make up a sample with a layup of $[0_8]$ (0 ° is along the length 110 mm direction). All samples mounted between spring-loaded heater plates with adjustable spacing were compacted to precise thickness values using accurately milled spacers. The spacers have low thermal conductivity and they are inserted away from heat transfer pathways in the devices. Samples were tested with four thicknesses ranging from 2.20 mm to 1.68 mm which results in fibre volume fraction ranging from 40.04 % to 52.43%. The devices cannot measure the compaction pressure directly. However, based on the compaction curve shown in Figure 4-5, to achieve the fibre volume fraction values, compaction pressures ranging from 0.02 MPa to 0.86 MPa are required. Table 5-1 shows the thickness, related fibre volume faction and required compaction pressure values of samples. For thermal conductivity measurements of each thickness, five repeats were conducted. The measurement results from these tests are the effective thermal conductivity of samples. The effective thermal conductivity is the combination of thermal conductivity of the carbon fibre tapes and the interlayer thermal contact conductance. The thermal conductivity of individual layer and interlayer thermal contact resistance cannot be separated using this method.

Table 5-1 Thickness, fibre volume fraction and related compaction pressure of TX1100 samples used for thermal conductivity measurement

Thickness (mm)	Fibre volume faction (%)	Compaction pressure (MPa)
2.20	40.04	0.02
2.00	44.04	0.08
1.84	47.87	0.25
1.68	52.43	0.86

5.2.1.2 Thermal conductivity measurement results

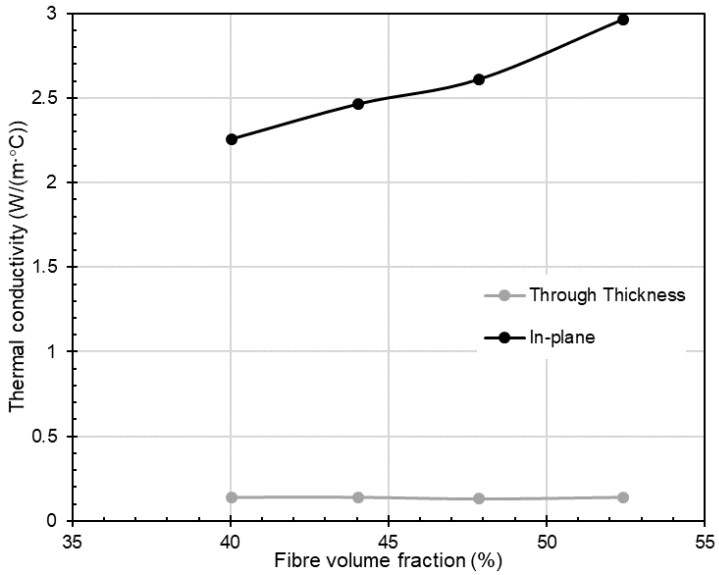

Figure 5-4 Effective in-plane and through-thickness thermal conductivity measurement results

Figure 5-4 shows the influence of fibre volume faction on the thermal conductivity of TX1100 dry carbon fibre tapes. The in-plane thermal conductivity of dry carbon tapes is significantly higher than the through-thickness thermal conductivity. For in-plane thermal conductivity, there is an almost linear increase with the increase of fibre volume fraction which is expected from rule of mixtures. However, it is unexpected through-thickness thermal conductivity remains almost constant for the four tested fibre volume fractions. Findings observed in these experiments display some differences from that in dry carbon fabric materials measurement results in the literature [139, 141, 142] where both in-plane and through-thickness thermal conductivity increase with the increase of fibre volume fraction. This difference is assumed to be caused by the pre-consolidation of TX1100 tapes during their fabrication process. Thermal conductivity measurement results for non-crimp fabric (NCF) materials in the literature [142], show that after three cycles of compaction, the in-plane thermal conductivity of NCF materials still increases with increasing fibre volume fraction, while the through-thickness thermal conductivity remains almost

constant. The pre-consolidation of TX1100 tapes has same effect as the three cycles of compaction in the literature [142].

The thermal conductivity of dry carbon fibres also is anisotropic in the in-plane direction. The in-plane thermal conductivity obtained from these experiments cannot be decoupled to thermal conductivities in fibre direction and transverse direction due to the measurement procedure. Thermal conductivity values obtained in this section are used in joule heating analytical models and finite element heat transfer model in later sections.

5.2.2 MDSC testing

Modulated differential scanning calorimeter (MDSC) tests were conducted using a DSC Q2000 (TA Instruments) device with temperature ranging from room temperature to 350 °C and the heating ramp rate of 2 °C/min. The modulation period is 60 s and the modulation amplitude is ± 1 °C. Three samples cut from TX1100 dry carbon fibre tapes were tested. The specific heat capacity of the tapes and the heat flow curves were obtained.

5.2.2.1 Specific heat capacity

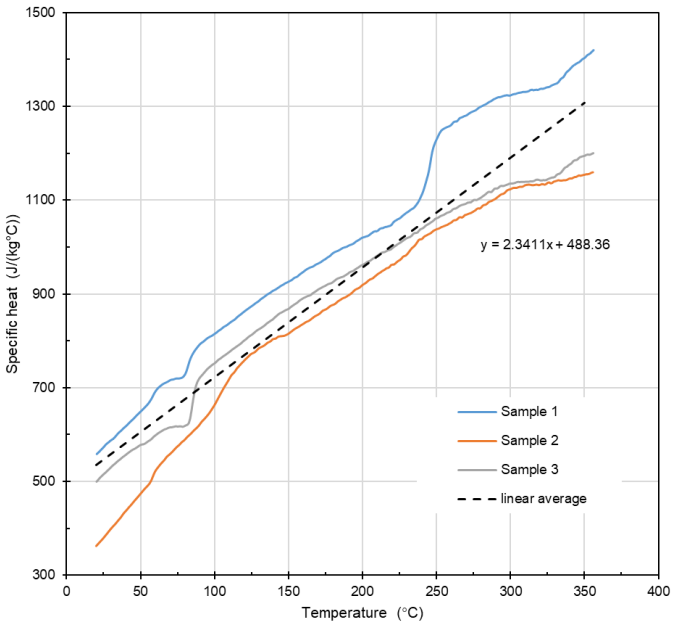

Figure 5-5 Specific heat measurement results from MDSC tests

Figure 5-5 shows the specific heat capacity measurement results for three samples. The specific heat capacity of dry carbon fibres increases with increasing temperature and their values at 350 °C are about 2.5 times as many as the values at room temperature. Three solid curves show a similar shape with value differences. The

samples for MDSC tests are very small (their weight is around 5 mg) and the veil and binder materials are not uniformly distributed in the very small samples which leads to the differences. A linear average fitted curve is plotted as a dashed line shown in Figure 5-5 to represent the temperature dependent specific heat capacity of dry carbon fibre tapes. The linearly fitted curve is used in joule heating analytical models and finite element heat transfer model in later sections.

5.2.2.2 Binder behaviour

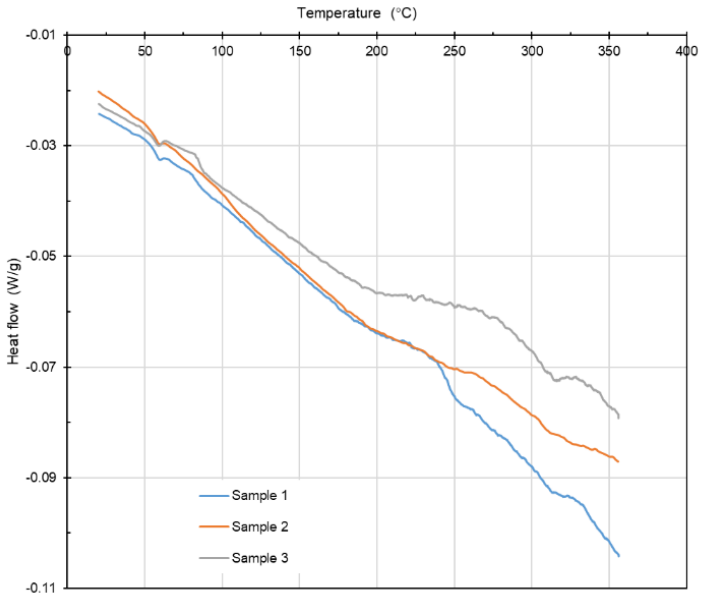

Figure 5-6 Heat flow measurement results in MDSC tests

Figure 5-6 shows the heat flow data for three samples. Non-uniformly distributed veils and binders again lead to the differences of three curves. Three transition temperatures (around 70 °C, 250 °C and 320 °C) are observed and these agree with the slope change of specific heat capacity curves shown in Figure 5-5. Carbon fibres are stable over this whole temperature range and the heat flow changes at three temperatures are related to the binder/veil state transition or reaction. The transition temperatures have no obvious link with the optimal temperature for peak peel resistance as shown in section 3.3.3. Research in [121] also shows that the transition temperatures are not optimal process temperatures for optimum fibre volume fraction of ADFP manufactured preforms.

5.3 Joule heating of dry carbon fibre tapes in ADFP configuration

5.3.1 Introduction

In state of art of ADFP, laser heating is commonly used but the laser heating creates health and safety issues [10]. For ADFP, joule heating could potentially be a suitable

heating method, especially for high speed deposition because it has high heating rates and fast response times [134]. However, applying joule heating in ADFP has two challenges: the contact resistance between carbon fibre tapes and electrodes, and cooling before nip point.

In the ADFP head, cylinder or roller electrodes are suitable for joule heating to ensure smooth feeding for carbon fibre tapes. The contacts between cylinder electrodes and carbon fibre tapes are not perfect and the electrical contact resistance therefore exists. The electrical contact resistance consumes energy and causes local heating therefore it needs to be reduced. Research in [138] characterised the contact resistance between carbon fibre tows and cylinder electrodes and it is found that the existence of contact resistance leads to the heating in the contact region and increasing fibre tension results in a decrease of contact resistance. However, the contact resistance between carbon fibre tapes used in ADFP and the cylinder electrodes has not been investigated. In this section, the contact resistance between TX1100 dry carbon fibre tape and copper cylinder electrodes is characterised under different contact angles, fibre tension levels and heating temperatures. An analytical model is built using measured electrical resistances to predict the heating temperature. The influence of contact resistance on the joule heating efficiency is also investigated.

Joule heating is a local heating method and only the tapes between the electrodes are heated. In ADFP, the tape is cooled when travelling from the joule heating area to the nip-point position due to convection, radiation and contact with cooler compaction roller. This cooling limits the deposition speed and brings difficulties for the nip point temperature control. In this section, an analytical model is built and experimentally validated to understand this cooling behaviour. The influence of the deposition speed and cooling region distance on the nip point temperature achieved by joule heating is investigated using the model.

5.3.2 Joule heating experiments

In this section, the electrical resistance and contact resistance between carbon fibre tapes and copper electrodes are characterised under different contact angle, fibre tension and heating temperature. Steady-state joule heating tests of carbon fibre tapes are conducted. Joule heating tests of carbon fibre tapes in an ADFP deposition head with fibre feeding are also conducted.

5.3.2.1 Characterisation of electrical resistance and contact resistance

A procedure used in literature [138] is used to measure the contact resistance between carbon fibre tapes and copper cylinder electrodes. A joule heating test rig as shown in Figure 5-7 is used to measure the contact resistance. The rig consists of two electrode tubes and a guide tube. The distance between the two electrode tubes can be changed. A digital multimeter (KEITHLEY 2110) with a four-wire arrangement is used to measure the electrical resistance between the two tubes shown in Figure 5-7. The total electrical resistance measured by the multimeter is the sum of the contact resistance of the two contact regions, the carbon fibre tape resistance and copper electrodes resistance. Copper electrodes resistance is ignored. The total resistance is measured with four different tape heating lengths (50 mm, 100 mm, 150 mm and 200 mm) between the two electrodes. The electrical resistance of the carbon fibre tape increases linearly with the increase of tape length. When the total resistance values for four tape lengths are plotted, the data points are fitted linearly and the intercept in y axis of the fitted line is the contact resistance. The resistances of carbon fibre tapes at different length are obtained by the total resistance subtracting the contact resistance. The influence of fibre tension and contact angle on the contact resistance can also be investigated using this rig. Fibre tension is applied by hanging weight at the one end of the carbon fibre tape. The contact angle on the right electrode where fibre tension is applied is a constant of 90° but the contact angle on the left electrode is changed by guiding fibre path using a copper tube. Four contact angles (31.0°, 42.7°, 82.4° and 116.1°) can be obtained by install the guiding tube in different locations.

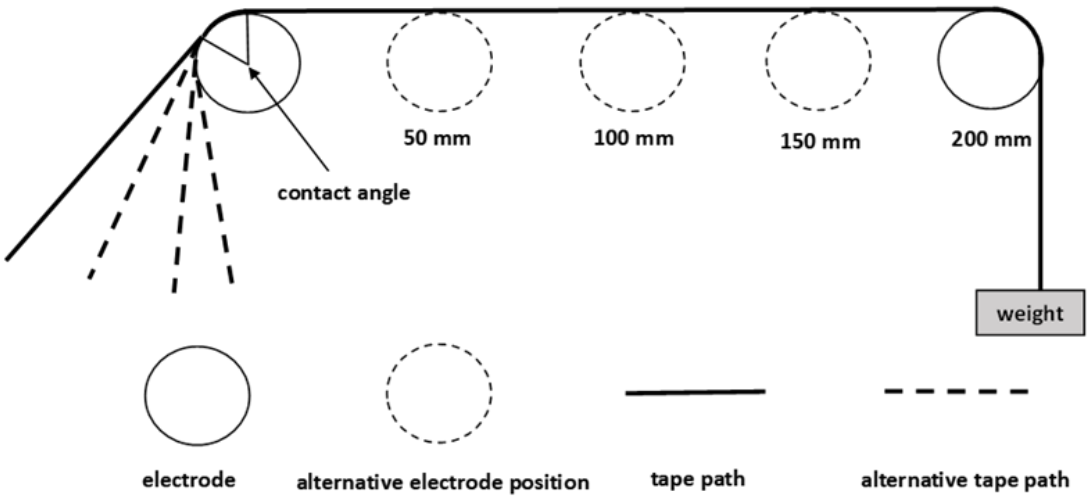

(a)

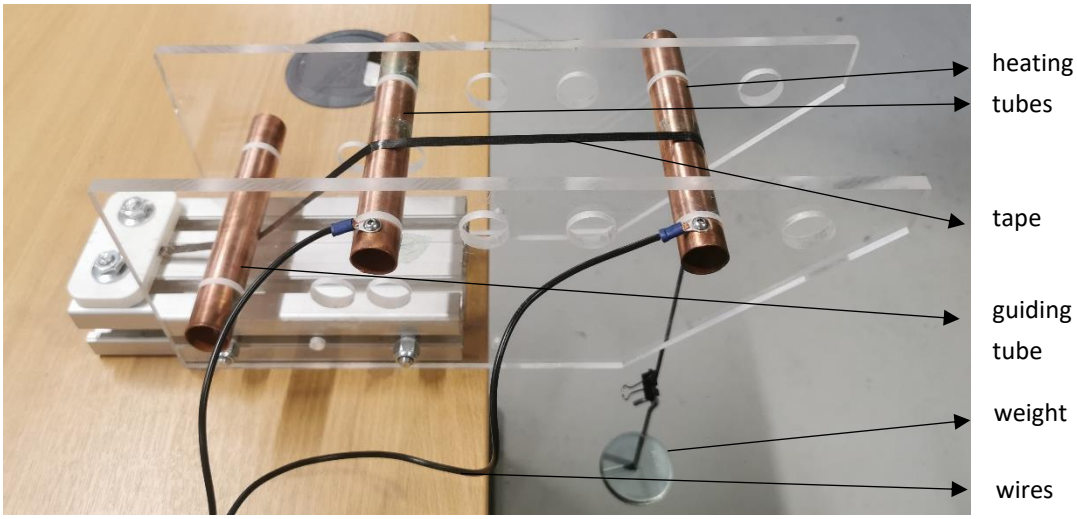

(b)

Figure 5-7 Joule heating rig (a) sketch (b) rig with a tape (Copper tubes on the top are used to change heating length. Guiding tube on the bottom is used to change contact angle. Two wires on the top copper tubes are connected to a multimeter for total resistance measurement.)

5.3.2.2 Static joule heating of carbon fibre tapes

In static joule heating tests, electrical currents pass though the joule heating rig shown in Figure 5-7 to heat the carbon fibre tapes. Figure 5-8 shows the electric circuit for static joule heating testing. A power supply (Velleman LABPS3010SM) is used to provide constant voltage to the circuit. A shunt resistor (PCN RXM50) with an electrical resistance of 0.1 Ω is used for the current measurement. A Beckhoff EL3164 analogue input terminal is used to measure the voltage across the shunt resistor. The current in the circuit is obtained from the Beckhoff terminal voltage values divided by the shunt resistor's electrical resistance of 0.1 Ω. The digital multimeter is used to measure the voltage between the two wires of the joule heating rig. The total resistance between the two wires in the joule heating rig is then obtained from the multimeter voltage value divided by the circuit current value Fibre tension and contact angle are applied using the same method as the electrical resistance measurement experiments.

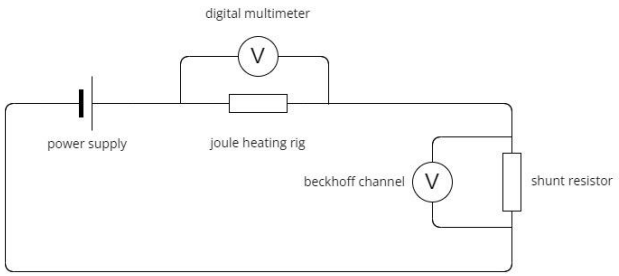

Figure 5-8 Electric circuit for static joule heating testing

In the static joule heating process, the carbon fibre tapes are heated up to a steady-state temperature in a few seconds. When the steady state is achieved, the circuit

current and multimeter voltage value are recorded. A FLIR C5 thermal camera is then used to measure the temperature of the carbon fibre tape. The average resulting temperature along the centreline of tape is recorded.

Using this static joule heating setup, the contact resistances between the carbon fibre tapes and copper electrodes at different temperature are also characterised. At each tape length, the tapes are heated to five different heating temperatures ranging between room temperature and 250 °C and the total resistances at different temperatures are measured. The total resistance versus heating temperature curves are fitted with quadratic polynomial equations. The equations are used to calculate the total resistance at a certain heating temperature for four tape lengths. The contact resistance at the certain heating temperature is the characterised using the method described in section 5.3.2.1.

5.3.2.3 Dynamic heating of joule heating

The dynamic joule heating test was conducted using a lab scale ADFP deposition head as shown in Figure 5-9. The carbon fibre tapes are heated between the two electrodes and then fed to the nip point with a constant velocity by a fibre feeding system. To simplify the experiment, the deposition head is stationary but feeds the carbon fibre tape under different velocities with joule heating. For the joule heating setup in the head, a constant voltage of 30 V is generated from a power supply and a duty cycle method developed in literature [134] is used for the control of power input of the joule heating. The details for the duty cycle method are described in section 6.3.1. A shunt resistor (PCN RXM50) with an electrical resistance of 0.1 Ω is also connected for the current measurement. A FLIR C5 thermal camera is used to measure the temperature of carbon fibre tape at the nip-point. Figure 5-10 shows the thermal camera measurement.

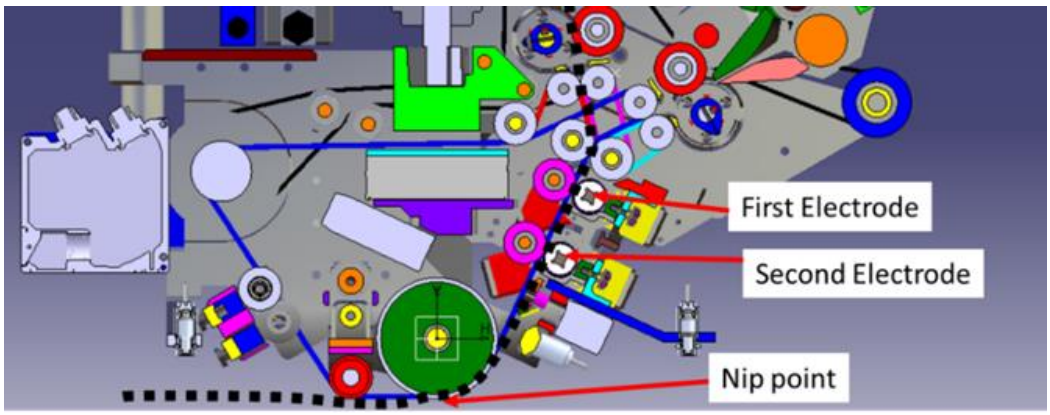

Figure 5-9 Joule heating setup in the ADFP deposition head (Dash line is the tape path. Tape is heated between two electrodes.)

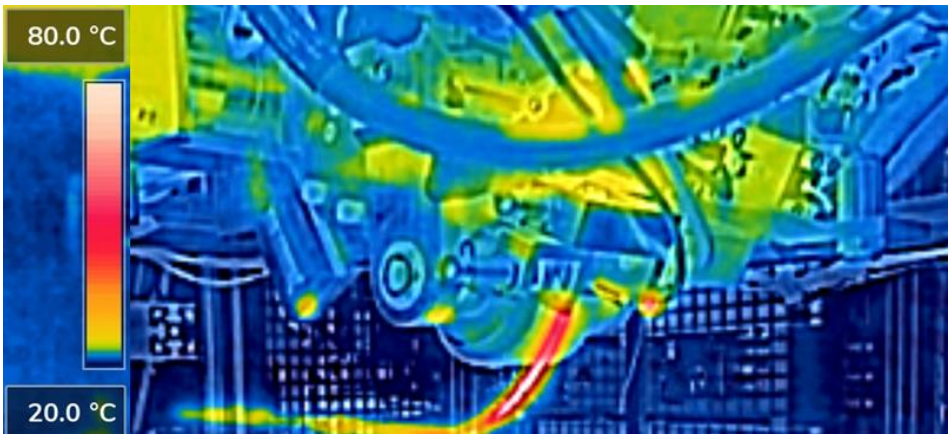

Figure 5-10 Thermal camera temperature measurement for dynamic joule heating test in the ADFP deposition head

5.3.2.4 Experimental results

Influence of residual deformation and surface finish of tapes on contact resistance

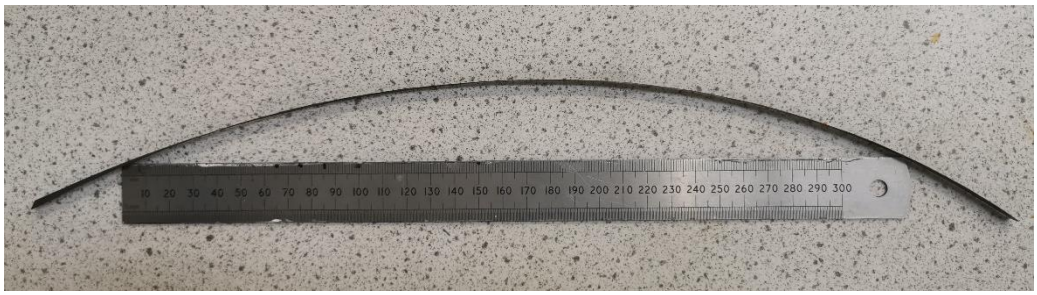

Figure 5-11 Tape with residual deformation after cutting from bobbin termed 'bent' tape (Top surface is veil surface and bottom surface is binder surface.)

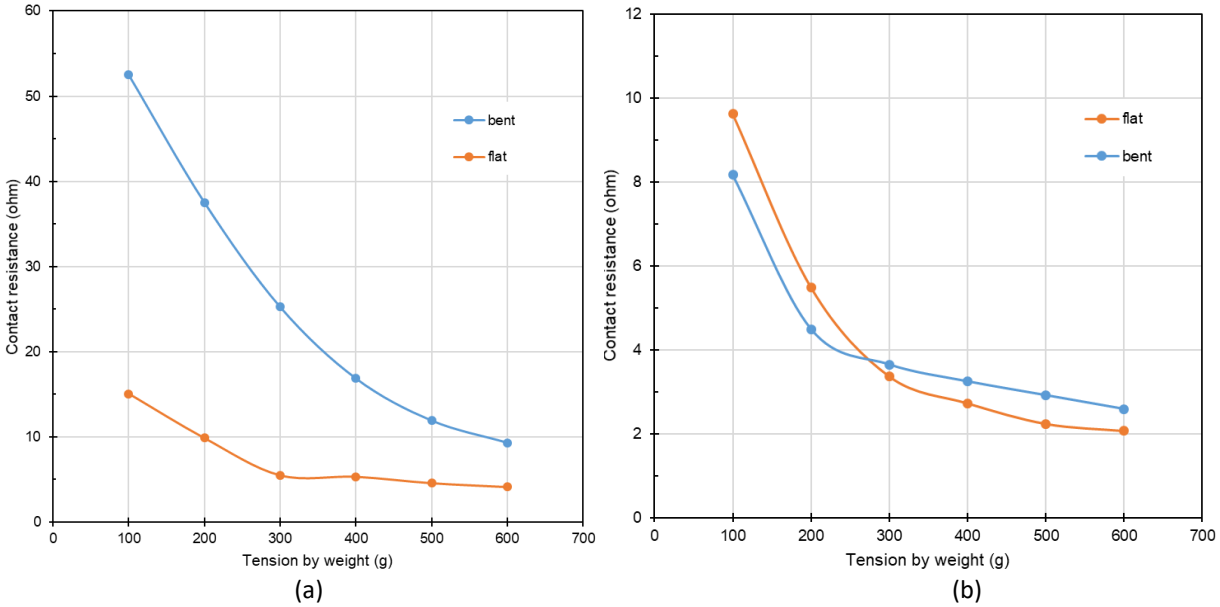

Figure 5-12 Contact resistance results of deformed and flattened carbon fibre tapes with (a) veil surface (b) binder surface contact with electrodes with 82.44° contact angle (difference y axis scales) under heating temperature around 50 °C

The TX1100 carbon fibre tapes were used in the tests. The binder surface and veil surface of TX1100 tapes have different surface finish which results in different contacts with electrodes and contact resistance. The tapes also exhibit residual bending deformation after cutting for bobbins as shown in Figure 5-11. This deformation also influences the contact with electrodes. To investigate the influence of residual deformation on the contact resistance, the carbon fibre tapes were compacted by a metal ruler to release the residual deformation and these tapes are termed 'flat' tapes. The tapes without compaction are termed 'bent' tapes. Figure 5-12 shows the influence of residual deformation and surface finish of tapes on the contact resistance. For veil surface contacting with electrodes, the residual deformation has significant influence on contact resistance. The contact resistance for bent tapes is dramatically larger than that for flat tapes at 100 g weight of tension (52.5 Ω vs 15.1 Ω). The differences decrease with the increase of the fibre tension since fibre tension could release some residual deformation. When veil surface faces electrodes, the direction of bend deformation is the opposite of the cylinder electrode curvature direction. This leads to poor contact and high contact resistance. For binder surface contacting with electrodes, the residual deformation has minimal influence on the contact resistance because the bending direction is the same with the cylinder electrode curvature direction. Results from later sections were obtained using flat tapes to avoid the influence of residual deformation.

The contact resistance for binder surface is lower than that for veil surface (9.6 Ω vs 15.1 Ω at 100 g tension and 2.1 Ω vs 4.1 Ω at 600 g tension). On the binder surface, binder powders are scattered while for veil surface, veil almost fully cover the carbon fibres. Therefore, carbon fibres have more effective contact area with electrode on the binder surface, which leads to lower contact resistance. Increasing fibre tension could generate better contact and then reduce this difference.

Influence of contact angle and fibre tension on contact resistance

Figure 5-13 shows the results of contact resistance for binder surface under different contact angles and fibre tension at room temperature. It is found that for all contact angles, when increasing the tension, the contact resistance drops significantly at low level of tensions and gradually reaches a plateau at high level of tension. Increasing fibre tension increases the number of filaments contacting with electrodes and the filament contact length, which decreases the contact resistance [138]. When most of filaments contact with electrodes, increasing fibre tension could not further decrease the contact resistance. Increasing contact angle can also lead to a decrease of contact resistance especially at low tension level because the contact area is larger with

higher contact angle. However, the contact angle is limited by the deposition hardware therefore in practical situations, increasing the tape tension is a more feasible way to reduce the contact resistance. It is also found that the contact resistance of 82.4° contact angle in Figure 5-13 is smaller than that in Figure 5-12 and Figure 5-14. The tests for Figure 5-13 were conducted firstly. After the testing, the electrodes show a few signs of abrasion and oxidation. It is assumed that the abrasion and oxidation lead to poorer contact and higher contact resistance results shown in Figure 5-12 and Figure 5-14.

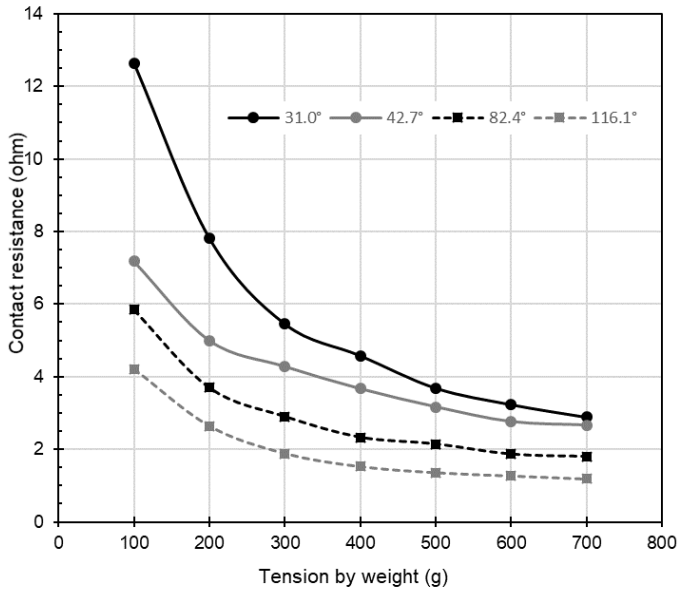

Figure 5-13 Contact resistance results without current passing in the circuit (at room temperature) under four different contact angles and seven different tension levels

Influence of heating temperature on contact resistance

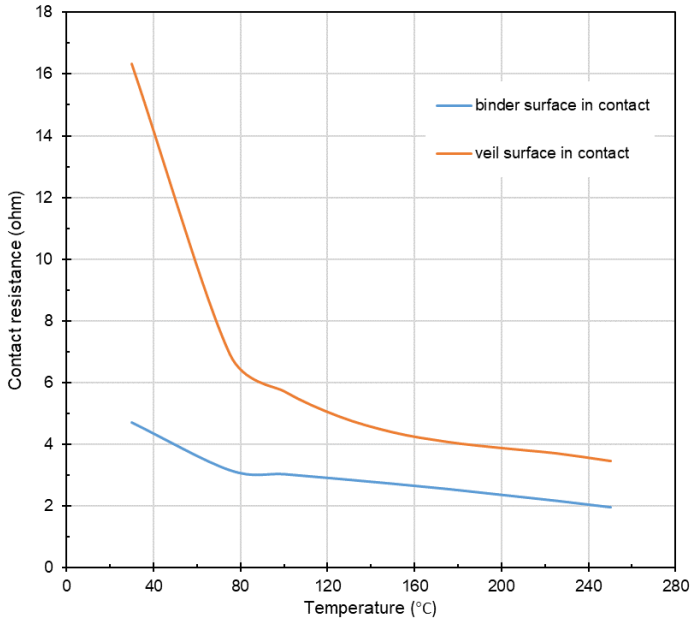

Figure 5-14 Contact resistances under different heating temperature with 82.4° contact angle and fibre tension by 300 g weight for binder surface in contact and 500 g for veil surface in contact

Figure 5-14 shows the influence of heating temperature on the contact resistance. For both binder surface and veil surface, the contact resistance decreases with the increase of heating temperature and there are slope changes for two curves around 70 °C. This slope change may link to the first transition temperature found in MDSC testing in 5.2.2.2. This needs further investigation with more data points because only three heating temperatures under 100 °C were used during the test. Research in literature [138] also shows that increasing heating temperature leads to significant drops of contact resistance and it is concluded that the transverse thermal expansion of carbon fibre filaments leads to better conformation on electrodes resulting in smaller contact resistance.

5.3.3 Joule heating analytical model

In this section, analytical models are built for joule heating using joule heating rig to calculate the efficiency of joule heating and steady state heating temperature. Another analytical model is also built for joule heating using the ADFP deposition head with fibre feeding to predict temperature when dry carbon fibre tapes reach the nip point.

5.3.3.1 Analytical model for static joule heating

Efficiency of joule heating

The two contact resistances and the fibre resistance are connected in series. The current passing through them is the same and represented as I. The power used on heating contact area P_c and carbon fibre tapes P_f can be calculated from equation (5.1-5.2) based on Joule's law. R_c and R_f is the total contact resistance and fibre tape resistance and their values are measured experimentally. The power efficiency of joule heating E is then calculated by equation (5.3).

$$P_c = I^2 R_c \tag{5.1}$$

$$P_f = I^2 R_f \tag{5.2}$$

$$E = \frac{P_f}{P_f + P_c} = \frac{I^2 R_f}{I^2 R_c + I^2 R_f} = \frac{R_f}{R_f + R_c} \tag{5.3}$$

Steady state heating temperature

When a steady state is achieved, the power from joule heating is equal to the power of radiation and convection cooling. This can be expressed in equation (5.4) according to heat transfer theory [149] and the steady state heating temperature T_s is then obtained.

$$I^2 R_f = hA(T_s - T_r) + \sigma \varepsilon A\left({T_s}^4 - {T_r}^4\right) \tag{5.4}$$

Where h is the convection coefficient of air and its value is 10.45 W/(m^{2}K). A is the

surface area of the carbon fibre tape which depends on the length of the carbon fibre tape in the heating area. T_r is the room temperature. σ is the Stefan-Boltzmann constant and its value is 5.67×10^{-8} $Wm^{-2}K^{-4}$. ε is the emissivity of the carbon fibre tape and a constant value of 0.9 is used for simplicity. I is the current in the electric circuit and it is measured from the static joule heating testing.

5.3.3.2 Analytical model for dynamic joule heating model

During ADFP deposition process, fibre tapes are heated between two electrodes before moving to the nip point with certain deposition speed. To predict the nip-point temperature, a one-dimensional transient heat transfer model considering the effect of deposition speed has been built. The model has a total length of 145 mm consisting of 40 mm-length joule heating region and 105 mm-length cooling region according to the dimension of the lab-scale ADFP machine. In this model, the heat transfer between the fibre tapes and the compaction roller is not considered. The one-dimensional transient heat equation with joule heating, conduction, convection and radiation can be expressed by equation (5.5).

$$\frac{\rho c_p}{k}\frac{\partial T}{\partial t} = \frac{\partial^2 T}{\partial x^2} + \frac{\dot{q}_{jh}}{k} - \frac{\dot{q}_{con}}{k} - \frac{\dot{q}_{rad}}{k} \tag{5.5}$$

Where T is the temperature of the carbon fire tape. ρ is the density of the carbon fibre tape. c_p is the specific heat capacity of the carbon fibre tape and the temperature dependent values characterised in section 5.2.2.1 are used. k is the thermal conductivity along the fibre direction of the carbon fibre tape and in-plane value characterised in section 5.2.1.2 is used. $\dot{q}_{jh}$, $\dot{q}_{con}$ and $\dot{q}_{rad}$ are the volumetric heat generation or dissipation by joule heating, convection and radiation respectively and they can be calculated by following equations.

$$\dot{q}_{jh} = \frac{I^2 R_f}{V} \tag{5.6}$$

$$\dot{q}_{con} = \frac{hA(T-T_r)}{V} \tag{5.7}$$

$$\dot{q}_{rad} = \frac{\sigma\varepsilon A(T^4-{T_r}^4)}{V} \tag{5.8}$$

Where I is the current in the electric circuit and it is measured from the dynamic joule heating testing. V is the volume of the carbon fibre tapes.

A finite-difference method is used for equation (5.5). The discretisation of time is shown in following equations.

$$t = p\Delta t \tag{5.9}$$

$$\frac{\partial T}{\partial t}\Big|_i = \frac{T_i^{p+1}-T_i^p}{\Delta t} \tag{5.10}$$

Where t is the time. Δt is the time interval. p is the integer to denote the time dependence of T. i is the integer to designate the location of discrete nodal points.

For the discretisation of the conduction heat transfer term, an explicit method with a forward-difference approximation is used and shown in equation (5.11).

$$\frac{\partial^2 T}{\partial x^2} = \frac{T_{i+1}^p + T_{i-1}^p - 2T_i^p}{(\Delta x)^2} \tag{5.11}$$

Where Δx is the length interval. Substituting equations (5.6-5.8) (5.10-5.11) into equation (5.5), equation (5.12) is then obtained. It is used for the joule heating region while for the cooling region the joule heating term is removed and the other terms are the same.

$$\frac{\rho c_p}{k}\frac{T_i^{p+1} - T_i^p}{\Delta t} = \frac{T_{i+1}^p + T_{i-1}^p - 2T_i^p}{(\Delta x)^2} + \frac{I^2 R_f}{kV} - \frac{hA\left(T_i^p - T_r\right)}{kV} - \frac{\sigma\varepsilon A\left({T_i^p}^4 - {T_r}^4\right)}{kV} \tag{5.12}$$

To simulate the movement of carbon fibre tapes, at the start of each time interval, the temperature distribution moves a certain distance along the discrete nodal points based on the deposition speed and the room temperature is assigned to the nodal points of the certain distance in the initial location of the model. Then the equation (5.12) is used to calculate the temperature of each nodal point.

5.3.3.3 Analytical model simulation results

Efficiency of joule heating

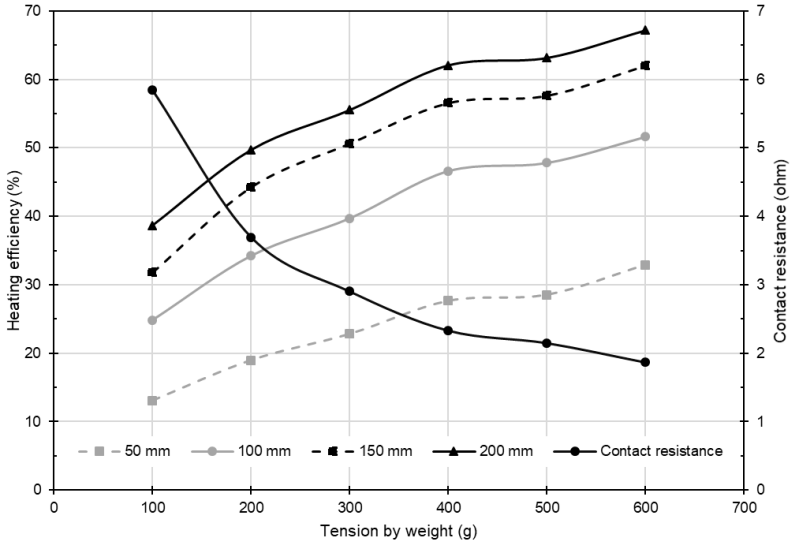

Figure 5-15 Joule heating efficiency results at contact angle of 82.4° under four different heating lengths (50 mm, 100 mm, 150 mm, 200 mm) and six different tension levels

Figure 5-15 shows the joule heating efficiency results calculated by equation (5.3) using the experimental contact resistance results. At fibre tension of 100 N, the tape resistance is smaller than the contact resistance. Therefore, the heating efficiencies are lower than 50 %. When fibre tension increases to 600 N, the heating efficiencies for the four lengths double approximately. It is also found that longer heating length, due to their higher resistance, leads to higher efficiency. It is recommended to

increase the length of heating region in the deposition head design to reduce the energy waste at the contact region.

Steady state heating temperature

Figure 5-16 shows the steady state heating temperature results from experiments and static analytical model from equation (5.4). It is found that reducing contact resistance results in a significant increase of heating temperature with a constant voltage supply. The results from the static analytical model show good agreement with the experimental data. The analytical model is then used to investigate the influence of contact resistance and heating region length on the steady state heating temperature. Figure 5-17 shows the benefits of reducing contact resistance by fibre tension. Decreasing contact resistance could increase heating temperature significantly. In the case of 50 mm heating length, the steady state heating temperature at tension of 600 N is more than three times of that at tension of 100 N. With a constant voltage supply, shorter heating length leads to higher heating temperature due to the lower resistance. If the power supply is limited, the heating length should be short enough to achieve enough heating temperature. However, if the power supply is sufficient, long heating length is recommended because it has higher heating efficiency and in real ADFP head, the tape has more heating time.

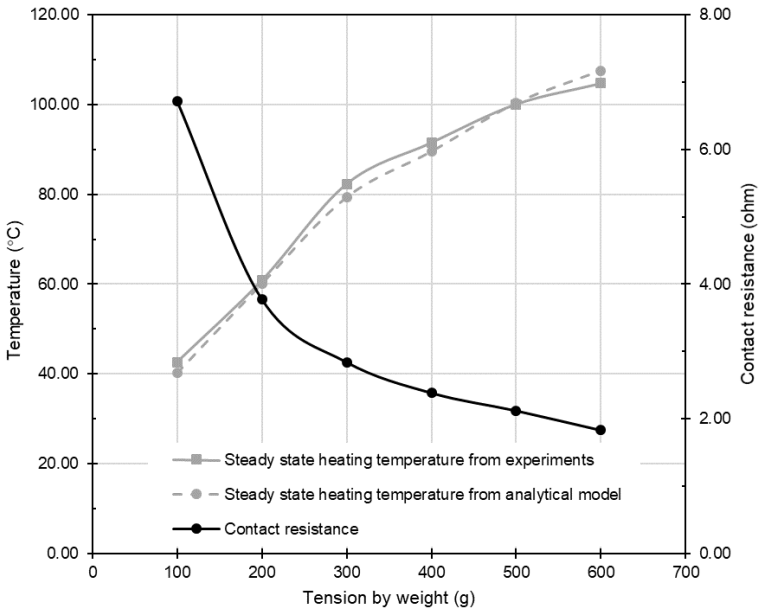

Figure 5-16 Static joule heating results for 50 mm length with 31.0° contact angle under a constant voltage supply

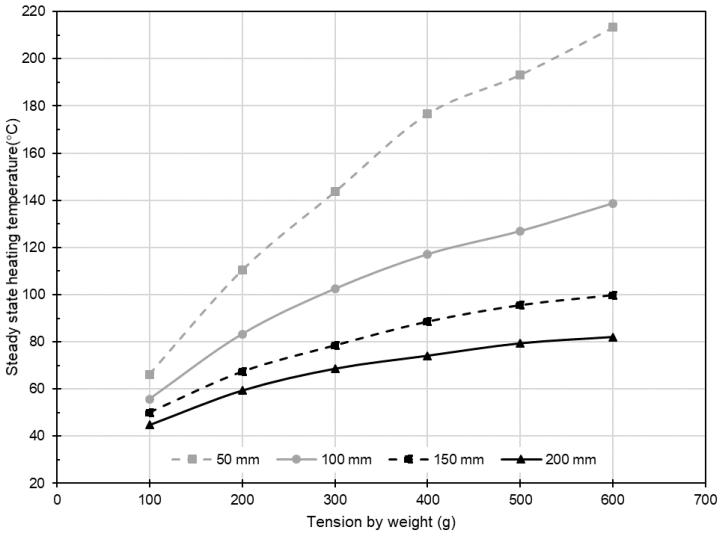

Figure 5-17 Analytical results of steady state heating temperature for 31.0° contact angle under four different heating lengths (50 mm, 100 mm, 150 mm, 200 mm) and six tension levels with a constant voltage of 5 V

Dynamic joule heating simulation results

To validate the dynamic analytical model, a simple joule heating testing with a step power input was conducted using the joule heating rig shown in Figure 5-7 and Figure 5-8. A thermocouple was attached to the surface of the tape to measure the temperature continuously. The measured current values from the shunt resistor are used as the input of the dynamic analytical model to generate the heating and cooling curve. The temperature calculated by the model agrees with the experimental data as shown in Figure 5-18. The equation (5.12) used in the model and the finite-difference method are then validated.

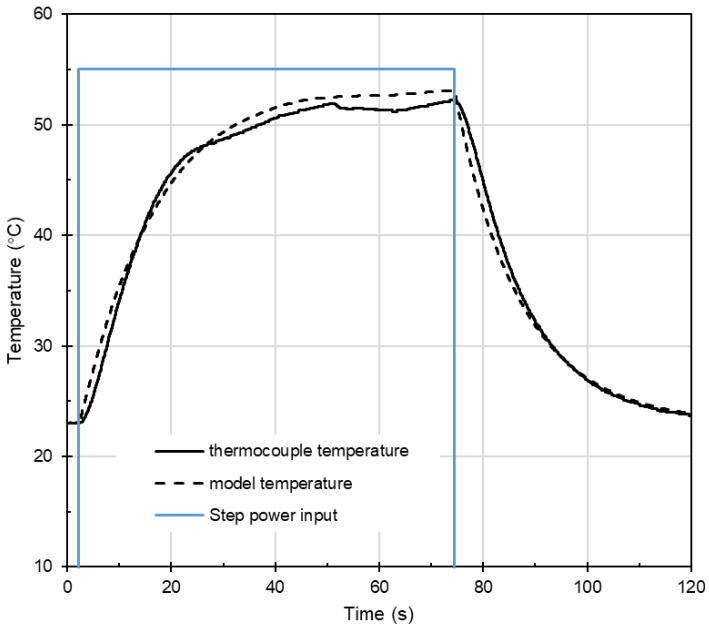

Figure 5-18 Joule heating and cooling curve of carbon fibre tape under step power input

Figure 5-19 shows the nip point temperature from dynamic joule heating with fibre feeding in the ADFP head. It is found that the nip point heating temperature increases approximately linearly with the increase of duty cycle. The model prediction agrees with the experimental data. The dynamic joule heating model is then validated. The model can be used to obtain the relationship between feeding speed, power input and the nip point temperature.

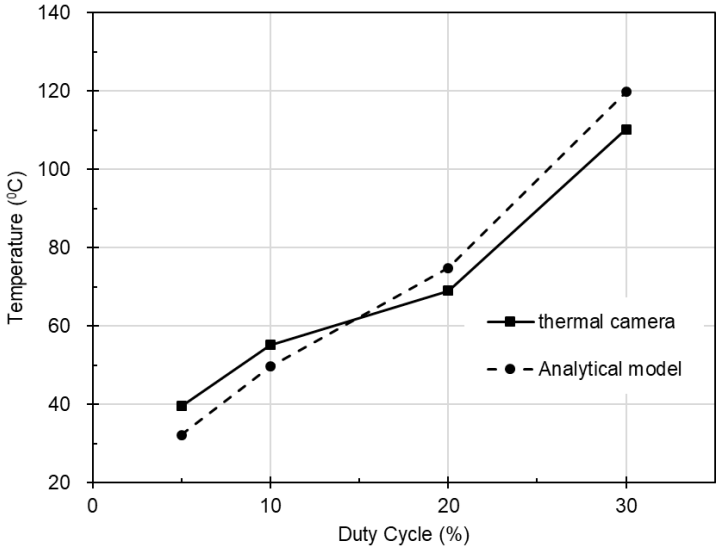

Figure 5-19 Nip point temperature from dynamic joule heating with 100 mm/s feeding velocity

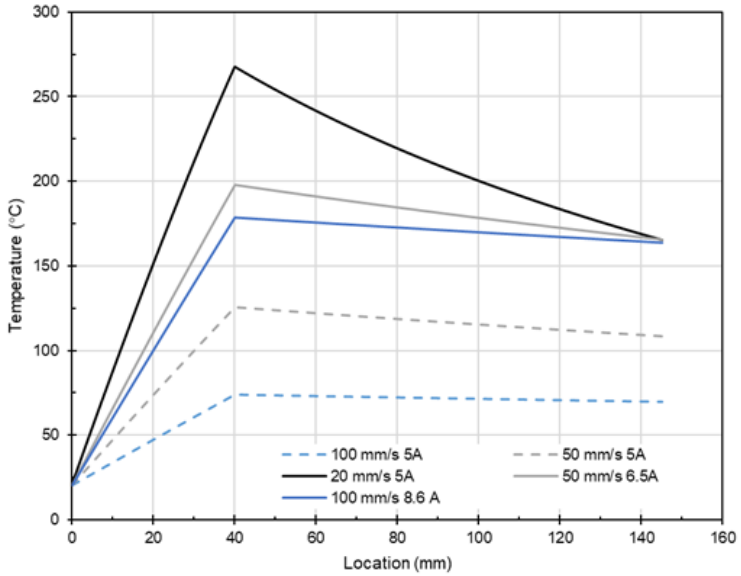

Figure 5-20 Model calculated temperature distribution in the ADFP head from heating region to the nip point (Heating region is from 0 to 40 mm. Cooling region is from 40 mm to 145mm. The right-hand end is the nip point)

Figure 5-20 shows the model predicted temperature distribution in the ADFP head from heating region to the nip point under different feeding velocity and current input. With same current supply, lower feeding speed leads to higher nip point

temperature because the tape has more heating time. The power supply should be adjusted for different feeding velocity to achieve the same nip point temperature and this model can provide guidance as shown in the solid lines in Figure 5-20. The lower feeding speed also leads to more cooling time. The black curve in the Figure 5-20 shows a near 100 °C temperature drop in the cooling area. In this situation, although the nip point temperature achieves the required temperature, the tape is overheated in the heating region which might degrade the binder in the carbon tapes. It is recommended that the distance between the end point of the heating region and the nip point should be minimised to reduce cooling effects.

5.4 FE model of heat transfer of ADFP process

Using the dynamic analytical model developed in the joule heating section 5.3.3.2, the temperature of carbon fibre tapes at the nip point can be obtained. The temperature history of the tapes after deposition is obtained using the model developed in this section.

5.4.1 FE model description

In the heat transfer model, a progressive activation of elements strategy where elements are activated step by step to simulate a dynamic process is used. This strategy can replicate the deposition process and it has been successfully used in the heat transfer analysis of additive manufacturing of thermoplastic composites [150] and steel [151], AFP process of thermoplastic composites [82, 152]. The whole model geometry with certain number of courses and layers, and the stacking sequence is defined as a normal FE model. In the analysis process, all elements are deactivated at the first solution step and then activated according to the deposition head position history in sequence to simulate the heating transfer in continuous ADFP deposition process. In each step, elements of carbon fibre tape representing a course with the nip point temperature which can be obtained from the dynamic joule heating model, are activated in the model and remain in the model in subsequent steps. The lay up speed is adjusted by altering the duration time of each step. This strategy is implemented in ABAQUS with the ‘model change’ interaction. Figure 5-21 shows a model example consisting two courses in a layer and deposition direction from the right hand end. In the first step, elements for the first pieces of tapes in the first course in the first layer are activated as shown in Figure 5-21 (a). After finishing the heat transfer analysis in the first step, second pieces of tapes in the first course in the first layer are then activated and heat transfer is analysed for all activated elements as shown in Figure 5-21 (b). Figure 5-21 (c) and (d) show the results from first step

for the second course in the first layer and first step for the second course in the second layer.

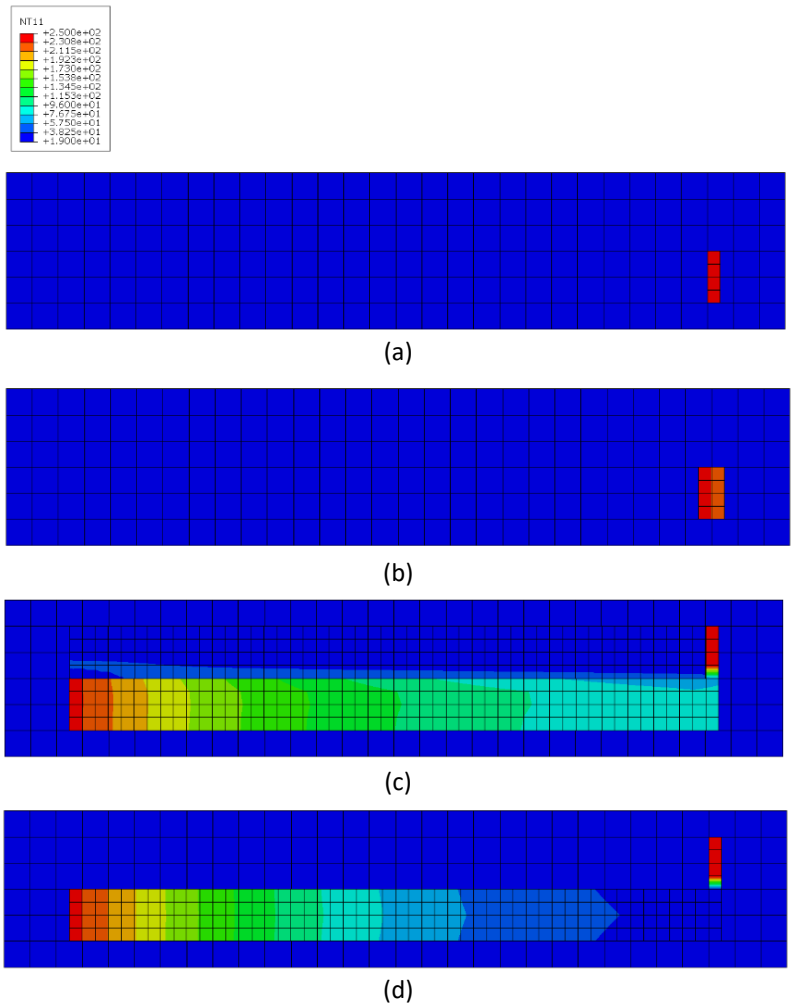

Figure 5-21 Element activation strategy for simulating continuous ADFP deposition with moving direction from right to left (a) first step for the first course in the first layer (b) second step for the first course in the first layer (c) first step for the second course in the first layer (d) first step for the second course in the second layer (Colour map shows the temperature distribution.)

A model consisting of five layers of carbon fibre tapes has been built using the above strategy. The layup is unidirectional ($[0_5]$). Each layer has two courses (four tapes per course) with dimensions of 300 mm × 50.8 mm × 0.275 mm. A tool with dimensions of 381 mm × 76.2 mm × 1 mm is also built in the model. An 8-node linear heat transfer brick (DC3D8) element is used for both carbon fibre tapes and the tool. Aluminium material thermal properties are assigned to the tool. For the material properties of the carbon fibre tapes, the linear fitted temperature dependent specific heat capacity values from section 5.2.2.1 are used. Effective thermal conductivity as characterised in section 5.2.1.2 is used and the interlayer thermal contact resistance is set to zero because thermal contact resistance cannot be separated from the experimental measurement of thermal conductivity. However, the measurement results can capture both the thermal conductivity of carbon fibre tape itself and the

interlayer thermal conductance (reverse of resistance). The thermal contact resistance between the carbon fibre tapes and the tool surface is also set to zero because no published data has been found. This zero thermal contact resistance could lead to an underestimation of the predicted temperature [85, 86, 153].The convective and radiative cooling of tapes is much smaller than conductive heat transfer to the substrate and the two cooling mechanisms have minimal influences on the temperature history of carbon fibre tapes according to the preliminary study using the model (differences are smaller than 5.4 %). Therefore, they are not considered in the model. No external heat flux is modelled in the model because the tapes at nip point are not heated. The elements are activated with a nip point temperature which could be the output of dynamic joule heating model in 5.3.3.2. History outputs for elements are requested and average temperature of all nodes within an element are calculated to obtain the temperature history of carbon fibre tapes.

5.4.2 Parameter analysis

In this section, the heat transfer model has been used to investigate the influence of compaction pressure, deposition velocity and heat input on the temperature history of carbon fibre tapes.

5.4.2.1 Influence of compaction pressure on temperature history

The compaction pressure only influences the thickness of carbon fibre tapes under compaction. But the tapes spring back after compaction. The TX1100 tape also has stable cyclic compaction performance and after a few times of compaction, it springs back to a relatively constant thickness (thickness before compaction) as shown in Figure 4-4. Because of the stable cyclic compaction performance of the TX1100 tape and short compaction time, the decrease of thickness under compaction is not modelled and a constant thickness is used for all five layers to simplify the model. The constant thickness also means constant fibre volume fraction of carbon fibre tapes and therefore constant thermal conductivity. The influence of compaction pressure is therefore not significant with the model as currently setup. Exaggerated conditions where all tapes have highest thermal conductivity values or lowest thermal conductivity values in section 5.2.1.2 are investigated using this model. It is found that the temperature histories show minimal differences (smaller than 3 °C) between high thermal conductivity inputs and low thermal conductivity inputs. The through-thickness heat transfer is dominant because of the large temperature differences in the through-thickness direction. But the through-thickness effective thermal conductivity of carbon fibre tape is constant independent of compaction

pressure therefore the heat transfer in through-thickness direction is almost the same. Changing compaction pressure only influences the in-plane heat transfer. Compaction pressure could influence the thermal contact resistance between the first layer of tape and the tool surface therefore it could influence the temperature history of first layer carbon fibre tapes but this needs further investigation in order to help to deposit first layer successfully.

5.4.2.2 Influence of deposition velocity on temperature history

Figure 5-22 and Figure 5-23 show the temperature history of carbon fibre tapes during the deposition of five layers with a deposition velocity of 60 mm/s and 600 mm/s and the heat inputs (nip point temperature) for the five layers kept constant. The temperature of the tape drops sharply just after contacting the cooler substrate and then decreases gradually over next one second for 600 mm/s deposition velocity or ten seconds for 60 mm/s deposition velocity. When hot carbon fibre tapes in later layers make contact with the previously deposited tapes, the temperature of the previously deposited tapes increases (as shown in 10, 20, 30, 40 s in Figure 5-22 and 1, 2, 3, 4 s in Figure 5-23) and then decreases due to conductive heat transfer to the lower layers. The increase in temperature of deposited tapes is termed 'reheating'. For the lower deposition velocity, deposited tapes have more time to transfer heat to lower layers and the tool. Heat is not accumulated much within the deposited substrates. When depositing the next layer, the reheating of deposited material is not significant (reheating temperature is around 70 °C as shown in Figure 5-22). For high deposition speed, previously deposited tapes are minimally cooled down when depositing the next layer. The reheating temperature is therefore high. In the case of 600 mm/s deposition velocity, the temperature of layer 4 can increase to around 130 °C for after layer 5 contacts with layer 4 as shown in Figure 5-23. If more layers are simulated in the model, this reheating temperature can increase to the binder activation temperature (around 150 °C) and could therefore lead to a softening of the binder bond. This could have a negative influence on the quality of manufactured preforms. This reheating of carbon fibre tapes due to later deposited layers therefore needs to be considered and possibly limited.

It is also found that for high deposition velocity, the temperature histories of different layers show large differences (around 25 °C temperature difference between adjacent layers at the time one second after deposition). These large differences could lead to different interlayer bonding properties which is not desired for manufacturing preforms with uniform quality across the whole thickness.

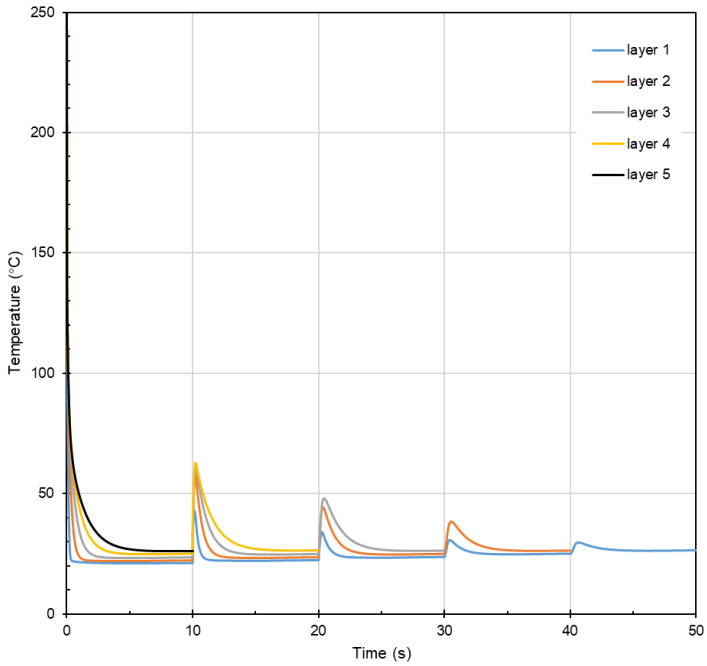

Figure 5-22 Temperature history of elements activated in the first step of each layer with deposition velocity of 60 mm/s with 250°C nip-point temperature of five layers

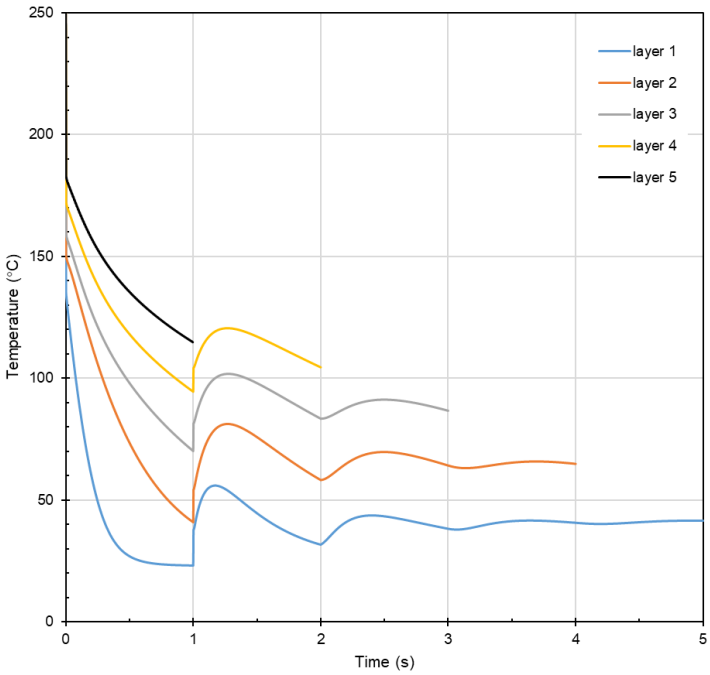

Figure 5-23 Temperature history of elements activated in the first step of each layer with deposition velocity 600 mm/s with 250°C nip point temperature of five layers

5.4.2.3 Influence of heat input and tool temperature on temperature history

The high reheating temperature and different temperature histories between layers observed for high deposition velocity are related to the accumulated heat in the previously deposited layers. Adjusting the heat input (nip point temperature) based on the substrate temperature is proposed to tackle the two issues. Table 5-2 shows

an example of manually optimised different heat inputs for different layers based on the substrate temperature at the time tapes is about to make contact with substrate.

Table 5-2 Different heat input based on the substrate temperature

Layer number	Heat input (nip point temperature) (°C)	Substrate Temperature (°C)
1	310	20.0
2	280	24.3
3	250	45.9
4	225	72.3
5	205	89.7

Figure 5-24 shows the temperature histories of five layers using the heat inputs shown in Table 5-2. The maximum reheating temperature is reduced from around 130 °C to around 110 °C compared with the temperature history results with constant heat input for all layers shown in Figure 5-23. Smaller differences of temperature history between adjacent layers are shown for all layers except layer 1. It is concluded that controlling heat input based on substrate temperature is somewhat effective in tackling the two challenges.

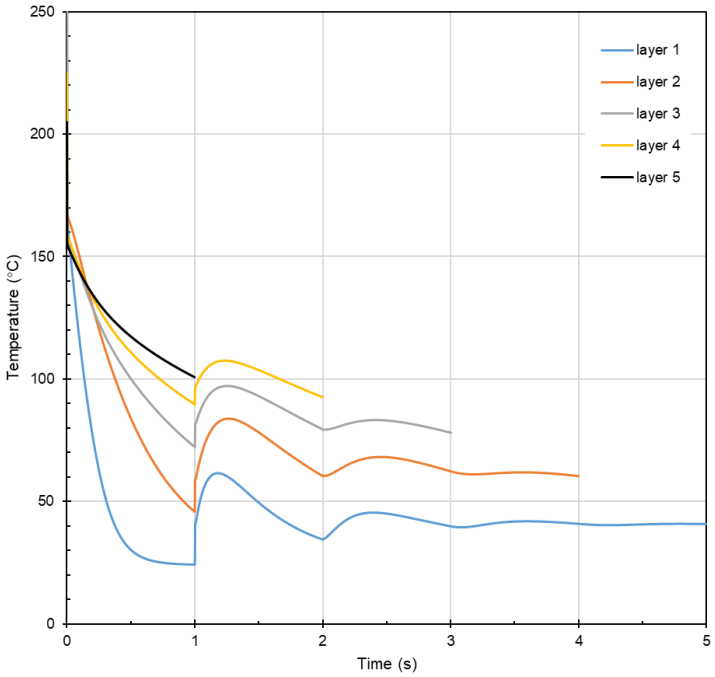

Figure 5-24 Temperature history of elements activated in the first step of each layer with different heat inputs for different layers at deposition velocity of 600 mm/s

To reduce the differences between the temperature history of first layer and subsequent layers, higher tool temperature is used. Because the tool temperature is altered, the heat inputs for different layers also need to be adjusted. A hotter tool with temperature of 40 °C is modelled with the heat inputs shown in Table 5-3. Figure

5-25 shows that differences between the temperature history of first layer and other layers are reduced. The maximum reheating temperature increases about 10 °C due to the hotter tool, but this heating is still less significant than the constant heat input using tool with room temperature as shown in Figure 5-23.

Table 5-3 Different heat input based on the substrate temperature when using hotter tool

Layer number	Heat input (nip point temperature) (°C)	Substrate Temperature (°C)
1	310	40.0
2	275	44.2
3	240	65.1
4	210	87.3
5	185	101.1

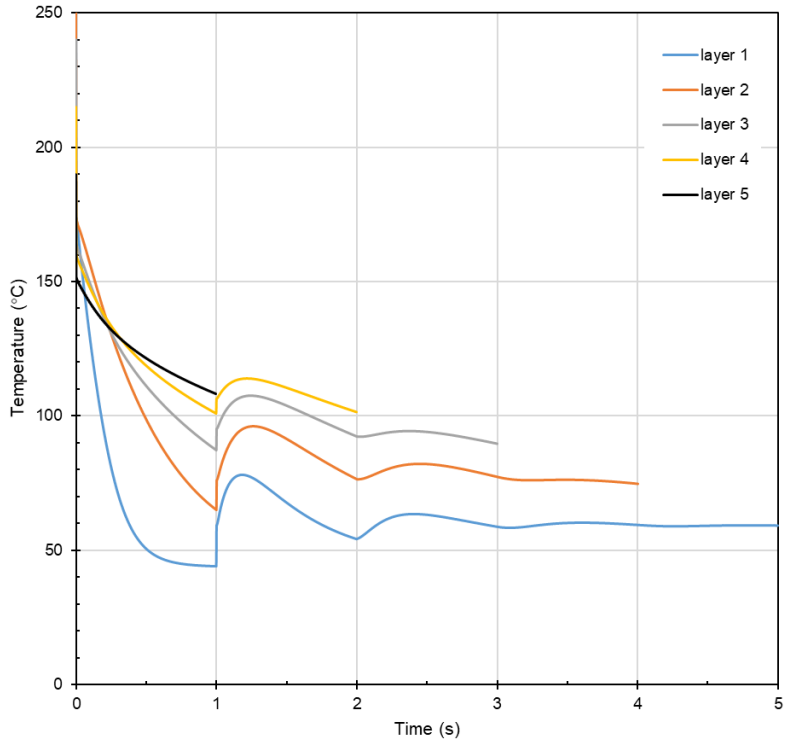

Figure 5-25 Temperature history of elements activated in the first step of each layer with different heat inputs for different layers and hotter tool at deposition velocity of 600 mm/s

5.5 Conclusions

In this chapter, the thermal properties of ADFP tapes are characterised then used in the developed models. The challenges of applying joule heating in ADFP process are investigated and tackled by characterising of the electrical contact resistance to increase the heating efficient and building analytical models to predict the joule

heating temperature. A dynamic FE heat transfer model is also built to investigate the influence of process conditions on the temperature history of deposited carbon fibre tapes. The following conclusions are obtained.

The in-plane thermal conductivity of TX1100 dry carbon fibre tapes increases linearly with the increase of fibre volume fraction but the through-thickness thermal conductivity of the tapes is independent of the fibre volume fraction. The pre-consolidation during the fabrication process of the tapes may contribute to this unexpectedly constant through-thickness thermal conductivity.

The electrical contact resistance between the carbon fibre tapes and cylinder copper electrodes at low levels of fibre tension is comparable or even higher than the electrical resistance of carbon fibre tapes. This results in low heating efficiency and heating temperature. Increasing fibre tension and contact angle can decrease the contact resistance and the joule heating efficiency is significantly increased. It is found that reducing contact resistance by increasing fibre tension can triple the heating temperature under same voltage supply.

When applying joule heating in the ADFP hardware, the cooling of tapes when travelling from the end of heating region to the nip point is significant especially at low deposition speed, therefore the cooling distance should be reduced as much as possible. The length of heating region should also be large enough because the carbon fibre tapes have more heating time and the energy wasted at the contact area is reduced. The established dynamic joule heating model predicts the nip point temperature after cooling under different deposition velocities. The predicted nip point temperature is used as the input of the heat transfer model for the whole ADFP process.

From the dynamic FE heat transfer model simulation results, the compaction pressure has minimal influence on the temperature history of deposited carbon fibre tapes except in the first layer deposition because the through-thickness thermal conductivity of the tape is independent of fibre volume fraction and compaction pressure. However, the compaction pressure can influence the thermal contact resistance between carbon fibre tapes and tool surfaces. The tool/tapes bonding is more challenging than the interlayer bonding and the temperature history of carbon fibre tapes in the first layer can influence the tool/tapes bonding quality. Therefore, the pressure dependent nature of the thermal contact resistance between carbon fibre tapes and tool surfaces needs to be characterised to refine the FE heat transfer

model and investigate the influence of compaction pressure on the temperature history of first layer of carbon fibre tapes. This can provide guidance for improving bonding quality between the first layer and the tool.

From the dynamic FE heat transfer model simulation results, it is found when deposition velocity is relatively high (600 mm/s), deposited tapes accumulate heat and have a relatively high temperature during the deposition of the next layer. This accumulated heat leads to undesired high reheating temperature of deposited tapes and significant differences of temperature histories of adjacent layers. It is also shown that adjusting heat inputs for different layers based on the substrate temperature could tackle the two challenges: high reheating temperature and different temperature histories of different layer of tapes. Using a hotter tool is also helpful to reduce the temperature history differences between first layer of carbon fibre tapes and the other layers.

In this chapter, the temperature history of carbon fibre tapes in the whole ADFP process including joule heating between electrodes, cooling before nip point and deposition on substrates, is fully captured. The observed results and developed models provide guidance of a real-time temperature control strategy proposed in 6.3.2.

6 Process parameter control of ADFP process

6.1 Introduction

Process parameters have a profound influence on the quality of ADFP manufactured preforms as evidenced in chapter 3. Precise process parameter control is desired to manufacture preforms with optimum quality. The deposition behaviour of carbon fibre tapes and simulation models developed in chapter 4 and chapter 5 provide foundations for this precise control. In this chapter, the understanding of deposition behaviour of tapes obtained in previous chapters is combined with capabilities of a lab-scale ADFP rig to implement precise parameter control.

Figure 6-1 shows the four-axis lab-scale ADFP rig. A deposition head in the rig has three movement axes, x axis (left and right in the Figure 6-1), z axis (up and down in the Figure 6-1) and c axis (rotation axis). A tool in the rig has y axis (front and back in the Figure 6-1) movement. The rig is designed to deposit up to four tapes with width of 6.35 mm. To provide process parameters feedback in real time, several sensors are installed: Axis encoders are installed to determine the position of each of the four axes. Three infrared (IR) thermometers (MICRO-EPSILON CT-SF15-C3) are installed to conduct contactless temperature measurement. One thermometer is used to measure the temperature in the joule heating region. The second one is used to measure the substrate temperature ahead of the nip point. The third one provides additional temperature measurement capability. A six degree of freedom force torque sensor (ATI Industrial Automation Axia80) can measure the forces and moments that act on the deposition head in all three orientations. A laser line scanner, which can measure surface profiles of the deposited material or the tool surface, is also included.

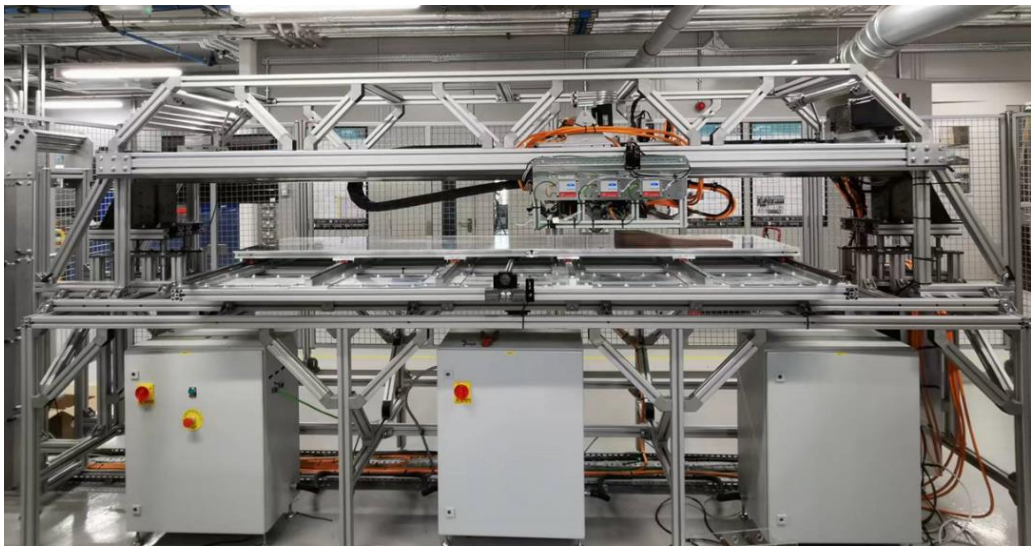

Figure 6-1 Lab-scale ADFP rig

An industrial PC (Beckhoff Automation) is used to control the rig and collect data from sensors. The industrial PC is a Windows based system which contains the programmable logic controller (PLC), Input/Output (I/O) terminals and Numerical Control (NC) within the same location, enabling real-time data exchange between each of them. Control codes for PLC are programmed using TwinCAT 3 (Beckhoff Automation) software. I/O terminals are used to collect data from sensors and send control commands to related devices.

Based on the deposition behaviours of tapes and the machine behaviour of the ADFP rig, a novel force control method is proposed and implemented for deposition on complex geometries. Two demonstrations are provided to show its effectiveness. A joule heating temperature control method is also developed and implemented. A real-time nip point temperature control framework is then proposed.

6.2 Compaction force control

Tapes used in ADFP process displays larger through-thickness deformation than thermoset prepregs during compaction in AFP as evidenced by the results in section 4.2, which means deposition head force control (particularly for thick, compliant substrates) is potentially more complex. Compliance of the deposition head and roller, material variability, and high deposition rates are known to contribute to final product variability. In many cases this variability cannot be designed out, this is therefore motivation to control machine parameters in real time based on force sensor feedback alongside models of machine and material behaviour. Complex tools, such as curved tools and tools with ramps, are commonly used in industrial applications which further complicates the control of compaction force at high speed. Work in this section shows that a single feedback controller does not work well for tools with complex geometry, therefore a model-based feed-forward control strategy is proposed to address these difficulties. The strategy is implemented on the lab ADFP rig and two demonstrations are given to show the effectiveness of proposed strategy.

6.2.1 Model-based feed-forward force feedback control strategy

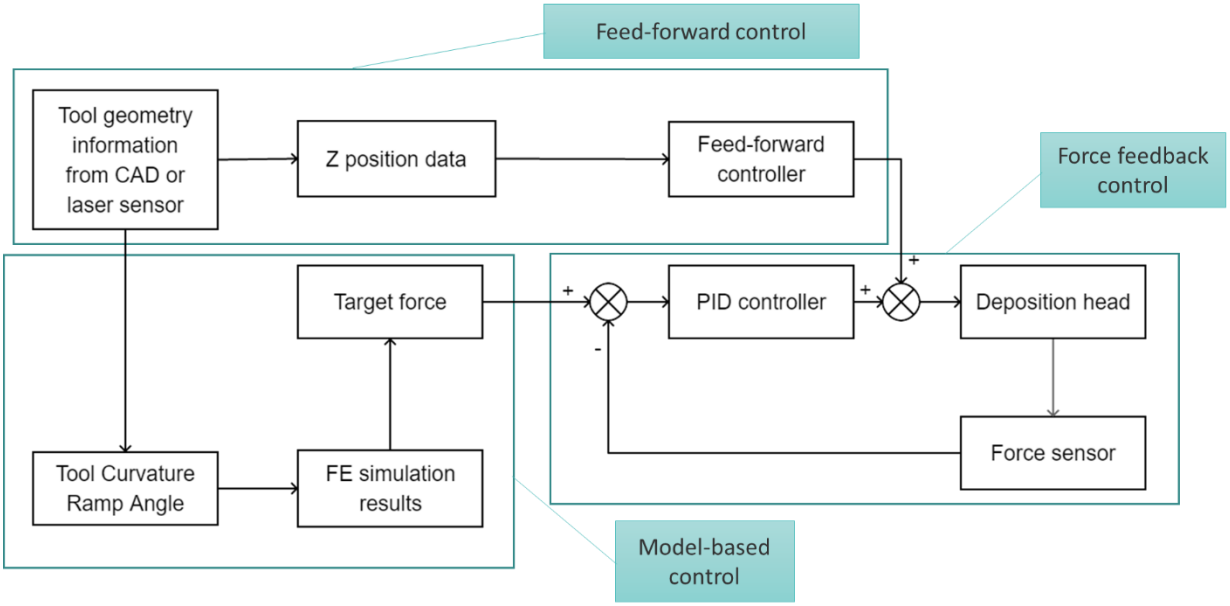

Figure 6-2 Flow chart for the model-based feed-forward force control strategy

Figure 6-2 shows the proposed force control strategy which consists of three main blocks: a force feedback control using proportional integral derivative (PID) controller, a feed-forward controller and a model-based control block. The tool geometry information can be obtained from design files of the tool or measured online using the laser line scanner. The tool geometry information is then transferred to the model based control block and the feed-forward controller. The model-based control block is used to calculate the target force based on tool geometry and models of machine and material behaviour. The feed-forward controller is used to handle tool geometry changes. The force feedback controller is used to handle the machine compliance and tape deformation. The outputs from the PID controller and the feed-forward controller are combined together and sent to the deposition head. Details of the three blocks are given in following sections.

6.2.1.1 Force feedback control

There are many potential sources of force error in the ADFP process including: the roller compliance and the large deformation of the dry fibre bed as shown in section 4.3, as well as material variability and machine compliance. A simple open-loop control method like a height based control from offline programming cannot eliminate the force errors from these multiple sources. A demonstration of height based control was conducted using the ADFP rig. The deposition head was firstly moved down to obtain a target compaction force of 50 N (as shown in Figure 6-3

when x position is zero). Z axis motion was then deactivated so that changes in height would not take place, and the deposition head started moving in the x direction. Figure 6-3 shows the force data when using a height based control method in the ADFP rig. It is found that the compaction force increases from 50 N to around 380 N when the deposition head arrives the middle area of the tool. The compaction force then decreases to around 100 N with further head movement. The maximum force error is about 330 N which is very large when compared with the target force 50 N. This is due to the bending deformation of the frame supporting the deposition head. The deflection of the frame causes compression on the compaction roller which leads to higher compaction force. A closed-loop feedback control method using online force data could potentially improve this error.

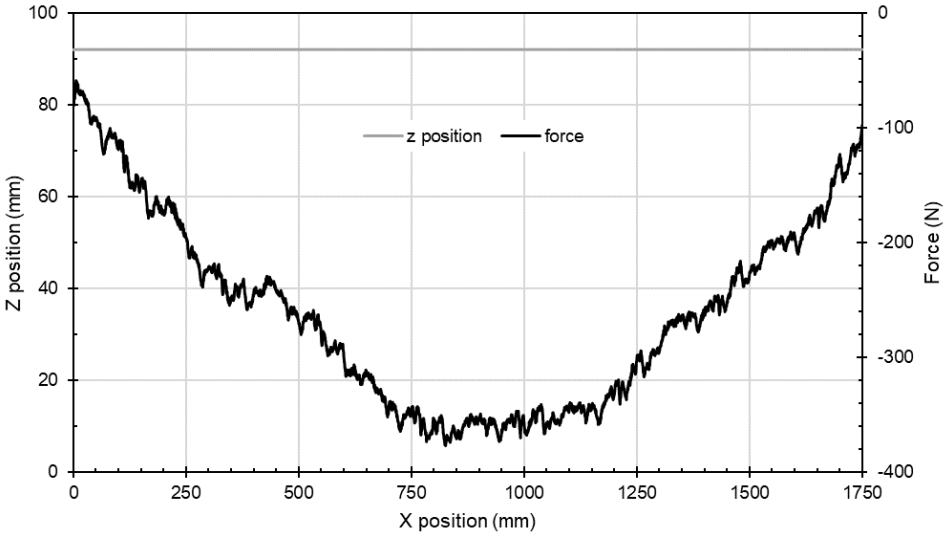

Figure 6-3 Force data when using a height based control method

A PID controller is chosen because it is relatively simple, robust and widely used in many industries. The PID controller is implemented using a built-in function block in the TwinCAT 3 software. The force sensor data in the z direction is inputted to the PID function block. The control output from the PID function block is sent to the motion control block of z axis to move up or down the deposition head in order to generate the desired force. The force sensor and encoder for the z axis have a sampling rate of 1 ms. This means the PID controller can generate control command every 1 ms. A Ziegler–Nichols method [154] is used to tune the PID controller manually. Three gains values: k_p of 0.01, T_i of 750 ms and T_d of 187.5 ms are then obtained. Figure 6-4 shows force and z position data when using the PID control method with target compaction force of 150 N. It is shown that most of the compaction force data ranges from 145 N to 155 N and the force error is around 3.3%. The deposition head moves up to overcome the deflection of the frame in order to

maintain the target force as shown in the z position curve. The PID control method shows good performance for simple flat tool geometry.

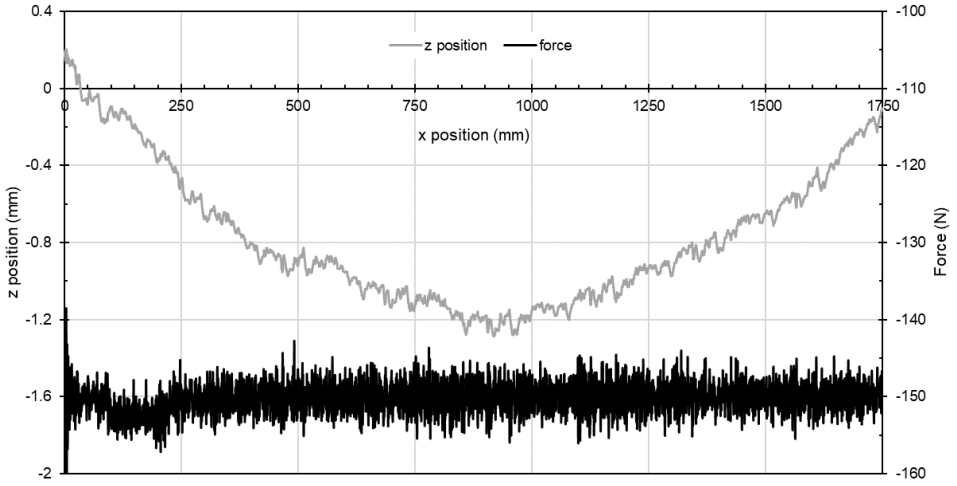

Figure 6-4 Force data when using a PID control method (negative direction in the z axis means moving head up)

6.2.1.2 Model based control

The model-based control method is used to provide target force for the force feedback controller. The target force is dependent on the compaction properties and geometries of tools. The roller compaction on dry fibres model developed in section 4.3.2 allows the derivation of target force windows for complex tools. Table 4-6 shows an example of target force windows for tools with different curvatures. For other complex tools, the same methodology shown in Figure 4-19 can be used to generate target force windows.

The target force is also dependent on the kinematics of the ADFP rig. When depositing on ramped tools, the force applied by the deposition head has an angle with the vertical direction of ramp surfaces because the ADFP rig lacks a rotational degree of freedom. Figure 6-5 shows the sketch for deposition on the tool with ramps. θ is the ramp angle. F is the force applied by the deposition head. This force is measured by the force sensor and sent to the feedback control loop. Ft is the force applying compaction to ramp surface or material surfaces. This force can be optimised using compaction model developed in section based on the compaction behaviour of tapes and compaction pressure requirement. When an optimised Ft is given, the equation $F=Ft/cos\theta$ is used to calculate the target force input F for the force feedback control loop.

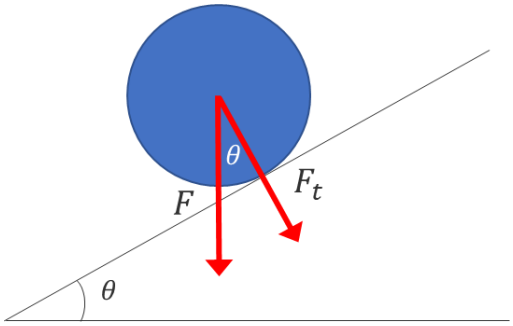

Figure 6-5 Sketch of roller compaction on ramp tool

6.2.1.3 Feed-forward control

The PID control method shows good performance for simple flat tool geometry. In practical applications, tapes are deposited on complex tools with geometry change. The feed-forward controller is therefore employed for rapid adaptation to tool geometry change based on knowledge of the underlying tool geometry. The geometry data in the compaction direction (z direction) along the deposition path derived from the tool geometry information is transferred to the feed-forward controller to pre-empt geometry changes. Due to the inertia of the deposition machine and the delay of control action (transportation lag), the deposition head cannot follow the tool geometry changes rapidly if the control output is sent to the deposition head at the location where geometry change occurs. A look-ahead distance, which is a function of deposition speed, is then introduced to compensate for the transportation lag. Figure 6-6 shows the concept of the look-ahead distance. The controller compares the geometry in the z direction of the tool at the current location with the geometry of the tool at the look-ahead distance location and generates control output to start moving the deposition head before the location where geometry change occurs.

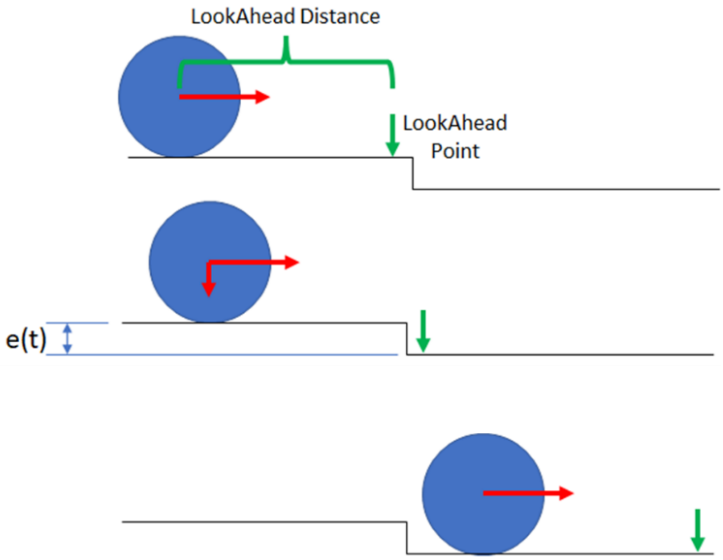

Figure 6-6 Sketch of feed-forward control strategy using a look-ahead distance

6.2.2 Demonstration on tool with steps

Figure 6-7 ADFP deposition head compaction on a tool with steps

A demonstration on a tool with steps was conducted using the lab-scale ADFP deposition rig as shown in Figure 6-7. There is no tape deposition in the demonstration for the simplicity. The tool has steps with a height of 5 mm (5 mm instant height decrease). For demonstration purposes, the geometry information is stored in the PLC in a format of a simple two-dimensional profile. Figure 6-8 shows the results from only using a PID control and using the proposed control strategy when the deposition speed is 20 mm/s and the target compaction force is 100 N. The force data response is similar for all five steps, therefore only the data for the first step is shown in the Figure 6-8. Figure 6-9 shows the adaption time and maximum force errors for only using a PID control and using the proposed control strategy. When only a PID controller is used, it took around 1 s for the compaction roller to contact the tool surface after the step (adaption time) and the compaction force dropped to around 30 N from 100 N during this time. It is therefore shown that a single PID controller does not perform well for the tools with steps even at a low deposition velocity of 20 mm/s. While for the proposed control strategy, it took around 0.6 s for the compaction roller to reach the tool surface (adaption time) and compaction force dropped to around 60 N. It is therefore shown that the proposed strategy is able to handle the tool geometry change and reduce the force error. In the future, the feed-forward controller can be further improved by optimising the look ahead distance and control parameters (like gain values).

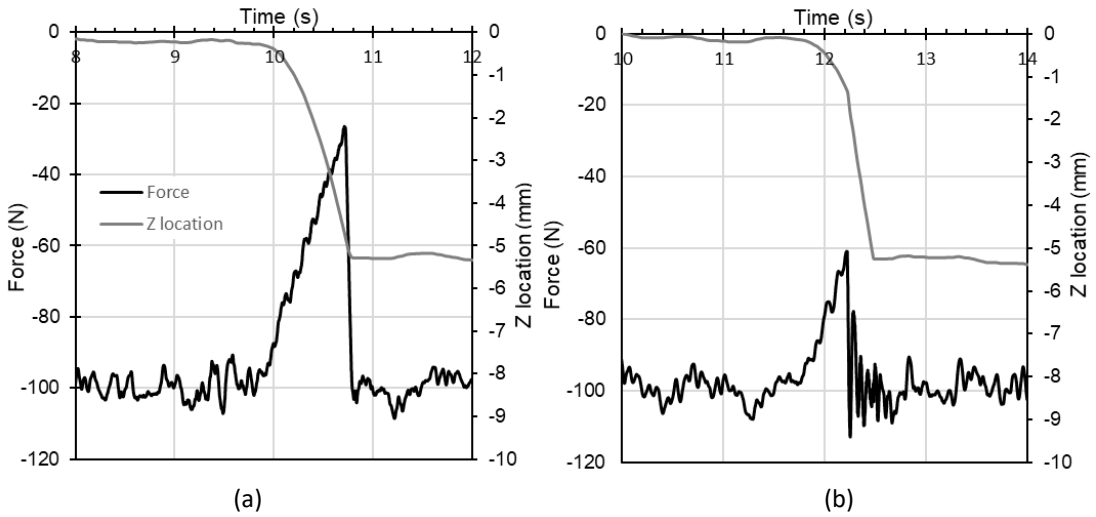

Figure 6-8 Compaction force data and z movement for the tool with steps using (a) PID control (b) Proposed control with deposition velocity of 20 mm/s, target compaction force of 100 N

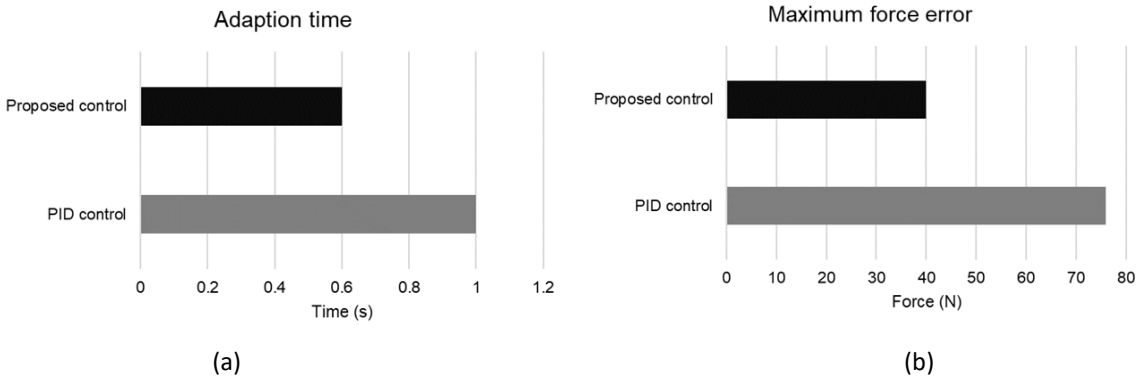

Figure 6-9 Benefits of proposed control over PID control in (a) adaption time (b) maximum force error

6.2.3 Demonstration on tool with ramps

A demonstration on a tool with ramps was also conducted using the lab-scale ADFP deposition rig as shown in Figure 6-10. There is no tape deposition in the demonstration for simplicity. The tool has two ramps with different ramp angles. For demonstration purposes, the geometry information is stored in the PLC in a format of a simple two dimensional profile. Two deposition velocities 20 mm/s and 100 mm/s were used and the target compaction force is 100 N. The performance of only using PID controller and using the proposed control method are compared.

Figure 6-10 ADFP deposition head compaction on tool with ramps

Figure 6-11 shows the force data from only using the PID controller. The performance of the PID controller is acceptable at the low deposition velocity. Only low level of force errors can be observed near the geometry change area as shown in the circles in Figure 6-11. Figure 6-12 shows the results under 100 mm/s deposition velocity from both PID control and proposed control method. It is noted that the force data has oscillations with large amplitude under 100 mm/s deposition. These oscillations are due to the vibration of the deposition head. The deposition head is not stiff enough for relatively high deposition velocity. Despite the large oscillations of force data, the advantage of the proposed control strategy over the PID control can still be observed. Larger force errors are observed near the edges of ramps for only PID control method, while most of the force data remains in the shaded area for the proposed method.

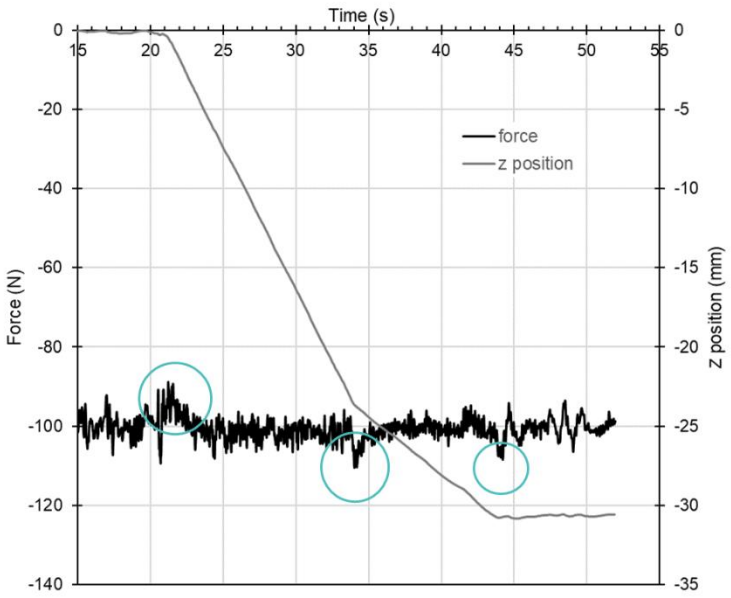

Figure 6-11 Compaction force data for PID control on the tool with ramps under deposition velocity of 20 mm/s with target compaction force of 100 N

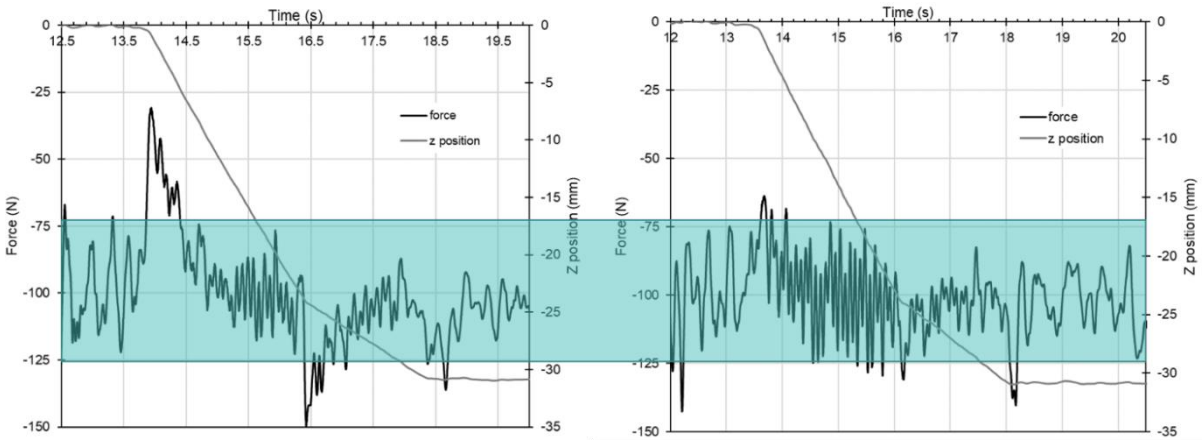

Figure 6-12 Compaction force data for (a) PID control (b) Proposed control on the tool with ramps under deposition velocity of 100 mm/s with target force of 100 N

The two simple demonstrations show the effectiveness of proposed method without tapes deposition. When depositing tapes on dry fibre bed, the proposed method could still have good performance for thin dry fibre substrate because the PID controller is robust and thin tapes substrate has minimal influence. While for thick dry fibre substrate, the PID controller parameters might need to be tuned according to the substrate thickness. Also tool geometry information from design files is not accurate enough to describe substrate information. An online substrate geometry measurement like via laser line scanner is required and it is used as the inputs for the model-based control block and the feed-forward controller.

6.3 Temperature control

Joule heating method is used in the ADFP rig and it is a local heating method where only tapes between two electrodes are heated. Tapes have a cooling period before reaching nip point. Two temperatures need to be controlled: the joule heating temperature between electrodes and the nip point temperature. In this section, a joule heating temperature control method is developed and implemented. To indirectly control the desired nip point temperature via control of the joule heating temperature between electrodes, a real-time model-based temperature control framework applying the knowledge and models developed in chapter 5 is proposed.

6.3.1 Joule heating temperature control

6.3.1.1 Pulse-width modulation power control method

In the ADFP rig, a constant 30 V is supplied to the joule heating circuit. A pulse width modulation method is used to adjust the power input. The joule heating input power is controlled by turning on and turn off the power supply in a cycle time periodically.

Figure 6-13 shows the principle of the method. t_{cycle} is the duty cycle time for switching on and switching off once. t_{on} is the time of power switching on and t_{off} is the time of power switching off. Duty cycle is defined by t_{on}/t_{cycle}. Duty cycle ranges from 0 to 1 meaning no power input to full power. These switching on and off actions are achieved by using a digital output signal to control a solid state relay connected to the joule heating circuit. When the digital output is '1', the solid state relay will the turn on the heating circuit continuously and when the digital output is '0', the solid state relay will cut off the circuit.

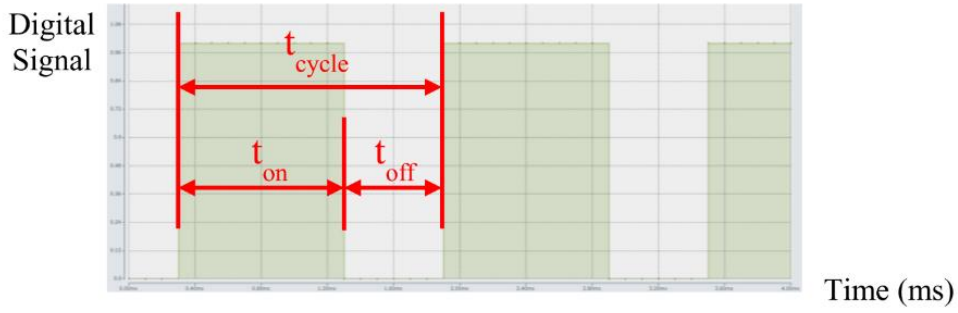

Figure 6-13 Pulse-width modulation method [146]

6.3.1.2 PID joule heating temperature control

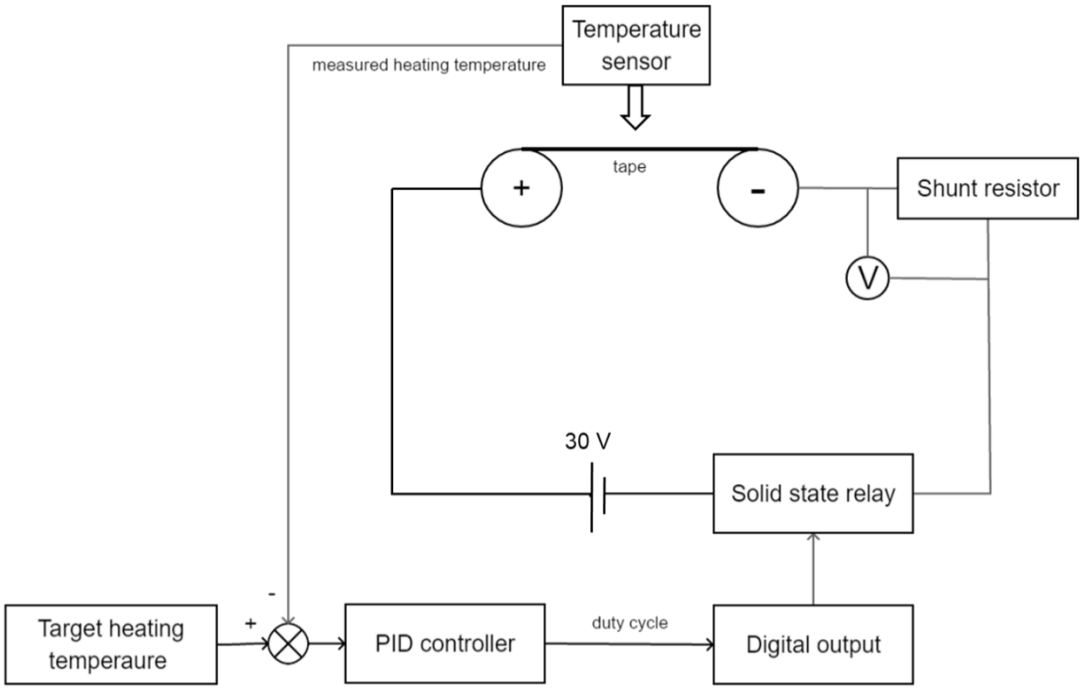

Figure 6-14 PID controller for joule heating temperature control with solid state relay in heating circuit

A closed-loop feedback control method is also required in the joule heating temperature control due to the material variability and temperature dependent properties of carbon fibre tapes. A PID controller is used to control the joule heating temperature. The PID controller is implemented using a built-in function block in the TwinCAT 3 software. The temperature sensor data is inputted to the PID function block. The control output is duty cycle which is sent to a solid-state relay to control the power input. Figure 6-14 shows the PID controller and the joule heating circuit with a solid state relay.

The PID temperature control with pulse-width modulation power control method is tested without fibre feeding using the joule heating rig shown in Figure 5-7 with a constant power supply of 15 V. The target temperature is 250 °C and duty cycle time is 50 ms. Figure 6-15 shows the temperature data with the closed-loop PID control method. It is found that temperature date is within the range from 247 °C to 250 °C and the average temperature data over the time period of 40 s is 248.9 °C. This average temperature is slightly lower than the target temperature. This lower resulting heating temperature is also observed for high target heating temperature situations. The cooling of tapes during t_{off} (the time when heating circuit is cut off) could lead to this slightly lower heating temperature. This issue is less concerning when the heating temperature is low because the cooling is less significant.

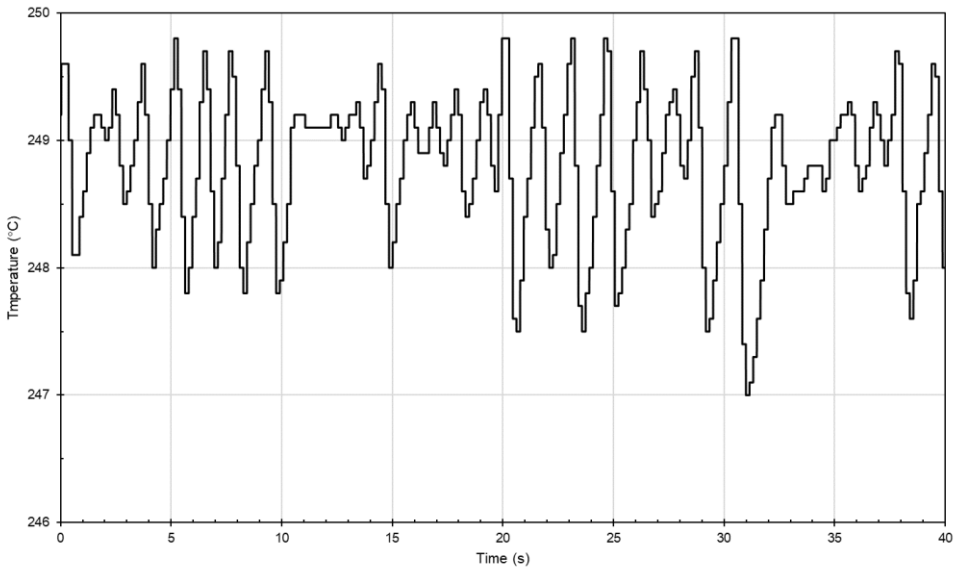

Figure 6-15 Temperature data with PID control of joule heating with target temperature of 250 °C duty cycle time of 50 ms (y axis scale from 246 °C to 250 °C)

Results shown in Figure 6-15 were generated from joule heating of static tapes without movement. Feeding movement of carbon fibre tapes could bring some variabilities for joule heating, such as contact resistance variability, feeding velocity variability and changes of fibre tension between two electrodes. However, the PID control method is robust and it is assumed that a similar level of control accuracy could be achieved for heating temperature control of tapes with feeding movement after fine tuning the PID controller. The temperature control accuracy using the developed method is significantly higher than laser heating of ADFP tapes using an open-loop heat power control based on a semi-empirical model in literature [75]. The open-loop method with the semi-empirical model in literature [75] has relatively high prediction confidence intervals of ± 12 % because the open-loop method cannot react with the variability of laser heating, and the model cannot capture all physics during the deposition.

6.3.2 Real-time model-based temperature control framework

From the conclusions of chapter 3 and chapter 5, the nip point temperature and temperature history after deposition could influence the quality of ADFP preforms. Applying control to the nip point temperature and resulting temperature history is ideal for quality control. However, the nip point temperature cannot be measured with the capability of deposition head as currently configured. Even if the nip point temperature can be measured by some methods, the measured nip point temperature is not directly helpful for the joule heating temperature control. Unlike laser heating, where heating directly enters in the nip point and the effects of control action based on the nip point temperature measurement take place in the nip point, joule heating only occurs between the two electrodes, therefore the effects of control action only take place between electrodes. These effects are ‘delayed’ when the heated tapes travel to the nip point due to the non-negligible cooling after the second electrode. A prediction of the delayed effects of control action taking place between the electrodes on nip point temperature is required. Additionally, the temperature history of deposited tapes also depends on the substrate temperature and substrate temperature measurement is required. Considering the delayed effects of control action and the effects of substrate temperature, a real-time temperature control framework based on models developed in chapter 5 is proposed to control the nip point temperature and temperature history to some extent.

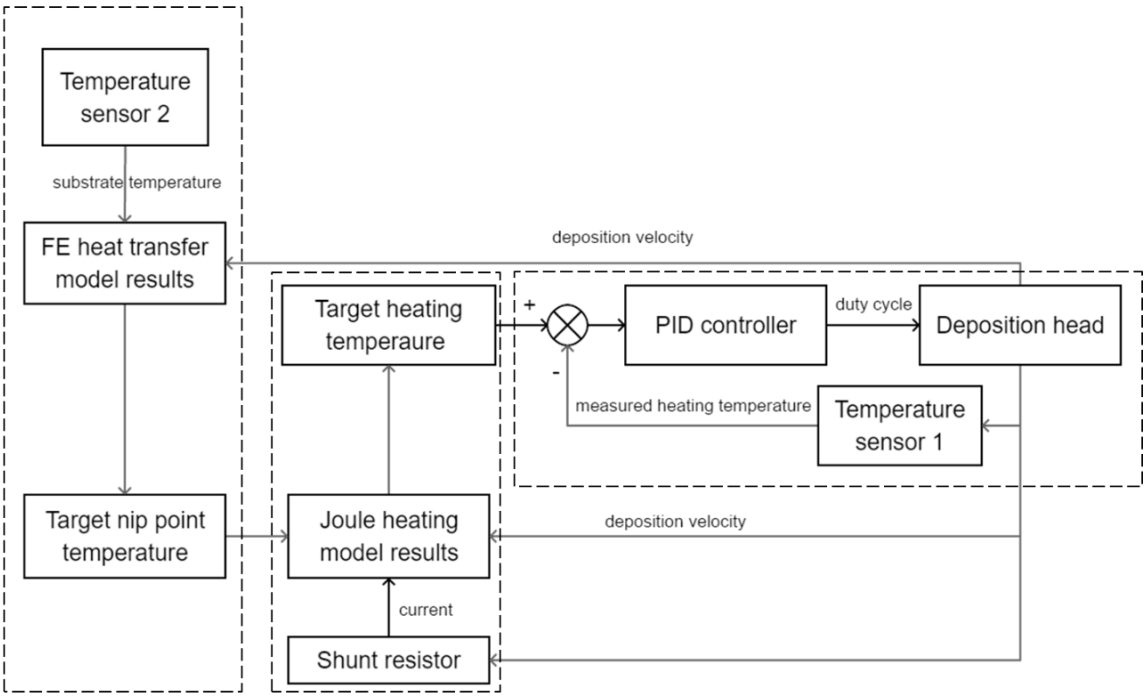

Figure 6-16 Real-time model-based temperature control framework

Figure 6-16 shows the proposed framework which consists of three main blocks. Figure 6-17 shows the sketch of heating unit in the ADFP rig. The block on the left-hand side of Figure 6-16 applies the knowledge obtained using the dynamic FE heat transfer model developed in section 5.4: controlling heating power based on the substrate temperature is helpful for improving preform quality. Substrate temperature is measured by 'Temperature sensor 2' shown in Figure 6-17 in real-time. Based on the measured substrate temperature, target temperature history and FE model results, an optimised nip point temperature target can be calculated dynamically and then inputted to the second block in the middle of Figure 6-16. This block applies the dynamic joule heating model developed in 5.3.3.2. The measured current and deposition velocity are combined with the dynamic joule heating model results to calculate the required joule heating temperature which can compensate for the cooling effects between the second roller and the nip point. The required joule heating temperature is then inputted to the closed-loop PID controller blocks on the right hand Figure 6-16. The joule heating temperature is measured by 'Temperature sensor 1' shown in Figure 6-17 in real-time.

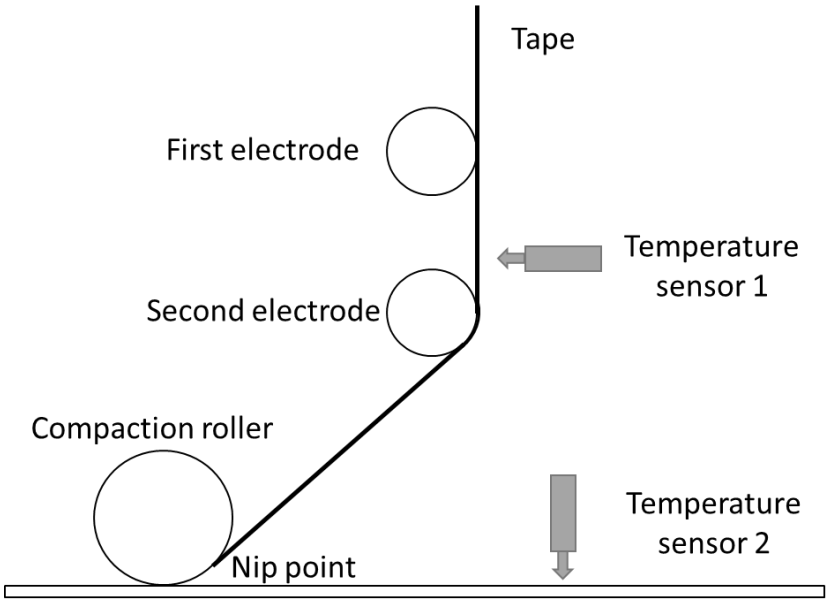

Figure 6-17 Sketch of temperature sensor location for proposed real-time model-based temperature control framework

This framework has not yet been implemented to the lab-scale ADFP rig because it has not been fully developed. The efficacy of this framework also depends on the sampling rate of sensors and the computing time of the models. The thermometers have a sampling rate of 150 ms. It is ideal that the real-time model computing time is less than 150 ms. For the dynamic joule heating model, the computing time is short and simulation interval time as shown in equation (5.9) can be optimised to further reduce computing time without losing significant prediction accuracy. For the dynamic FE heat transfer model, there are two methods which could help to reduce the computing time: The model can be simplified by reducing the time of interests and dimension of interests, like a one-dimensional model simulating temperature history in a period of 1 s; The model could generate large number of simulation results under different process conditions and the results could be used to train a machine learning based model.

6.4 Conclusion

In this chapter, the capability of the lab-scale ADFP rig is introduced. Control methods for compaction force and heating temperature in ADFP process are developed with the help of the understanding and models of ADFP tapes behaviour obtained in chapter 4 and chapter 5. The following conclusions are obtained.

A model-based feed-forward force control method is developed in order to handle the large deformation of carbon fibre tapes and deposition on complex tools. The force control method is implemented in the ADFP rig. Two demonstrations using tools with ramps and steps are conducted and it is shown that smaller force errors and more rapid response to tool geometry change are obtained using the proposed force control method compared to the traditional PID control method. For tool with significant geometry change (such as high steps) or deposition with high velocity, the proposed model-based feed-forward force control method is a better option than traditional PID control method.

A PID controller with a pulse-width modulation power control method is developed for joule heating temperature control between two electrodes. The method is implemented and tested using a joule heating rig. A high level of control accuracy can be achieved. For a target heating temperature of 250 °C, the joule heating temperature error is less than 1.6 %. This is achieved without fibre feeding movement and the fibre feed movement could bring fibre tension changes which might lead to contact resistance variation and heating temperature variation. However, fine tuning of the PID controller could in some extent handle variation due to fibre tension changes and it will be conducted in the future.

A real-time model-based temperature control framework is proposed to indirectly control nip point temperature by controlling the local joule heating temperature with the help of the dynamic joule heating model and the FE heat transfer model developed in chapter 5. The framework can be implemented in the lab-scale ADFP rig when it is fully developed and the models are simplified to achieve fast real-time computing.

7 Conclusions and Future Work

7.1 Conclusions

ADFP has the potential for manufacturing preforms with high rate and high quality, but this is currently limited by poor understanding of the material behaviour of ADFP tapes under relevant process conditions. In this thesis, to improve the quality of ADFP manufactured preforms by improved understanding the deposition behaviour of carbon fibre tapes, the influence of key process parameters on the bonding quality of ADFP manufactured preforms is firstly investigated. The material behaviour of dry carbon fibre tapes under roller compaction and joule heating is then investigated. Simulation models are built to aid understanding and provide guidance for accurate process parameter control. Real-time model-based process parameter control methods are developed and implemented to the lab-scale ADFP rig. The following conclusions are obtained:

Although commercial ADFP tapes are relatively expensive and highly engineered, they have a more stable and stiffer performance in the through-thickness direction than normal dry carbon fibre tows and fabrics. The commercial tapes exhibit less deformation under compaction than normal tows, which reduces the difficulty of compaction force control. The thickness and compaction response of the tapes have a minimal change after a few compaction cycles in cyclic compaction testing. This means that debulking cycles for the tapes after deposition might be minimised. The effective through-thickness thermal conductivity of the tapes is found to be independent of the fibre volume fraction. This leads to relatively simple understanding and modelling of temperature history of deposited tapes. A long term goal is to improve ADFP process or deposition hardware to reduce the demand on high performance expensive highly engineered tapes in order to reduce material costs.

The interlayer bonding quality of ADFP manufactured preforms is significantly lower than that of both preforms manufactured by long term isothermal consolidation and that of AFP manufactured prepreg preforms. Therefore, process parameters for ADFP need to be chosen carefully and controlled precisely. For the influence of process parameters on the interlayer bonding quality, increasing heating temperature above a critical temperature increases the interlayer bonding but peak bonding quality is observed at 233 °C for TX1100 tapes. Low levels of compaction force are helpful for improving bonding quality but excessive compaction forces have a negative influence on the bonding quality. This negative influence of excessive

forces agrees with the research on the fibre volume fraction of ADFP manufactured preforms [120, 121] and interlayer bonding of AFP-manufactured thermoplastic composites [143].

A roller compaction on dry fibre bed finite element model is built with experimentally characterised non-linear compaction response of the tapes. The model is validated using a pressure measurement film. The model is used to analyse the roller compaction pressure distribution on a dry fibre bed with complex shaped tools. Target force windows are obtained for curved tools based on the compaction pressure requirement and the compaction pressure distribution. The target force windows are also used as the input of the controller used in compaction force control. It is recommended that compliant compaction rollers should be used in ADFP process because pressure distribution on curved tools generated by the compliant compaction rollers is more uniform.

Two main challenges have been found in attempting the application of joule heating methods in an ADFP configuration: the electrical contact resistance between carbon fibre tapes and cylinder electrodes reduces the joule heating efficiency and temperature; the rapid cooling upon leaving the joule heating region brings difficulties for nip point temperature control. It is found that the contact resistance can be reduced significantly by increasing the fibre tension and the contact angle between tapes and electrodes. An experimentally validated dynamic joule heating analytical model is built to predict the joule heating temperature in the heating region and the nip point temperature after cooling under different deposition velocity. It is shown that the cooling before nip point is significant especially when the deposition velocity is low.

A dynamic FE heat transfer model is built using experimentally characterised thermal conductivity and specific heat of the tapes to simulate the temperature history of deposited tapes. From the simulation results, two challenges have been found: ‘reheating’ of carbon fibre tapes and different temperature histories of different layers. It is found that adjusting the nip point temperature based on knowledge of the substrate temperature could address the two challenges: the maximum reheating temperature shows a 15% drop and differences of temperature history is reduced.

A model-based feed-forward force control method is developed and implemented in the ADFP rig in order to handle the large deformation of carbon fibre tapes and

compaction rollers and to more accurately control deposition on complex tools. Target force windows generated by the roller compaction model are used as the input of the controller. Two demonstrations of deposition on tools with ramps and steps are conducted and it is shown that a 47 % smaller force error and more rapid response to tool geometry change are obtained using the proposed force control method.

A PID controller with a pulse-width modulation power control method is developed and implemented in the joule heating rig for joule heating temperature control between two electrodes. A high level of heating temperature control accuracy temperature (error is less than 1.6 %) can be achieved. A real-time model-based temperature control framework is proposed to indirectly control nip point temperature. The target nip point temperature is calculated dynamically according to the substrate temperature measurement and the learning from dynamic FE heat transfer model. The target heating temperature for the PID controller is calculated based on calculated target nip point temperature and the joule heating model. The framework will be implemented in the lab-scale ADFP rig when it is fully developed.

7.2 Future work

The following work could be conducted in order to further improve the quality of ADFP manufactured preforms in the future.

1. Implement the proposed model-based real-time temperature control framework.

To implement the framework, the PID controller of joule heating temperature control between two electrodes needs to be tuned with the tape feeding movement to handle the heating temperature variation due to the inevitable variation of fibre tension during tape feeding. The dynamic FE heat transfer model needs experimental validation before simplification.

2. Investigate the influence of high deposition velocity on the quality of ADFP manufactured preforms.

The influence of deposition velocity on the quality of ADFP manufactured preforms has been investigated at low deposition velocities (from 2 mm/s to 20 mm/s) and the results are not highly conclusive due to the mock ADFP setup in this work as discussed in 3.3.4. It is recommended to manufacture samples under different deposition velocity with real ADFP consolidation to investigate the influence of deposition velocity. To manufacture good preforms at higher rates, the influence of high

deposition velocity (around 1 m/s) on the quality of ADFP manufactured preforms is also required to be investigated.

3. Test the proposed force control method in more challenging scenarios: with tape deposition, deposition on thick substrates and high velocity deposition.

The model-based feed-forward force control method shows effectiveness without carbon fibre tapes deposition. The deformation of tapes especially for thick substrate could bring more variabilities and difficulties which influence of efficiency of the force control method. High velocity deposition could also bring more variability and difficulties such as vibration of deposition head or roller, high requirement of cycle time of PLC and controllers. Therefore, the controllers in the proposed method may need adjustment and turning in these more challenging scenarios.

4. Investigate influence of process parameters on the tool/first layer bonding quality.

Sufficient tool/tapes bonding is believed to be more challenging to obtain than interlayer bonding. To deposit the first layer successfully, the influence of process parameters on the tool/first layer bonding needs to be investigated for the purpose of process parameter optimisation. Understanding the temperature history of tapes in first layer is beneficial to investigate the bonding formation. The dynamic FE model could predict the temperature history of the first layer but the compaction pressure dependent tool/first layer thermal contact resistance needs to be characterised in order to improve the accuracy of temperature history prediction.

References

[1] Tsai SW. Double–Double: New Family of Composite Laminates. AIAA Journal. 2021;59:4293-305.

[2] Demir E, Yousefi-Louyeh P, Yildiz M. Design of variable stiffness composite structures using lamination parameters with fiber steering constraint. Composites Part B: Engineering. 2019;165:733-46.

[3] Brasington A, Sacco C, Halbritter J, Wehbe R, Harik R. Automated fiber placement: A review of history, current technologies, and future paths forward. Composites Part C: Open Access. 2021;6.

[4] Zhang L, Wang X, Pei J, Zhou Y. Review of automated fibre placement and its prospects for advanced composites. Journal of Materials Science. 2020;55:7121-55.

[5] Kollmannsberger A, Lichtinger R, Hohenester F, Ebel C, Drechsler K. Numerical analysis of the temperature profile during the laser-assisted automated fiber placement of CFRP tapes with thermoplastic matrix. Journal of Thermoplastic Composite Materials. 2017;31:1563-86.

[6] Assadi M, Field T. AFP Processing of Dry Fiber Carbon Materials (DFP) for Improved Rates and Reliability. SAE Technical Paper Series2020.

[7] Kadiyala AK, Portela A, Devlin K, Lee S, O'Carroll A, Jones D, et al. Mechanical evaluation and failure analysis of composite laminates manufactured using automated dry fibre tape placement followed by liquid resin infusion. Composites Science and Technology. 2021;201.

[8] Liu YN, Yuan C, Liu C, Pan J, Dong Q. Study on the resin infusion process based on automated fiber placement fabricated dry fiber preform. Sci Rep. 2019;9:7440.

[9] Veldenz L, Di Francesco M, Giddings P, Kim BC, Potter K. Material selection for automated dry fiber placement using the analytical hierarchy process. Advanced Manufacturing: Polymer & Composites Science. 2019;4:83-96.

[10] Potter K. 6 - Automated fibre placement. In: Harper L, Clifford M, editors. Design and Manufacture of Structural Composites: Woodhead Publishing; 2023. p. 125-43.

[11] Cassola S, Duhovic M, Schmidt T, May D. Machine learning for polymer composites process simulation – a review. Composites Part B: Engineering. 2022;246.

[12] Crossley RJ, Schubel PJ, De Focatiis DSA. Time–temperature equivalence in the tack and dynamic stiffness of polymer prepreg and its application to automated composites manufacturing. Composites Part A: Applied Science and Manufacturing. 2013;52:126-33.

[13] Crossley RJ, Schubel PJ, Warrior NA. Experimental determination and control of prepreg tack for automated manufacture. Plastics, Rubber and Composites. 2013;40:363-8.

[14] Crossley RJ, Schubel PJ, Warrior NA. The experimental determination of prepreg tack and dynamic stiffness. Composites Part A: Applied Science and Manufacturing. 2012;43:423-34.
[15] Endruweit A, Ghose S, Johnson BA, Kelly S, De Focatiis DS, Warrior NA. Tack testing to Aid Optimisation of Process Parameters for Automated Material Placement in an Industrial Environment. Annual International Conference on Composite Materials (ICCM 21), Xi'an2017. p. 20-5.
[16] Endruweit A, Choong GYH, Ghose S, Johnson BA, Younkin DR, Warrior NA, et al. Characterisation of tack for uni-directional prepreg tape employing a continuous application-and-peel test method. Composites Part A: Applied Science and Manufacturing. 2018;114:295-306.
[17] Wang Y, Mahapatra S, Belnoue JPH, Ivanov DS, Hallett SR. Understanding tack behaviour during prepreg-based composites' processing. Composites Part A: Applied Science and Manufacturing. 2023;164.
[18] Bakhshi N, Hojjati M. An experimental and simulative study on the defects appeared during tow steering in automated fiber placement. Composites Part A: Applied Science and Manufacturing. 2018;113:122-31.
[19] Wang Y, Mahapatra S, P.-H. Belnoue J, Ivanov DS, Hallett SR. Modelling the effect of process conditions on steering-induced defects in automated fibre placement (AFP). Composites Part A: Applied Science and Manufacturing. 2023;173.
[20] Rao S, Umer R, Thomas J, Cantwell WJ. Investigation of peel resistance during the fibre placement process. Journal of Reinforced Plastics and Composites. 2015;35:275-86.
[21] Stokes-Griffin CM, Kollmannsberger A, Compston P, Drechsler K. The effect of processing temperature on wedge peel strength of CF/PA 6 laminates manufactured in a laser tape placement process. Composites Part A: Applied Science and Manufacturing. 2019;121:84-91.
[22] Satheesh B, Tonejc M, Potakowskyj L, Pletz M, Fauster E, Kaynak B, et al. Peel strength characterisation on ply/ply interface using wedge and T-peel/pull-type tests. Polymers and Polymer Composites. 2018;26:431-45.
[23] Comer A, Hammond P, Ray D, Lyons J, Obande W, Jones D, et al. Wedge peel interlaminar toughness of carbon-fibre/PEEK thermoplastic laminates manufactured by laser-assisted automated-tape-placement (LATP). SETEC. 2014;14:10-1.
[24] Khan MA, Mitschang P, Schledjewski R. Parametric study on processing parameters and resulting part quality through thermoplastic tape placement process. Journal of Composite Materials. 2013;47:485-99.

[25] Khan MA, Mitschang P, Schledjewski R. Identification of some optimal parameters to achieve higher laminate quality through tape placement process. Advances in Polymer Technology. 2010;29:98-111.
[26] Zhao P, Shirinzadeh B, Shi Y, Cheuk S, Clark L. Multi-pass layup process for thermoplastic composites using robotic fiber placement. Robotics and Computer-Integrated Manufacturing. 2018;49:277-84.
[27] Zhao P, Shirinzadeh B, Shi Y, Cheuk S, Clark L. Improved uniform degree of multi-layer interlaminar bonding strength for composite laminate. Journal of Reinforced Plastics and Composites. 2017;36:1211-24.
[28] Çelik O, Peeters D, Dransfeld C, Teuwen J. Intimate contact development during laser assisted fiber placement: Microstructure and effect of process parameters. Composites Part A: Applied Science and Manufacturing. 2020;134.
[29] Aized T, Shirinzadeh B. Robotic fiber placement process analysis and optimization using response surface method. The International Journal of Advanced Manufacturing Technology. 2010;55:393-404.
[30] Cheng J, Zhao D, Liu K, Wang Y. Process modeling and parameter optimization based on assumed inherent sensor inversion for composite automated placement. Journal of Reinforced Plastics and Composites. 2016;36:226-38.
[31] Han Z, Sun S, Fu H, Fu Y. Multi-Scale Low-Entropy Method for Optimizing the Processing Parameters during Automated Fiber Placement. Materials (Basel). 2017;10.
[32] Han Z, Sun S, Fu Y, Fu H. Multiscale analysis of the correlation of processing parameters on viscidity of composites fabricated by automated fiber placement. Materials Research Express. 2017;4.
[33] Han Z, Sun S, Shao Z, Fu H. Multiscale Collaborative Optimization of Processing Parameters for Carbon Fiber/Epoxy Laminates Fabricated by High-Speed Automated Fiber Placement. Advances in Materials Science and Engineering. 2016;2016:1-14.
[34] Albazzan MA, Harik R, Tatting BF, Gürdal Z. Efficient design optimization of nonconventional laminated composites using lamination parameters: A state of the art. Composite Structures. 2019;209:362-74.
[35] Montemurro M, Pagani A, Fiordilino GA, Pailhès J, Carrera E. A general multi-scale two-level optimisation strategy for designing composite stiffened panels. Composite Structures. 2018;201:968-79.
[36] Wehbe R, Harik R, Gurdal Z. In-plane tow deformations due to steering in automated fiber placement2019.
[37] Kim BC, Weaver PM, Potter K. Manufacturing characteristics of the continuous tow shearing method for manufacturing of variable angle tow composites. Composites Part A: Applied Science and Manufacturing. 2014;61:141-51.

[38] Zhao C, Xiao J, Huang W, Huang X, Gu S. Layup quality evaluation of fiber trajectory based on prepreg tow deformability for automated fiber placement. Journal of Reinforced Plastics and Composites. 2016;35:1576-85.
[39] Zhang P, Sun R, Zhao X, Hu L. Placement suitability criteria of composite tape for mould surface in automated tape placement. Chinese Journal of Aeronautics. 2015;28:1574-81.
[40] Montemurro M, Catapano A. On the effective integration of manufacturability constraints within the multi-scale methodology for designing variable angle-tow laminates. Composite Structures. 2017;161:145-59.
[41] Arian Nik M, Fayazbakhsh K, Pasini D, Lessard L. Optimization of variable stiffness composites with embedded defects induced by Automated Fiber Placement. Composite Structures. 2014;107:160-6.
[42] Rousseau G, Wehbe R, Halbritter J, Harik R. Automated Fiber Placement Path Planning: A state-of-the-art review. Computer-Aided Design and Applications. 2018;16:172-203.
[43] Harik R, Saidy C, Williams S, Gurdal Z, Grimsley B. Automated fiber placement defect identity cards: cause, anticipation, existence, significance, and progression2018.
[44] Heinecke F, Willberg C. Manufacturing-Induced Imperfections in Composite Parts Manufactured via Automated Fiber Placement. Journal of Composites Science. 2019;3.
[45] Oromiehie E, Prusty BG, Compston P, Rajan G. Automated fibre placement based composite structures: Review on the defects, impacts and inspections techniques. Composite Structures. 2019;224.
[46] Lichtinger R, Lacalle J, Hinterhölzl R, Beier U, Drechsler K. Simulation and experimental validation of gaps and bridging in the automated fiber placement process. Science and Engineering of Composite Materials. 2015;22.
[47] Belnoue JPH, Mesogitis T, Nixon-Pearson OJ, Kratz J, Ivanov DS, Partridge IK, et al. Understanding and predicting defect formation in automated fibre placement pre-preg laminates. Composites Part A: Applied Science and Manufacturing. 2017;102:196-206.
[48] Rajan S, Sutton MA, Wehbe R, Tatting B, Gürdal Z, Kidane A, et al. Experimental investigation of prepreg slit tape wrinkling during automated fiber placement process using StereoDIC. Composites Part B: Engineering. 2019;160:546-57.
[49] Croft K, Lessard L, Pasini D, Hojjati M, Chen J, Yousefpour A. Experimental study of the effect of automated fiber placement induced defects on performance of composite laminates. Composites Part A: Applied Science and Manufacturing. 2011;42:484-91.

[50] Lan M, Cartié D, Davies P, Baley C. Influence of embedded gap and overlap fiber placement defects on the microstructure and shear and compression properties of carbon–epoxy laminates. Composites Part A: Applied Science and Manufacturing. 2016;82:198-207.

[51] Guin WE, Jackson JR, Bosley CM. Effects of tow-to-tow gaps in composite laminates fabricated via automated fiber placement. Composites Part A: Applied Science and Manufacturing. 2018;115:66-75.

[52] Elsherbini YM, Hoa SV. Experimental and numerical investigation of the effect of gaps on fatigue behavior of unidirectional carbon/epoxy automated fiber placement laminates. Journal of Composite Materials. 2016;51:759-72.

[53] Shadmehri F, Ioachim O, Pahud O, Brunel J, Landry A, Hoa V, et al. Laser-vision inspection system for automated fiber placement (AFP) process. 20th International conference on composite materials Copenhagen2015.

[54] Cemenska J, Rudberg T, Henscheid M. Automated in-process inspection system for AFP machines. Additive Manufacturing of Aerospace Composite Structures: Fabrication and Reliability. 2017;8:35.

[55] Denkena B, Schmidt C, Völtzer K, Hocke T. Thermographic online monitoring system for Automated Fiber Placement processes. Composites Part B: Engineering. 2016;97:239-43.

[56] Gregory ED, Juarez PD. In-situ thermography of automated fiber placement parts. AIP conference proceedings: AIP Publishing; 2018.

[57] Oromiehie E, Prusty BG, Compston P, Rajan G. In situ process monitoring for automated fibre placement using fibre Bragg grating sensors. Structural Health Monitoring. 2016;15:706-14.

[58] Schmidt C, Schultz C, Weber P, Denkena B. Evaluation of eddy current testing for quality assurance and process monitoring of automated fiber placement. Composites Part B: Engineering. 2014;56:109-16.

[59] Budelmann D, Detampel H, Schmidt C, Meiners D. Interaction of process parameters and material properties with regard to prepreg tack in automated lay-up and draping processes. Composites Part A: Applied Science and Manufacturing. 2019;117:308-16.

[60] Tierney J, Gillespie JW. Modeling of In Situ Strength Development for the Thermoplastic Composite Tow Placement Process. Journal of Composite Materials. 2006;40:1487-506.

[61] Oromiehie E, Prusty GB, Compston PP, Rajan G. The influence of consolidation force on the performance of AFP manufactured laminates. 21st International Conference on Composite Materials (ICCM-21). Xi'an2017.

[62] Liu X, Qian S, Ye Y, Xu Q, Li X. Effect of process parameters on mode-II interlaminar fracture toughness and fractographic features of automated fibre placement prepreg laminates. Journal of Composite Materials. 2021.
[63] Miao Q, Dai Z, Ma G, Niu F, Wu D. Effect of consolidation force on interlaminar shear strength of CF/PEEK laminates manufactured by laser-assisted forming. Composite Structures. 2021;266.
[64] Oromiehie E, Gain AK, Prusty BG. Processing parameter optimisation for automated fibre placement (AFP) manufactured thermoplastic composites. Composite Structures. 2021;272.
[65] Bakhshi N, Hojjati M. Effect of compaction roller on layup quality and defects formation in automated fiber placement. Journal of Reinforced Plastics and Composites. 2019.
[66] Cheng J, Zhao D, Chen H, Zhang Y, Wang Y. Effect of the attitude fine-adjustment of compaction roller on automated fiber placement defects and trajectory. Journal of Reinforced Plastics and Composites. 2019.
[67] Jiang J, He Y, Ke Y. Pressure distribution for automated fiber placement and design optimization of compaction rollers. Journal of Reinforced Plastics and Composites. 2019.
[68] Ammar MMA, Shirinzadeh B. The Role of Compaction Roller in Defining the Layup Quality and Laminate Porosity in Robotic Fiber Placement. 2021 24th International Conference on Mechatronics Technology (ICMT)2021. p. 1-6.
[69] Chu Q, Li Y, Xiao J, Huan D, Zhang X. Placeability restricted by in-complete contact between laying roller and mould in an automated fiber placement process. Journal of Reinforced Plastics and Composites. 2018;37:475-89.
[70] Venkatesan C, Zulkifli F, Silva A. Effects of processing parameters of infrared-based automated fiber placement on mechanical performance of carbon fiber-reinforced thermoplastic composite. Composite Structures. 2023;309.
[71] Qu W, He R, Cheng L, Yang D, Gao J, Wang H, et al. Placement suitability analysis of automated fiber placement on curved surfaces considering the influence of prepreg tow, roller and AFP machine. Composite Structures. 2021;262.
[72] Jiang J, He Y, Wang H, Ke Y. Modeling and experimental validation of compaction pressure distribution for automated fiber placement. Composite Structures. 2021;256.
[73] He Y, Jiang J, Qu W, Ke Y. Compaction pressure distribution and pressure uniformity of segmented rollers for automated fiber placement. Journal of Reinforced Plastics and Composites. 2021.
[74] Hörmann P, Stelzl D, Lichtinger R, Van Nieuwenhove S, Mazón Carro G, Drechsler K. On the numerical prediction of radiative heat transfer for thermoset automated

fiber placement. Composites Part A, Applied science and manufacturing. 2014;67:282-8.
[75] Di Francesco M, Veldenz L, Dell'Anno G, Potter K. Heater power control for multi-material, variable speed Automated Fibre Placement. Composites Part A: Applied Science and Manufacturing. 2017;101:408-21.
[76] Schledjewski R, Yadav N. Parameter Selection for Peel Strength Optimization of Thermoplastic CF-PA6 for Humm3TM. Key engineering materials. 2019;809:297-302.
[77] Stokes-Griffin C, Compston P. A combined optical-thermal model for near-infrared laser heating of thermoplastic composites in an automated tape placement process. Composites Part A: Applied Science and Manufacturing. 2015;75:104-15.
[78] Stokes-Griffin CM, Compston P, Matuszyk TI, Cardew-Hall MJ. Thermal modelling of the laser-assisted thermoplastic tape placement process. Journal of Thermoplastic Composite Materials. 2013;28:1445-62.
[79] Weiler T, Emonts M, Wollenburg L, Janssen H. Transient thermal analysis of laser-assisted thermoplastic tape placement at high process speeds by use of analytical solutions. Journal of Thermoplastic Composite Materials. 2018;31:311-38.
[80] Donough MJ, Shafaq, St John NA, Philips AW, Gangadhara Prusty B. Process modelling of In-situ consolidated thermoplastic composite by automated fibre placement – A review. Composites Part A: Applied Science and Manufacturing. 2022;163.
[81] Hassan N, Thompson JE, Batra RC, Hulcher AB, Song X, Loos AC. A Heat Transfer Analysis of the Fiber Placement Composite Manufacturing Process. Journal of Reinforced Plastics and Composites. 2005;24:869-88.
[82] Li Z, Yang T, Du Y. Dynamic finite element simulation and transient temperature field analysis in thermoplastic composite tape lay-up process. Journal of Thermoplastic Composite Materials. 2015;28:558-73.
[83] Lichtinger R, Hörmann P, Stelzl D, Hinterhölzl R. The effects of heat input on adjacent paths during Automated Fibre Placement. Composites Part A: Applied Science and Manufacturing. 2015;68:387-97.
[84] Qu W, Pan H, Yang D, Li J, Ke Y. As-built FE thermal analysis for complex curved structures in automated fiber placement. Simulation Modelling Practice and Theory. 2022;118.
[85] Barasinski A, Leygue A, Soccard E, Poitou A. Identification of non uniform thermal contact resistance in automated tape placement process. International Journal of Material Forming. 2013;7:479-86.
[86] Levy A, Heider D, Tierney J, Gillespie JW. Inter-layer thermal contact resistance evolution with the degree of intimate contact in the processing of thermoplastic composite laminates. Journal of Composite Materials. 2013;48:491-503.

[87] Moghadamazad M, Hoa SV. Models for heat transfer in thermoplastic composites made by automated fiber placement using hot gas torch. Composites Part C: Open Access. 2022;7.
[88] Chen M, Jiang M, Liu X, Wu B. Intelligent Inspection System Based on Infrared Vision for Automated Fiber Placement. 2018 IEEE International Conference on Mechatronics and Automation (ICMA): IEEE; 2018. p. 918-23.
[89] Sebastian Zambal CE, Michael Clarke, John Klintworth, Pierre-Yves Mechin. A digital twin for composite parts manufacturing Effects of defects analysis based on manufacturing data. 2018 IEEE 16th International Conference on Industrial Informatics (INDIN). Porto, Portugal: IEEE; 2018.
[90] Brüning J, Denkena B, Dittrich MA, Hocke T. Machine Learning Approach for Optimization of Automated Fiber Placement Processes. Procedia CIRP. 2017;66:74-8.
[91] Ojeda IdJG, Patrouix O, Aoustin Y. Pressure based approach for Automated Fiber Placement (AFP) with sensor based feedback loop and flexible component in the effector. IFAC-PapersOnLine. 2017;50:794-9.
[92] Gonzalez Ojeda IDJ, Patrouix O, Aoustin Y. Dynamic Tool Center Point (DTCP) implementing in Automated Fiber Placement (AFP). the third International Symposium on Automated Composites Manufacturing (ACM1). Montreal, Canada2017.
[93] Uhart M, Patrouix O, Aoustin Y. Controlling the tape's gap in robotized fiber placement process using a visual servoing external hybrid control scheme. The International symposium Aircraft Materials (ACMA2014)2014.
[94] Krombholz C, Perner M, Bock M, Röstermundt D. Improving the production quality of the advanced automated fiber placement process by means of online path correction. 28th congress of the international council of the aeronautical sciences2012. p. 3922-31.
[95] Uhart M, Patrouix O, Aoustin Y. Improving manufacturing of aeronautical parts with an enhanced industrial Robotised Fibre Placement Cell using an external force-vision scheme. International Journal on Interactive Design and Manufacturing (IJIDeM). 2015;10:15-35.
[96] Heinecke F, Wille T. In-situ structural evaluation during the fibre deposition process of composite manufacturing. CEAS Aeronautical Journal. 2018;9:123-33.
[97] Yadav N, Schledjewski R. Inline tape width control for thermoplastic automated tape layup. Composites Part A: Applied Science and Manufacturing. 2022;163.
[98] Nguyen DH, Sun X, Tretiak I, Valverde MA, Kratz J. Automatic process control of an automated fibre placement machine. Composites Part A: Applied Science and Manufacturing. 2023;168.

[99] Druiff PPJ, Ma K, Visrolia A, Arruda M, Palardy-Sim M, Bolduc S, et al. A Smart Interface For Machine Learning Based Data-Driven Automated Fibre Placement. The Composites and Advanced Materials Expo 20212021.
[100] Brasington A, Halbritter J, Godbold M, Kirkpatrick M, Sacco C, Harik R. Mapping of multimodality data for manufacturing analyses in automated fiber placement. Composites Part B: Engineering. 2023;263.
[101] Sloan J. Infused wing sheds light on aerocomposites future. Composites World2018.
[102] Lombetti D, Dell'Anno G, Skordos A, Partridge I. Delamination performance of tufted carbon/epoxy composites made by automated dry fibre placement. 19th International Conference on Composite Materials, ICCM 20132013.
[103] Rimmel O, May D, Mitschang P. Impact of stitching on permeability and mechanical properties of preforms manufactured by dry fiber placement. Polymer Composites. 2019;40:1631-42.
[104] Kadiyala AK, O'Shaughnessy T, Lee S, Portela A, Comer A. Influence of environmental conditioning on mechanical properties of carbon dry fibre preformed thermoplastic matrix composites manufactured via automated placement-resin infusion process. Composites Communications. 2021;27.
[105] Neunkirchen S, Schledjewski R. Tack measurement of bindered rovings for the dry fiber winding process. Polymer Composites. 2021.
[106] Matveev MY, Schubel PJ, Long AC, Jones IA. Understanding the buckling behaviour of steered tows in Automated Dry Fibre Placement (ADFP). Composites Part A: Applied Science and Manufacturing. 2016;90:451-6.
[107] Rohatgi V, Lee LJ. Moldability of Tackified Fiber Preforms in Liquid Composite Molding. Journal of Composite Materials. 1997;31:720-44.
[108] Brody JC, Gillespie Jr. JW. Reactive and non-reactive binders in glass/vinyl ester composites. Polymer Composites. 2005;26:377-87.
[109] Schmidt S, Mahrholz T, Kühn A, Wierach P. Powder binders used for the manufacturing of wind turbine rotor blades. Part 1. Characterization of resin-binder interaction and preform properties. Polymer Composites. 2018;39:708-17.
[110] Shih C-H, Lee LJ. Tackification of Textile Fiber Preforms in Resin Transfer Molding. Journal of Composite Materials. 2001;35:1954-81.
[111] Tanoglu M, Robert S, Heider D, McKnight S, Brachos V, Gillespie Jr J. Effects of thermoplastic preforming binder on the properties of S2-glass fabric reinforced epoxy composites. International journal of adhesion and adhesives. 2001;21:187-95.
[112] Dickert M, Ziegmann G. Influence of binder on the mechanical properties and the permeability of a non-crimp carbon fabric preform. ECCM15 - 15TH EUROPEAN CONFERENCE ON COMPOSITE MATERIALS. Venice2012.

[113] Agogue R, Chebil N, Deleglise-Lagardere M, Beauchene P, Park CH. Efficient Permeability Measurement and Numerical Simulation of the Resin Flow in Low Permeability Preform Fabricated by Automated Dry Fiber Placement. Applied Composite Materials. 2017;25:1169-82.
[114] Rimmel O, Becker D, Mitschang P. Maximizing the out-of-plane-permeability of preforms manufactured by dry fiber placement. Advanced Manufacturing: Polymer & Composites Science. 2017;2:93-102.
[115] Aziz AR, Ali MA, Zeng X, Umer R, Schubel P, Cantwell WJ. Transverse permeability of dry fiber preforms manufactured by automated fiber placement. Composites Science and Technology. 2017;152:57-67.
[116] Veldenz L, Astwood S, Giddings P, Kim BC, Potter K. Infusion characteristics of preforms manufactured by Automated Dry Fibre Placement. 2017.
[117] Matveev MY, Ball FG, Jones IA, Long AC, Schubel PJ, Tretyakov MV. Uncertainty in geometry of fibre preforms manufactured with Automated Dry Fibre Placement and its effects on permeability. Journal of Composite Materials. 2017;52:2255-69.
[118] Ehsani F, Hoa SV, Shadmehri F. Effect of gaps on preform and laminate made by automated dry fiber placement and resin infusion. Composites Part A: Applied Science and Manufacturing. 2023;173.
[119] Kelly PA. Transverse compression properties of composite reinforcements. Composite Reinforcements for Optimum Performance: Elsevier Ltd; 2011. p. 333-66.
[120] Di Francesco M. Laser-assisted Automated Fibre Placement Process Development [EngD Thesis]: University of Bristol, 2017.
[121] Veldenz L. Automated Dry Fibre Placement and Infusion Process Development for Complex Geometries [EngD Thesis]: University of Bristol, 2019.
[122] Nixon-Pearson OJ, Belnoue J-H, Ivanov DS, Potter KD, Hallett SR. An experimental investigation of the consolidation behaviour of uncured prepregs under processing conditions. Journal of Composite Materials. 2016;51:1911-24.
[123] Swery EE, Allen T, Kelly P. Predicting compaction-induced deformations of meso-scale textile models efficiently. Journal of Composite Materials. 2016;51:2517-27.
[124] Potluri P, Sagar TV. Compaction modelling of textile preforms for composite structures. Composite Structures. 2008;86:177-85.
[125] Lin H, Sherburn M, Crookston J, Long AC, Clifford MJ, Jones IA. Finite element modelling of fabric compression. Modelling and Simulation in Materials Science and Engineering. 2008;16.
[126] Nguyen QT, Vidal-Sallé E, Boisse P, Park CH, Saouab A, Bréard J, et al. Mesoscopic scale analyses of textile composite reinforcement compaction. Composites Part B: Engineering. 2013;44:231-41.

[127] Wu W, Li W. A novel material for simulation on compaction behavior of glass fiber non-crimp fabric. Composite Structures. 2019;219:8-16.
[128] Comas-Cardona S, Le Grognec P, Binetruy C, Krawczak P. Unidirectional compression of fibre reinforcements. Part 1: A non-linear elastic-plastic behaviour. Composites Science and Technology. 2007;67:507-14.
[129] Wei K, Liang D, Mei M, Yang X, Chen L. A viscoelastic model of compression and relaxation behaviors in preforming process for carbon fiber fabrics with binder. Composites Part B: Engineering. 2019;158:1-9.
[130] Belhaj M, Deleglise M, Comas-Cardona S, Demouveau H, Binetruy C, Duval C, et al. Dry fiber automated placement of carbon fibrous preforms. Composites Part B: Engineering. 2013;50:107-11.
[131] Kabachi MA, Danzi M, Arreguin S, Ermanni P. Experimental study on the influence of cyclic compaction on the fiber-bed permeability, quasi-static and dynamic compaction responses. Composites Part A: Applied Science and Manufacturing. 2019;125.
[132] Lectez A-S, El Azzouzi K, Binetruy C, Comas-Cardona S, Verron E, Lebrun J-M. Three-dimensional mechanical properties of dry carbon fiber tows subjected to cyclic compressive loading. Journal of Composite Materials. 2018;52:2661-77.
[133] Helber F, Amann A, Carosella S, Middendorf P. Intrinsic fibre heating: a novel approach for automated dry fibre placement. IOP Conf Ser: Mater Sci Eng: IOP Publishing; 2018. p. 12064.
[134] Evans AD, Turner TA, Endruweit A. Development of automated dry fibre placement for high rate deposition. ICCM International Conferences on Composite Materials2019.
[135] Fukuda H. Processing of carbon fiber reinforced plastics by means of Joule heating. Advanced Composite Materials. 1994;3:153-61.
[136] Raji A-RO, Varadhachary T, Nan K, Wang T, Lin J, Ji Y, et al. Composites of Graphene Nanoribbon Stacks and Epoxy for Joule Heating and Deicing of Surfaces. ACS Applied Materials & Interfaces. 2016;8:3551-6.
[137] Çelik M, Maguire JM, Noble T, Robert C, Ó Brádaigh CM. Numerical and experimental investigation of Joule heating in a carbon fibre powder epoxy towpregging line. Composites Part A: Applied Science and Manufacturing. 2023;164.
[138] Çelik M, Noble T, Haseeb A, Maguire J, Robert C, Ó Brádaigh CM. Contact resistance heating of unidirectional carbon fibre tows in a powder-epoxy towpregging line. Plastics, Rubber and Composites. 2022;51:383-92.
[139] Ma L, Srivastava R, Barpanda D, Fowler T, Theophanous T, Verghese N. An inverse approach to characterize anisotropic thermal conductivities of a dry fibrous preform composite. Journal of Reinforced Plastics and Composites. 2013;32:1916-27.

[140] YAMASHITA Y, YAMADA H, MIYAKE H. Effective thermal conductivity of plain weave fabric and its composite material made from high strength fibers. Journal of Textile Engineering. 2008;54:111-9.
[141] Villière M, Lecointe D, Sobotka V, Boyard N, Delaunay D. Experimental determination and modeling of thermal conductivity tensor of carbon/epoxy composite. Composites Part A: Applied Science and Manufacturing. 2013;46:60-8.
[142] El-Hage Y, Hind S, Robitaille F. Thermal conductivity of textile reinforcements for composites. Journal of Textiles and Fibrous Materials. 2018;1.
[143] Zhang C, Duan Y, Xiao H, Wang B, Ming Y, Zhu Y, et al. The effects of processing parameters on the wedge peel strength of CF/PEEK laminates manufactured using a laser tape placement process. The International Journal of Advanced Manufacturing Technology. 2022.
[144] Forcellese A, Mancia T, Russo AC, Simoncini M, Vita A. Robotic automated fiber placement of carbon fiber towpregs. Materials and Manufacturing Processes. 2021;37:539-47.
[145] Sherburn M. Geometric and Mechanical Modelling of Textiles: University of Nottingham, 2007.
[146] Evans AD, Turner TA, Endruweit A. Development of Automated Dry Fibre Placement for High Rate Deposition. 22nd International Conference on Composite Materials (ICCM22). Melbourne2019.
[147] Dharmalingam AS, Hemmer J, Lectez AS, Binetruy C, Comas-Cardona S. Evolution of single carbon and glass fibrous tow cross-sections in dry and lubricated states during compaction perpendicular to the fibers. Composites Part B: Engineering. 2018;148:235-42.
[148] Hind S, Robitaille F. Measurement, modeling, and variability of thermal conductivity for structural polymer composites. Polymer Composites. 2009:NA-NA.
[149] Incropera FP. Introduction to heat transfer / Frank P. Incropera ... [et al.]. 5th ed. ed. Hoboken, N.J.: Hoboken, N.J. : John Wiley & Sons, 2007.
[150] Brenken B, Barocio E, Favaloro A, Kunc V, Pipes RB. Development and validation of extrusion deposition additive manufacturing process simulations. Additive Manufacturing. 2019;25:218-26.
[151] Nie Z, Wang G, McGuffin-Cawley JD, Narayanan B, Zhang S, Schwam D, et al. Experimental study and modeling of H13 steel deposition using laser hot-wire additive manufacturing. Journal of Materials Processing Technology. 2016;235:171-86.
[152] Zhao Q, Hoa SV, Gao ZJ. Thermal stresses in rings of thermoplastic composites made by automated fiber placement process. Science and Engineering of Composite Materials. 2011;18:35-49.

[153] Çelik O, Hosseini SMA, Baran I, Grouve WJB, Akkerman R, Peeters DMJ, et al. The influence of inter-laminar thermal contact resistance on the cooling of material during laser assisted fiber placement. Composites Part A: Applied Science and Manufacturing. 2021;145.

[154] Ziegler JG, Nichols NB. Optimum settings for automatic controllers. Transactions of the American society of mechanical engineers. 1942;64:759-65.